CFD Analysis of a Helical Coil Based Energy Storage Integrated with Solar Water Heating System

By

Saqib Ayuob

Reg. No: 00000275171

Session 2018-20

Supervised by

Dr. Mariam Mahmood

US-Pakistan Center for Advanced Studies in Energy (USPCAS-E)

National University of Sciences and Technology (NUST)

H-12, Islamabad 44000, Pakistan

June 2022

CFD Analysis of a Helical Coil Based Energy Storage Integrated with Solar Water Heating System

By

Saqib Ayuob

Reg # 00000275171

Session 2018-20

Supervised by

Dr. Mariam Mahmood

A Thesis Submitted to the U.S-Pakistan Center for Advanced Studies in Energy in partial fulfilment of the requirements for the degree of MASTER of SCIENCE in THERMAL ENERGY ENGINEERING

US-Pakistan Center for Advanced Studies in Energy (USPCAS-E)

National University of Sciences and Technology (NUST)

H-12, Islamabad 44000, Pakistan

June 2022

THESIS ACCEPTANCE CERTIFICATE

Certified that final copy of MS/MPhil thesis written by **Mr. Saqib Ayuob (Registration No. 00000275171)**, of U.S.-Pakistan Centre for Advanced Studies in Energy has been vetted by undersigned, found complete in all respects as per NUST Statues/Regulations, is within the similarity indices limit and is accepted as partial fulfilment for the award of MS/MPhil degree. It is further certified that necessary amendments as pointed out by GEC members of the scholar have also been incorporated in the said thesis.

Signature: _____

Name of Supervisor: Dr. Mariam Mahmood

Date: _____

Signature (HoD): _____

Date: _____

Signature (Dean/Principal): _____

Date: _____

.

Certificate

This is to certify that work in this thesis has been carried out by **Mr. Saqib Ayuob** and completed under my supervision in, US-Pakistan Center for Advanced Studies in Energy (USPCAS-E), National University of Sciences and Technology, H-12, Islamabad, Pakistan.

Supervisor: _____

Dr. Mariam Mahmood
USPCAS-E
NUST, Islamabad

GEC member 1: _____

Prof. Dr. Adeel Waqas
USPCAS-E
NUST, Islamabad

GEC member 2: _____

Dr. Majid Ali
USPCAS-E
NUST, Islamabad

GEC member 3: _____

Dr. Nadia Shahzad
USPCAS-E
NUST, Islamabad

HOD-TEE: _____

Dr. Majid Ali
USPCAS-E
NUST, Islamabad

Dean/Principal: _____

Prof. Dr. Adeel Waqas
USPCAS-E
NUST, Islamabad

Acknowledgment

I would like to take some time at the end of this thesis to thank all the individuals without whom this project was never feasible. Although it is just my name on the cover, many individuals have contributed in their own manner to the studies, and I thank them for that.

My supervisor, Dr. Mariam Mahmood, you developed an invaluable room for me to do this study in the best possible manner and to develop myself as a researcher. I substantially appreciate the liberty you gave me to discover my own route, the advice and help you gave me when it was necessary. Your friendly guidance and professional advice were invaluable throughout all the work phases.

I would also like to take a moment to thank Dr. Adeel Waqas, Dr. Majid Ali, and Dr. Nadia Shahzad, members of the GEC Committee. I am proud and honoured that you accepted my committee's presence.

Thank you

Saqib Ayuob

Dedication

I would like to wholeheartedly dedicate my thesis to my beloved parents, who have been a constant source of inspiration and strength with continuous moral, spiritual and emotional support.

To my brothers, sister, mentor, and friends who shared their words of advice and encouragement to help me finish this study.

Abstract

Storage tanks based on helical coil heat exchangers are an integral part of solar water heating (SWH) systems and require optimal design configuration to achieve maximum heat transfer and a longer storage period. This study is focused on thermal analysis of a vertical helical coil-based water storage tank and derivation of inner and outer Nusselt number correlations by considering the storage tank as well as helical coil and catering to both forced and natural convection effects. A fluid-fluid conjugate heat transfer transient state model is validated with experiments performed with 50/50% water-glycol mixture as HTF at flow rates of 2 and 3 L/minute in a solar water heating system, while water remains at static flow condition inside the tank. To reduce the computational cost, a symmetrical downsized model is also designed and validated, which showed a mean absolute percentage error of 3.25%. In order to derive the mathematical correlations, alterations were made to the validated model by using coils with curvature ratios ranging from 0.09-0.184 with HTF flow rates in laminar flow regimes, ranging from 30 to 100 liters per hour at temperatures from 40^{o}C to 80^{o}C. Furthermore, Nu_i mathematical correlations based on M number, curvature ratio, and Prandtl number showed good agreement with correlations derived by past investigators. Similarly, the outer Nusselt number of the coil was related to Rayleigh's number and the derived relations showed good agreement with the past studies, while $Nu_o = 0.1996 (Ra_{do}^{0.326})$ showed the least error of 2.06%. Later on, thermal stratification analysis helped to understand that coil position and aspect ratio determine the thermocline developed inside the storage tank and hot water storage for longer periods. Finally, a comparative study was carried out to determine the variation in inner and outer HTC with different geometric parameters of helical coil.

Keywords: Thermal Energy Storage (TES), Nusselt Number, Helical Coil, Computational Fluid Dynamics (CFD), Thermal Stratification

Table of Contents

List of Figures

List of Tables

List of Publications

“Development and Validation of Nusselt number correlations for a Helical Coil Based Energy Storage Integrated with Solar Water Heating System’’. Saqib Ayuob, Mariam Mahmood, Naveed Ahmad, Adeel Waqas, Hamza Saeed, Muhammad Bilal Sajid, Majid Ali, Nadia Shahzad

EST-D-22-00865- Journal of Energy Storage (Under review).

Nomenclature

List of symbols

A	surface area of the coil
C_p	specific heat at constant pressure (J/kg.K)
d	diameter of the tube (m)
D	mean helix diameter (m)
D_e	Dean number
$\triangle T_i$	temperature difference between the mean bulk temperature of the hot fluid and internal surface of coil (K)
$\triangle T_o$	temperature difference between the external surface of the coil and mean bulk temperature of the water (K)
H	height of the coil
h	convective heat transfer coefficient ($W/m^2.K$)
k	thermal conductivity (W/m.K)
L_c	Characteristic length (m)
M	dimensionless number
$\dot{m}$	mass flow rate (kg/s)
Nu	Nusselt number
P	pitch of the coil (m)
Pr	Prandtl number
Q	Heat transferred (W)
Ra	Rayleigh's number
Re	Reynolds number
Re_{cr}	critical Reynolds number
T_{in}	temperature of the hot fluid at the inlet (K)
T_{out}	temperature pf the hot fluid at the outlet (K)
T_s	mean outer surface temperature of the coil (K)
T_w	mean bulk temperature of the water inside the tank
V	volume (m^3)

Abbreviations

CFD	Computational Fluid Dynamics
2D	Two Dimensional
3D	Three Dimensional
RANS	Reynolds Average Navier Stokes
TES	Thermal Energy Storage
AEDB	Alternate Energy Development Board
USPCASE	United States Pakistan Centre of Advanced studies in Energy

Greek symbols

α	thermal diffusivity (m^2/s)
β	thermal expansion coefficient (1/K)
δ	curvature ratio (d_i/D)
μ	dynamic viscosity (kg/m.s)
ν	kinematic viscosity (μ/ρ) (m^2/s)
ρ	density (kg/m^3)

Subscript

c	coil
H	height
L	length
i	inner
o	outer

Chapter 1: Introduction

1.1 Motivation

For centuries, people have relied upon expending conventional energy sources to harvest energy, but in today's world burning off non-renewable fuels such as oil, gas, and coal for energy needs is turning out to be a problem. Ecological change is one of the best characteristic troubles that we have ever stood up to, and the essential driver behind it is our dependence on petroleum derivatives. Utilizing coal, oil and other oil-based goods is the fundamental method by which we produce power, however, it likewise stimulates overwhelming centralizations of pollutants in our air and water.

Currently, there is a worldwide requisite for clean and sustainable power sources, since fossil fuels are non-renewable and require limited resources, which are gradually diminishing because of high cost and ecologically damaging retrieval practices. For the recent few decades, we have come to depend progressively more on the world's supply of petroleum derivatives, and that supply is quickly running out. As the enthusiasm for non-renewable energy sources has extended, the cost of using them has moreover extended and consistently we end up with greater and greater energy bills. In this manner, the prerequisite for reasonable and achievable assets is colossally required. Powerful and increasingly practical elective choices are geothermal energy, biomass and biofuels, sunlight-based energy, hydro-energy, and wind energy, in contrast to non-renewable energy sources these sources of energy never run out. With a much lower effect on the earth, using supportable power protects our planet by essentially diminishing the aggregate of carbon discharges that we produce. By utilizing economical power sources, we likewise decrease our dependence on non-sustainable power sources, for example, gas and oil which suggests that we can avoid the expanding cost of energy charges and grow our energy security.

1.2 Solar Energy

Solar power is energy in the form of heat from the sun and radiant light that is further transformed into thermal and electrical energy. It is one of the cleanest and abundant renewable energy sources available. In the upper atmosphere, the earth receives around

174 petawatts (PW) of solar radiation [1]. Around 70% of the solar radiation gets absorbed while the rest is reflected back to space. The majority of the earth's population lives in areas where solar irradiance levels are 150 to 300 watts/m^2, or 3.5 to 70 kWh/m^2 per day [2]. In 2000, World Energy Council published an estimate for the global solar potential to be around 1600 to 49800 exajoules per annum [3]. Therefore, solar technologies utilize this energy for different applications, which varies from proving light for a conducive inner environment to the generation of electricity. It is also used for heating water for different domestic and industrial applications.

1.3 Solar energy potential in Pakistan

As the interest in energy continues developing far and wide, countries are using various sources to produce and disseminate capacity to customers. Ongoing numbers demonstrate that nations meet as much as 80 percent of their energy prerequisite from non-renewable energy sources, for example, oil, natural gas and coal while the remaining 20% necessities are met by nuclear (5.8%), hydro (2.5%), wind, sun-powered, biofuel, wood and biogas (10.8%). Over the most recent five years, there has been a solid move from the utilization of non-renewable energy sources to renewable sources for power production with about 66% of new generation investment going in renewables [4].

In Pakistan, the total installed power generation capacity is about 25,000 MW. In 2017, Pakistan acquired just about one-third of power from gas, almost 31% from furnace oil and 26% from hydel, followed by approximately 6% from nuclear and just 2% from sustainable sources. Production from hydel is occasional in nature, resulting in more dependence on non-renewable energy sources amid the cooler months of the year [5]. Also, because of the absence of local fossil fuel resources and high rates of these fuels in the global markets, the nation is confronting challenges of power shortage. All these obstacles together have adversely influenced industrial development in the country. As a result, the country's economy has been continually deteriorating. For emerging countries such as Pakistan, exploring renewable energy resources represents a great alternative for power production [6].

Pakistan is blessed with huge solar energy potential. It is situated on the sunny belt where days are mostly sunny, long with high solar radiation. Some locations even have an annual

average sunshine duration of 8-8.5 hrs [7]. The daily mean global irradiation falling on a horizontal surface is around 200-250 watt/m^2[8]. A research was conducted by the Alternative Energy Development Board of Pakistan (AEDB) in collaboration with the National Renewable Energy Laboratory (NERL), USA to determine the approximate solar energy potential of Pakistan. The solar potential was estimated to be around 1.6 TWh per year [9]. Furthermore, from Figure 1-1 it can be observed that some of the southern parts of Pakistan had solar irradiance above 5 kWh/m^2 per day, which is considered ideal for solar technologies [10]. Solar irradiance for Islamabad is quite reasonable and as investigated by I. Ulfat et al [11], in the region, solar energy can be efficiently utilized for decreasing the dependence on conventional fuels.

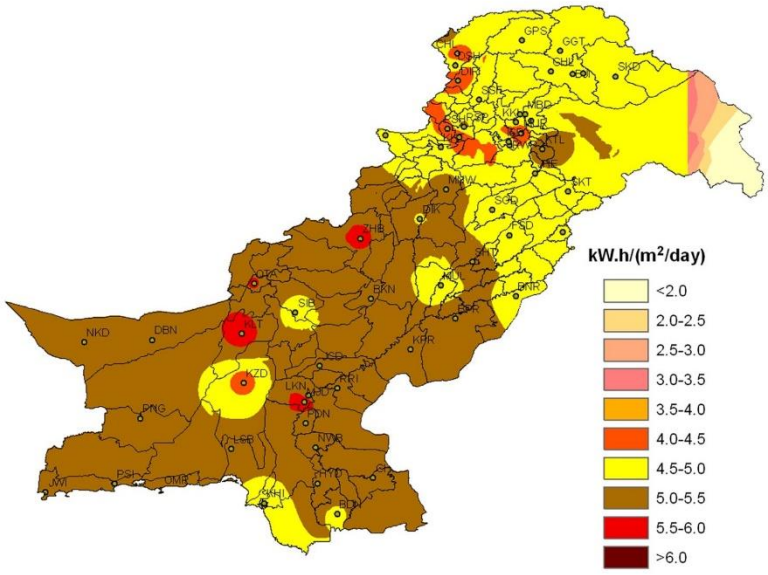

Figure 1-1 Annual solar radiations of Pakistan [10]

1.4 Types of solar technologies

There are generally 3 major technologies through which solar energy is utilized:

1. Photovoltaic (PV) module
2. Concentrated solar power (CSP)
3. Solar thermal collectors

1.4.1 Photovoltaic (PV) module

Photovoltaic (PV) module or solar panel is photovoltaic cells assembled on a structure for installation. Photovoltaic modules use photons from sunlight to produce DC electricity through the photovoltaic effect. PV modules usually use thin-film cell or crystalline silicon-based cells, and the back layer or the top layer act as a load-carrying element. Initially, PV modules constructed were rigid, but now thin-film-based semi-flexible modules are also available. Cells of the modules are connected in parallel to achieve the desired current and connected in series to get the necessary voltage. The power of the PV module is determined by taking the product of voltage and current. An assembly of photovoltaic modules is called a Photovoltaic panel, and a collection of interconnected PV panels is called a solar array as shown in Figure 1-2 [12]. Solar cell's first major application was to be used as an alternative power source for a satellite in 1958. Nowadays, with advancement in technologies, it could be a major contributor to decreasing our dependency on fossil fuel.

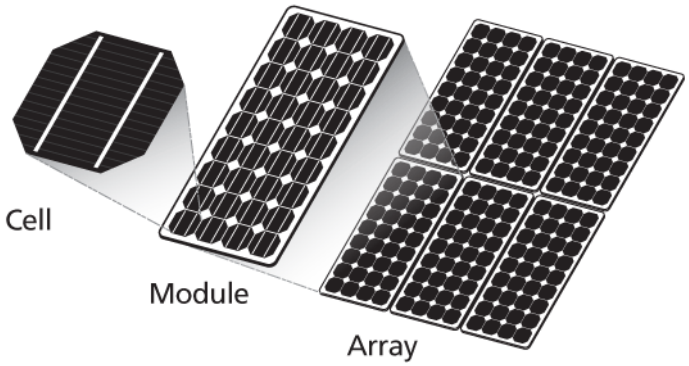

Figure 1-2 Solar cell, PV module and Solar array [12]

1.4.2 Concentrated solar power (CSP)

Concentrated solar power technology generates electricity by concentrating sunlight from a large area onto a receiver as seen in Figure 1-3. Thermal energy at the receiver is used to drive a heat engine which is further connected to an electrical generator to generate electricity. This thermal energy could also be used to facilitate a thermochemical reaction. Solar energy from such a large area is concentrated with help of mirrors and a tracking system. Concentrated solar power plants with thermal storage use synthetic oil or molten salt as a medium for storing thermal energy. These thermal energy storage mediums are

further stored in insulated tanks. Later, when required, oil or molten salt is used for generating steam in the boiler, then the steam is used for driving the turbine to generate electricity. CSP plants with thermal energy storage are dispatchable and also self-sustainable just like conventional power plants and also without pollution. CSP plants with thermal energy storage systems also operate on the Brayton cycle using air instead of steam for producing electricity [13].

Figure 1-3 Concentrated solar power plant [13]

1.4.3 Solar thermal collectors

Solar thermal collector gathers thermal energy from sunlight. It consists of an aperture area and an absorber area. The aperture area size is approximately the same as the absorber area and it is the part that receives the solar radiation, while the absorber area is the part that absorbs the solar radiation. Furthermore, thermal energy from the absorber is collected through cooling pipes that contain water, glycol, or a mixture of water and glycol as a working fluid. Afterward, working fluid is flown through the thermal energy storage unit so that heat gets transferred from the working fluid to the thermal energy storage for later use. Solar thermal collectors are of different types such as flat plate collectors, evacuated tube collectors, and evacuated flat plate collectors.

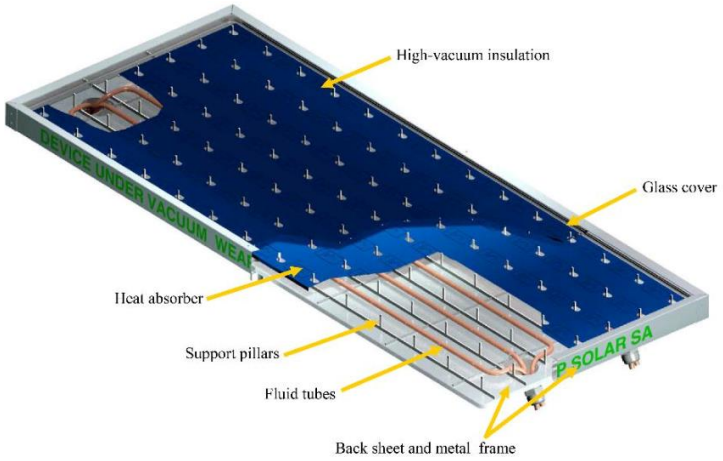

Figure 1-4 Evacuated flat plate solar thermal collector [14]

Evacuated flat plate collector (EFPC), in Figure 1-4 [14], is one of the most efficient thermal collectors. A vacuum is induced between the glass cover and the absorber area so that the heat losses from the absorber to the environment due to convection could be prevented. Moreover, the bottom part of the absorber is padded with a thermal insulator so that the heat loss from the bottom of the collector could also be prevented. EFPC is the collector further used in our research.

Although solar energy is quite useful in overcoming lot of energy related challenges, but it also has its share of disadvantages. Amount of solar energy to be consumed is directly related to space required which prompts the requirement of large spaces for installation of solar projects. Weather dependency and lack of solar energy during night-time is one of the major challenges. Which leads to its dependency on different energy storage technologies, that causes increase in capital cost for solar projects.

1.5 Thermal energy storage (TES)

At present thermal energy storage (TES) is an active field in applied energy [15]. It encompasses energy efficiency and conservation. It affects the efficiency by shifting the load to the off-peak hours and reduce the expenditure effectively. In the case of solar energy, it conserves energy during the daytime and uses the same during the night. It also helps in reducing the intermittence behaviour of renewable sources [16]. The main advantage of the thermal energy storage system is its integration with the existing system,

and this alone can save a lot of the cost of retrofitting. The basic working principle of the TES systems is shown below in Figure 1-5 [17].

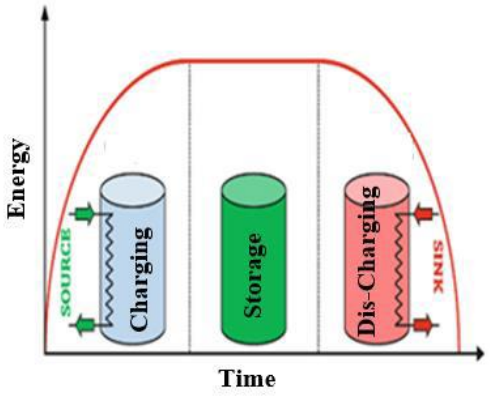

Figure 1-5 Schematic of thermal energy storage system [17]

The figure above shows a simple TES system. The system is charged with a source during the charging phase. The source can be solar thermal, electric, or natural gas. After the system is fully charged the energy is stored in a storage tank and is sent to the load/ sink when required, which can be seen in the graph.

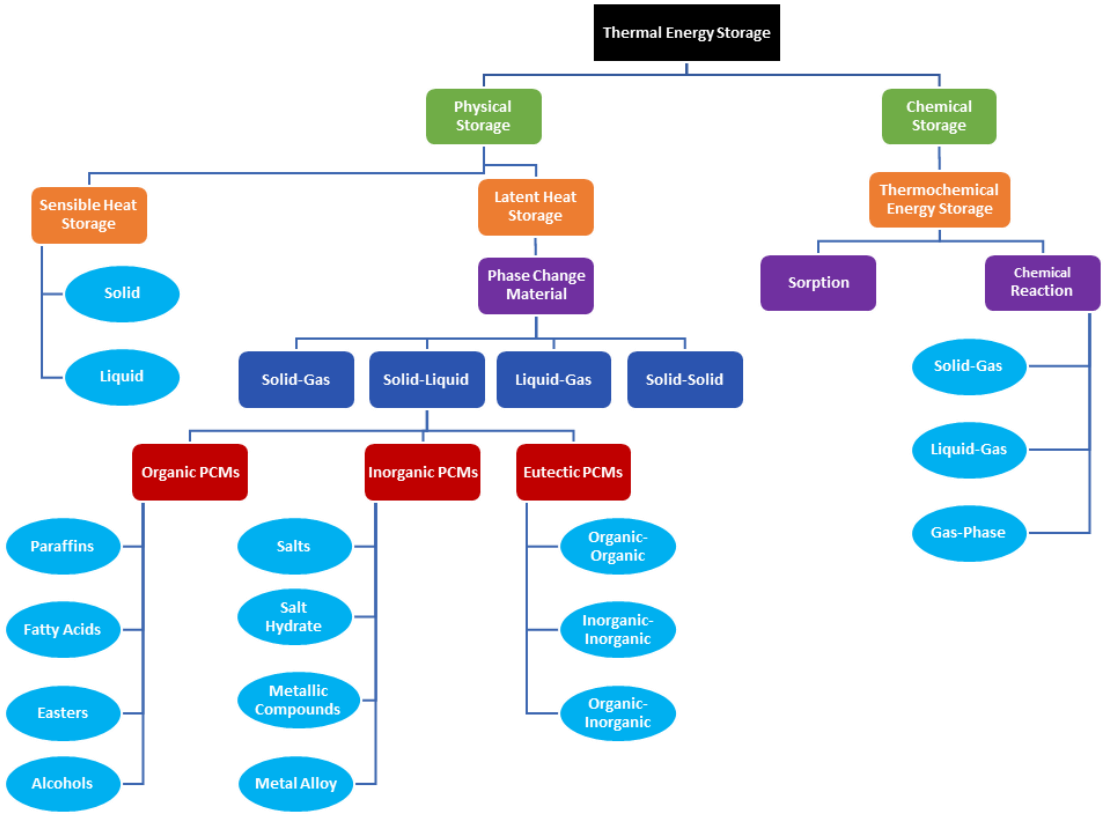

Figure 1-6 Types of thermal energy storage systems

TES systems can be further divided into many categories as per the applications or the material used for storage. The different kind of thermal storage is shown in Figure 1-6. TES systems can broadly be classified into two major categories one is known as physical storage that does not involve the chemical changes of the substance and the other is known as chemical or thermochemical storage that involve the chemical changes of the substance during each thermal cycle and hence reduces the durability of the system. Physical storage is further divided into two major categories i.e., Sensible (which does not change phase during the thermal cycle) and Latent (which changes phase during the thermal cycle, solid-liquid, liquid-gas, etc.). In our research, sensible heat storage medium water is used, because it could be directly used in hot water applications for winters, and in summers it could be used as a source of heat for any due thermal process.

1.6 Heat Exchangers

A heat exchanger is a system that is used for the transfer of thermal energy in the form of heat from one medium to another. The phenomenon of heat exchange takes place between two or more fluids. Heat exchangers are used in heating as well as cooling operations [18]. Fluids between which the phenomenon of heat exchange take place are usually separated employing a solid wall to prevent the mixing of the fluids. But in some applications fluids also come in direct contact [19]. Heat exchangers have enormous applications in HVAC, power plants, process plants, manufacturing industries, etc.

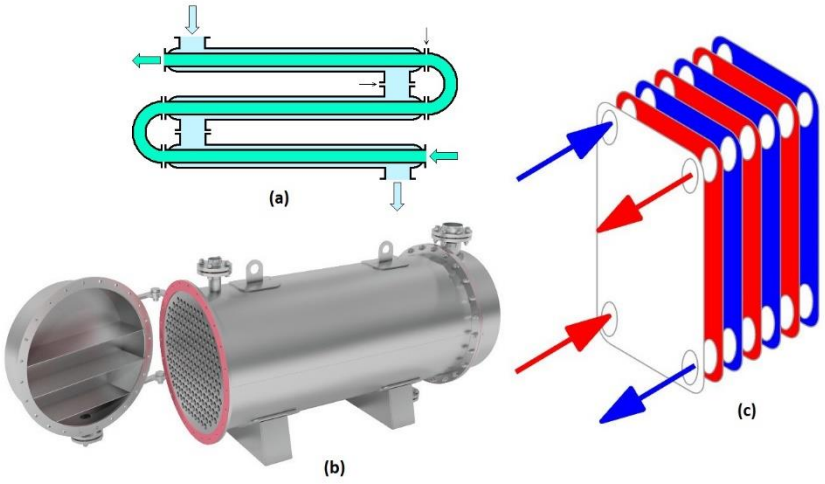

Figure 1-7 (a) Double pipe, (b) Shell and tube, (c) Flat plate heat exchanger [20]

Heat exchangers are of many types but the most common types are double pipe heat, shell and tube, and flat plate heat exchanger as shown in below Figure 1-7 [20]. If heat exchangers are classified based on the fluid flow, they are primarily divided into 3 types. Parallel flow, counterflow, and cross-flow heat exchanger. In a parallel-flow heat exchanger, hot and cold fluid both enters from the same side and flows in parallel to one another during heat transfer. In a counter-flow heat exchanger, both fluids enter from the opposite side and travel anti-parallel to one another. While in crossflow, both fluids flow perpendicular to one another in the exchanger.

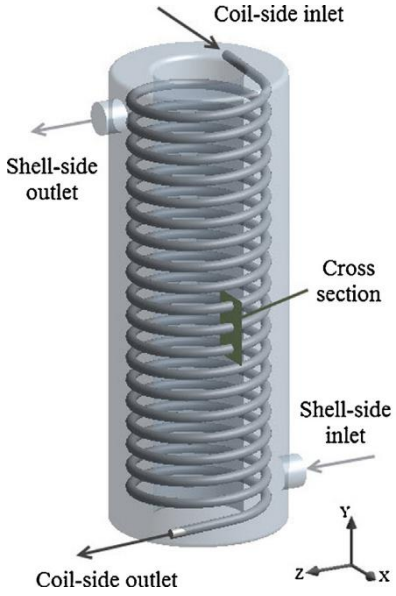

Figure 1-8 Shell and coiled tube heat exchanger [21]

In the case of thermal energy storage, when water is used as the medium for energy storage, a shell and coiled tube heat exchanger are normally used. Water remains in the tank (also be assumed as a shell), while the coiled tube with the running hot fluid is immersed inside the tank. Hot fluid flows through the top of the coil and exits from the bottom. At the time of charging water remains inside the tank at the static position while in the dynamic state water inlet is from the bottom part of the tank and the outlet is from the top in this state it also acts as a counter-flow heat exchanger as shown in Figure 1-8 [21]. Coiled tube heat exchangers are used because they are more compact with high area density [22]. It can be used anywhere with requirements of greater heat transfer with a lesser volume of the exchanger available.

In this research a CFD based analysis is performed to deduce a mathematical corelation for inner and outer Nusselt numbers for vertical helical coil-based storage by using 50/50% water glycol solution as a heat transfer fluid.

1.7 Aims and objectives

In reference to the current energy situation in Pakistan, research is necessary to be accomplished to achieve an efficient system and develop a proper design procedure for the energy devices and equipment. To address this major issue and achieve the desired goals, this research aims to achieve the following purposes.

First, an experimental setup of solar collectors and TES needs to be established. Then, data is needed to be extracted from the TES tank at different dates. A CFD-based model is to be created, whose results are in agreement with the experimental results. After validation, more simulations would be run on the same model by altering its geometric parameters, and mathematical correlation for the inner Nusselt number with 50% water-glycol solution as a working fluid would be extracted. In the same way, a mathematical correlation for the outer Nusselt number would also be extracted and both correlations would be compared with the correlations present in the literature. Moreover, analysis on how the different positions of the coil affect the thermal profile of the storage tank. Lastly, a parametric analysis on variation in inner and external HTC of helical coil with geometric parameters are studied.

1.8 Scope and limitations

The scope of this study is to create a validated CFD-based model for helical coil-based storage tank and derive inner and outer Nusselt number relations based on simulations. Later on, parametric analysis of storage tank on the basis of position of coil and relation of HTC with different geometric parameters of helical coil are discussed.

The limitation in this study is that only 50/50% water-glycol solution is used as heat transfer fluid, and the Nusselt number mathematical relations derived are only for the laminar flow regime. Moreover, thermal properties of the materials used in the simulations are taken constant.

1.9 Thesis outline

The detailed sections of this study are summarized below.

Chapter 2: - This chapter will summarize the work done on the deducing the Nusselt number correlations for helical coiled based heat exchanger for different fluids in the past. Furthermore, studies carried on thermal stratification inside the storage tank and how different aspects affect the thermocline.

Chapter 3: - In this chapter, details on the methodology of the research is initially defined. Furthermore, establishment of the experimental setup, specifications of variety of equipment's used and also the procedure followed for extracting the data are elaborated.

Chapter 4: - In this chapter, the whole CFD aspect of the research is discussed. From the modelling of the storage tank to defining the thermal properties and the boundary conditions are explained. Lastly, results of the initial simulation and its validation with the experimental data is studied.

Chapter 5: - This chapter will sum up the results of the CFD analysis. Mathematical correlations for inner and outer Nusselt number will be deduced and the correlations will further be validated with the correlations produced by the past investigators. Finally, thermal stratification analysis will be carried out and some outcomes would be discussed.

Chapter 6: - This chapter will be comprised of conclusion, recommendation and the work which could be carried out in the future.

Summary

For a growing economy of a world, it is a necessary requirement to have a sustainable with reliable source of cheap energy. Renewable energy particularly solar energy has shown a huge potential to meet that demand. Pakistan possesses promising solar energy potential to meet up their energy requirements which is elaborated in this chapter. This chapter include brief and basic details related to Solar power systems. This describes basic technologies that are used for using solar source of energy. Furthermore, different thermal energy storage medium that can be used for storing the solar thermal energy are discussed. Moreover, different types of heat exchangers that are normally used for transferring heat energy from one medium to another are elaborated in this chapter.

References

[1] P.L. Wagner, V. Smil, General Energetics: Energy in the Biosphere and Civilization, Geogr. Rev. 83 (1993) 110. https://doi.org/10.2307/215395.

[2] Karthik Karuppu. Venk Sitaraman. NVICO., Solar Assessment Guidance : A guide for solar trainee, trainer & assessor examination., NOTION Press, 2019.

[3] United Nations Development Programme, United Nations Department of Economic and Social Affairs, World Energy Council, World Energy Assessment, 2000. https://doi.org/10.2105/AJPH.64.12.1166-b.

[4] A.A. Durrani, I.A. Khan, M.I. Ahmad, Analysis of Electric Power Generation Growth in Pakistan: Falling into the Vicious Cycle of Coal, Eng 2021, Vol. 2, Pages 296-311. 2 (2021) 296–311. https://doi.org/10.3390/ENG2030019.

[5] S.Z. Farooqui, Prospects of renewables penetration in the energy mix of Pakistan, Renew. Sustain. Energy Rev. 29 (2014) 693–700. https://doi.org/10.1016/J.RSER.2013.08.083.

[6] A. Ghafoor, T.U. Rehman, A. Munir, M. Ahmad, M. Iqbal, Current status and overview of renewable energy potential in Pakistan for continuous energy sustainability, Renew. Sustain. Energy Rev. 60 (2016) 1332–1342. https://doi.org/10.1016/J.RSER.2016.03.020.

[7] U.K. Mirza, M. Mercedes Maroto-Valer, N. Ahmad, Status and outlook of solar energy use in Pakistan, Renew. Sustain. Energy Rev. 7 (2003) 501–514. https://doi.org/10.1016/j.rser.2003.06.002.

[8] M.A. Chaudhry, R. Raza, S.A. Hayat, Renewable energy technologies in Pakistan: Prospects and challenges, (n.d.). https://doi.org/10.1016/j.rser.2008.09.025.

[9] S.R. Shakeel, J. Takala, W. Shakeel, Renewable energy sources in power generation in Pakistan, Renew. Sustain. Energy Rev. 64 (2016) 421–434. https://doi.org/10.1016/j.rser.2016.06.016.

[10] S. Adnan, H. Khan, S. Haider, R. Mahmood, A.H. Khan, Impacts of aerosols on

available solar energy at Mbour, Cit. J. Renew. Sustain. Energy. 4 (2012) 13105. https://doi.org/10.1063/1.4712051.

[11] I. Ulfat, F. Javed, F.A. Abbasi, F. Kanwal, A. Usman, M. Jahangir, F. Ahmed, Estimation of Solar Energy Potential for Islamabad, Pakistan, Energy Procedia. 18 (2012) 1496–1500. https://doi.org/10.1016/J.EGYPRO.2012.05.166.

[12] A. Salman, M.I. Khalil, W. Mukhtar, M. Farooq, S.A. Siddique, M. Saad, Comprehensive Overview of Basic Photovoltaic (PV) Power System, (2014).

[13] 247Solar and Masen Ink Agreement for First Operational Next Generation Concentrated Solar Power Plant – HELIOSCSP, (2019). https://helioscsp.com/247solar-and-masen-ink-agreement-for-first-operational-next-generation-concentrated-solar-power-plant/.

[14] W. Murillo-torres, A. Montero-izquierdo, A review of the state-of-the-art of solar thermal collectors applied in the industry Una revisión de los últimos avances de los colectores solares térmicos aplicados en la industria, (2022).

[15] I. Sarbu, C. Sebarchievici, A comprehensive review of thermal energy storage, Sustain. 10 (2018). https://doi.org/10.3390/su10010191.

[16] I. Dinçer, M. (Marc A.. Rosen, John Wiley & Sons, Thermal energy storage systems and applications, 2021.

[17] How Phase Change Materials (PCM) Works — Steemit, (2018). https://steemit.com/science/@badet/how-phase-change-materials-pcm-works.

[18] A.T. Al-Sammarraie, K. Vafai, Heat transfer augmentation through convergence angles in a pipe, An Int. J. Comput. Methodol. 72 (2017) 197–214. https://doi.org/10.1080/10407782.2017.1372670.

[19] S. (Sadık) Kakaç, H. Liu, Heat exchangers : selection, rating, and thermal design, (2002) 501.

[20] Central States Industrial, Types of Heat Exchangers, (2022). https://www.csidesigns.com/blog/articles/types-of-heat-exchangers.

[21] S. Bahrehmand, A. Abbassi, Heat transfer and performance analysis of nanofluid flow in helically coiled tube heat exchangers, Chem. Eng. Res. Des. 109 (2016) 628–637. https://doi.org/10.1016/J.CHERD.2016.03.022.

[22] U.E. Inyang, I.J. Uwa, U.E. Inyang, I.J. Uwa, Heat Transfer in Helical Coil Heat Exchanger, Adv. Chem. Eng. Sci. 12 (2021) 26–39. https://doi.org/10.4236/ACES.2022.121003.

Chapter 2: Literature Review

2.1 Outline

Solar energy is a renewable and clean source of energy that can also be scaled to our requirements. Moreover, it is largely applied in the industrial as well as domestic sectors. According to a study, Pakistan has a solar potential of 1600,000 MW annually [1]. By keeping in consideration of the energy crisis Pakistan facing right now, solar energy could be a definite solution. Solar collectors absorb solar energy, in form of radiation, and then the absorbed energy is used for heating water. Water is usually stored in a tank, which ultimately acts as energy storage. However, water is heated inside the tank with the help of a helical coil-based heat exchanger. Helically coiled tubes have a better heat transfer coefficient as compared to a heat exchanger with straight tubes because helical coiled-based heat exchangers are more compact and have a large surface area to volume ratio which results in a high volumetric heat rating. They are also cheap, easy to manufacture, and could easily be integrated with the storage tank. The hot fluid is passed through the coil, and water inside the tank gets heated up due to natural convection, and the total amount of heat transfer from the hot fluid to the water inside the tank mainly depends upon the internal and external convection, conduction through the pipe also plays a significant role in the heat transfer process. Subsequently, inner and outer heat transfer coefficients greatly influence the amount of heat transferred. It has been observed through the literature review that there is ample evidence to support the notion that a helical tube augments the inner heat transfer coefficient [2]. Whenever a fluid is passed through the helical coil, despite just the main flow, as in the straight pipes, there also exist a secondary flow inside the helical tubes and this secondary flow is due to the centrifugal forces. The longitudinal pressure gradient inside the pipe gives rise to a secondary flow pattern which leads to a higher internal heat transfer coefficient. Streamline flows in the straight pipe converts into curved streamlines which in result delivers comparatively a higher rate of heat transfer. Henceforth, this results in large applications of the helical coiled-based heat exchanger from domestic to industrial sector. In domestic applications, a water tank is generally heated through hot water from a boiler, solar setup, or electric heater [3]. If the hot fluid is used as the source of heat, helically coiled tubes are mainly used as heat

exchangers inside the tank. Furthermore, in industrial applications, helical coiled-based heat exchangers are used in HVAC applications, power plants, process industries, waste heat recovery plants, and different thermal processing industries [4] such as: (1) In many HVAC applications refrigerants are condensed in helical coils by transferring heat with ambient or with another cold fluid passing through the shell and helical tube heat exchanger, (2) Vertical counterflow shell and helical coil heat exchanger based steam generators are used in nuclear power plants for the production of steam to drive the turbine [5]. (3) In chemical industries, polyethylene is produced by the oxidation of ethylene, and to remove the heat of reaction, helical coil-based heat exchangers are used.

2.2 Helical coil-based heat exchanger

2.2.1 Inner Nusselt number of helical coils

Most of the research done in the past practiced simplified boundary conditions, for investigating heat transfer coefficients. For example, using constant heat flux or constant temperature as boundary condition [6–9] conducted CFD analysis on helical tubes and studied the influence of different geometric parameters of a helical coil, pitch coil diameter, and pitch tube diameter. Eventually, concluded that parameters like heat transfer coefficients and Nusselt number of a straight tube in a tube are less than the helical tube in tube heat exchangers. Schmidt [10] did a comparison between straight pipe with the coiled tube, and studied the effects of curvature on the heat transfer. Lastly, they came up with mathematical correlations, through experimentation.

$$\boldsymbol{Nu = 3.65 + 0.08[1 + 0.8(\delta^{0.9})]Re^{[0.5+0.2903\,\delta^{0.194}]}Pr^{\frac{1}{3}}} \quad \textbf{(1)}$$

$0.0123 < d/D < 0.203,\ 100 < Re < Re_{cr}$

$$\boldsymbol{Nu = 0.023\left[1 + 14.8(1 + \delta)\left(\delta^{\frac{1}{3}}\right)\right]Re^{[0.8-0.22\,\delta^{0.1}]}} \quad \textbf{(2)}$$

$0.0123 < d/D < 0.203,\ Re_{cr} < Re < 22000$

Xin & Ebadian [11] carried out experimentation on helical tubes. They used 3 different types of working fluids: ethylene glycol, water, and air. Experimentations were performed on uniformly heated 5 helical tubes. No considerable ramifications were observed due to

the variation of coil pitch and torsion. Moreover, new correlations were developed from the set of data achieved through experimentation.

$$\boldsymbol{Nu = (2.153 + 0.318 De^{0.643}) Pr^{0.177}} \quad \textbf{(3)}$$

$20 < De < 2000$, $0.7 < Pr < 175$, $0.0267 < d/D < 0.0884$

$$\boldsymbol{Nu = 0.00619\, Re^{0.92} Pr^{0.4} (1 + 3.455\, \delta)} \quad \textbf{(4)}$$

$5 \times 10^3 < Re < 10^5$

$0.7 < Pr < 5$, $0.0267 < d/D < 0.0884$

Jayakumar [12] analyzed the helical coil-based heat exchanger by using water as a heat transportation media. Analyses of the heat exchanger were done by considering temperature-dependent properties of water, and conjugate heat transfer. Experimental results were compared with simulated results by using FLUENT 6.2. Furthermore, a mathematical co-relation was established to predict the inner heat transfer coefficient of the coil. Jayakumar [13] also conducted a CFD-based analysis by flowing a single-phase fluid from the helical tubes. Hot water as a working fluid, they changed the coil parameters such as pitch, diameter of the pipe, and diameter of the coil, and studied their effects on heat transfer. Moreover, a correlation was deduced from the experimental data to predict the Nusselt number. The ranges of the parameters used in the correlation are described as

$$\boldsymbol{Nu = 0.116 Re^{0.71} Pr^{0.4} \delta^{0.11}} \quad \textbf{(5)}$$

$14000 < Re < 70000$, $3000 < De < 22000$

$3.0 < Pr < 5.0$, $0.05 < \delta < 0.2$

Mahmoudi et al. [14] Investigated that utilization of TiO2/water nanofluid as heat transfer fluid leads to an increase in Nusselt number. Further, an increase in the curvature ratio of the coil subsequently leads to an increase in Dean number, which causes improvement in the heat transfer, even at fixed Reynolds number. Xu et al. [15] Experimentally studied the heat transfer in the helical coil by using supercritical CO2 as the working fluid. In addition, the experiment was studied based on exergy analysis. Different parameters such as the diameter of the tube, heat flux, and mass flux were examined to determine their effects on dimensionless exergy destruction. Thus, results delineate that dimensionless

exergy losses caused by flow friction are quite less than the dimensionless exergy destruction due to the irreversibilities of heat transfer.

2.2.2 Outer Nusselt number of helical coils

Considerable work has been done on the inner heat transfer coefficient of the helical coil but the same trend is not observed for outer heat transfer coefficients. Ali [16] experimented by submersing a vertical coil in the water and flowing hot water through the helical coil. Furthermore, external heat transfer coefficients were calculated and correlations were developed between the Nusselt number and Rayleigh number. Co relations were devised by taking height and length as the characteristic length.

$$\boldsymbol{Nu_L = 0.685\ (Ra_L)^{0.295}} \quad \textbf{(6)}$$

d_o = 0.012m, $3 \times 10^{12} \leq Ra_L \leq 8 \times 10^{14}$

$$\boldsymbol{Nu_L = 0.00044\ (Ra_L)^{0.516}} \quad \textbf{(7)}$$

d_o = 0.008m, $6 \times 10^{11} \leq Ra_L \leq 1 \times 10^{14}$

$$\boldsymbol{Nu_H = 0.257\ (Ra_H)^{0.323}} \quad \textbf{(8)}$$

d_o = 0.012m, $6 \times 10^{8} \leq Ra_H \leq 3 \times 10^{11}$

Furthermore, studies were carried out on heat transfer by steady-state natural convection [17]. Coiled tubes of various curvature ratios and number of turns were submerged in oil. Subsequently, based on heat transfer data and by using coil length as a characteristic length, numerous correlations were developed. Finally, a general correlation was formulated based on the present and past research heat transfer data.

$$\mathbf{Nu_L = 0.287\ (Ra_L)^{0.323}} \quad \textbf{(9)}$$

δ = 0.03, $7.35 \times 10^{11} \leq Ra_L \leq 5.5 \times 10^{14}$

$$\mathbf{Nu_L = 1.733\ (Ra_L)^{0.264}} \quad \textbf{(10)}$$

δ = 0.01, $4.37 \times 10^{10} \leq Ra_L \leq 2.24 \times 10^{13}$

$$\mathbf{Nu_L = 0.714\ (Ra_L)^{0.294}} \quad \textbf{(11)}$$

$4.35 \times 10^{10} \leq Ra_L \leq 8.0 \times 10^{14}$

Fernandez & Seara [3] did a thermal analysis of a coil submerged in a domestic water storage tank. Two experimental arrangements were investigated. In the initial configuration, the coil was placed at the bottom of the tank, and in the second configuration, the coil was placed at the top of the tank. Results were extracted from the experimental setup and co-relations were developed by considering the diameter of the pipe, length of the tube, and coil height as characteristic length.

$$\boldsymbol{Nu_{do} = 0.4998\ (Ra_{do})^{0.2633}} \quad \textbf{(12)}$$

$4.67 \times 10^6 \leq Ra_{do} \leq 3.54 \times 10^7$

$$\boldsymbol{Nu_{L} = 1.709\ (Ra_{L})^{0.2633}} \quad \textbf{(13)}$$

$1.97 \times 10^{14} \leq Ra_{L} \leq 1.49 \times 10^{15}$

$$\boldsymbol{Nu_{H} = 0.818\ (Ra_{H})^{0.2633}} \quad \textbf{(14)}$$

$5.31 \times 10^9 \leq Ra_{H} \leq 4.02 \times 10^{10}$

Thermal stratification of hot water in the storage has been studied experimentally [18]. Data were extracted for tanks with different aspect ratios, mass flow rates. Effects of different configurations of inlet and outlet on the thermal stratification were also investigated. Finally, the data were correlated to propose a relation for the design of an optimized hot water-based thermal energy storage tank.

The whole purpose of thermal stratification is to prevent mixing during the dynamic as well as the static condition of the tank. Different models were studied in the paper [19], and different geometrical parameters of the tank were studied. And a survey was done in order to study the performance improvement of different methods and how performance was quantified.

A studied was carried out to determine the major factors which affect the performance of stratified thermal energy storage systems [20]. The aspect ratio of the tank, inlet velocity, and temperature difference between inlet of hot fluid and water were taken into consideration. Results were deduced that thermal stratification improves by lowering inlet velocities and with increased temperature differences.

2.2.3 Characteristics of coil

Figure 2-1 represents the basic geometry of the helical pipe. The inner diameter of the pipe is di and the outer diameter of the pipe is do. Similarly, the diameter of the coil is D_c, which is measured from the center of the pipe. The diameter of the coil is also known as pitch circle diameter (PCD). If the coil is being projected, the angle made by the turn of the coil with respect to the plane perpendicular to the axis of the coil is known as the helical angle, α.

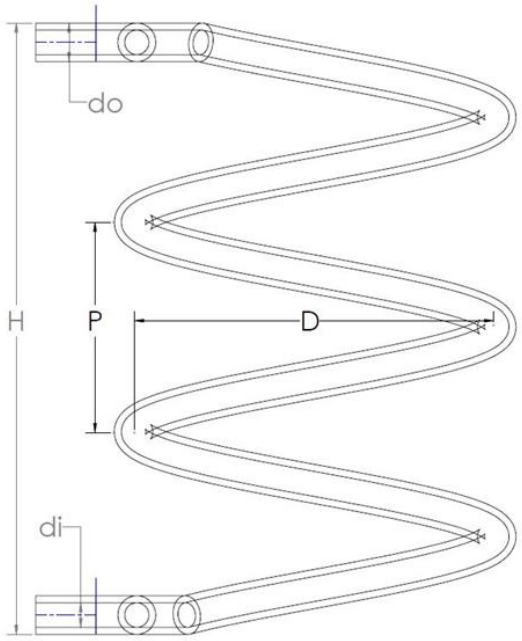

Figure 2-1 Geometry of helical pipe

Furthermore, the gap between two consecutive turns of the coil is called pitch, P. Lastly, the Ratio of pipe internal diameter to coil diameter is known as the inner curvature ratio, δ_i. And, the ratio of pipe external diameter to coil diameter is known as the outer curvature ratio, δ_o.

2.3 Dimensionless numbers

As Reynolds number is mainly used for the study of fluid flow in straight pipes, Dean number is applicable for the study of fluid flow in curved channels and pipes. Dean number is defined as,

$$\boldsymbol{De = Re\sqrt{\frac{d_i}{D}}} \quad \textbf{(15)}$$

While, Reynolds number is, $\boldsymbol{Re = \frac{\rho v L_c}{\mu}}$

Researchers have already identified better heat transfer in coils due to complex flow patterns. The effects of centrifugal forces on the fluid depending upon the curvature of the coil, while torsional effects on the fluid are governed by the helix angle or the pitch of the coil. Moreover, the transition from laminar to turbulent flow in a coil is not the same as the transition of the hydrodynamic nature of the fluid in a straight pipe. So, the critical Reynolds number of a coil is not similar to a straight pipe, hence, it depends on the geometric parameters. Schmidt [10] advised a correlation for determining the critical Reynolds number of the coil.

$$\boldsymbol{Re_{cr} = 2300\left[1 + 8.6\left(\frac{r_i}{R_c}\right)^{0.45}\right]} \quad \textbf{(16)}$$

Due to complex flow patterns, the determination of the hydrodynamic nature of working fluid in the helical coils is different from straight pipes, so more work is done to sort out this problem. Hence, based on experimental results and considering the effects of curvature ratio on fluid flow, Mujawar et al. [21]deduced a new dimensionless number 'M'. Lastly, criteria were also derived to determine lamina flow in a coil with any curvature ratio.

$$\boldsymbol{M = \frac{Re^{0.64}}{0.26\left(\frac{r_i}{R_c}\right)^{0.18}} \leq 2100} \quad \textbf{(17)}$$

In heat transfer problems and applications another dimensionless number that have great significance is the Prandtl number. It is the ratio of momentum diffusivity and thermal diffusivity [22].

$$\boldsymbol{Pr = \frac{\nu}{\alpha}} \quad \textbf{(18)}$$

This dimensionless number does not contain any length scale, instead, it is a number that relied on the fluid and its state. When Pr values are very small (Pr << 1) it means thermal diffusivity is dominant in the working fluid, and in the case of very large values (Pr >> 1) momentum diffusivity is the dominant behavior.

In the field of fluid mechanics, a dimensionless number related to natural convection (or buoyancy-driven flow) is Rayleigh's number. Arithmetically, it is defined as the product of Grashof number and Prandtl number. In the same way, it can also be interpreted as the ratio of buoyancy forces and viscosity forces multiplied by the ratio of momentum diffusivity and thermal diffusivity.

$$\boldsymbol{Ra} = \frac{\boldsymbol{g\beta {L_c}^3 (T_s - T_w)}}{\boldsymbol{\nu\alpha}} \quad \textbf{(19)}$$

2.4 Numerical modelling

Numerical methods are defined by John D. Anderson as:

"CFD is the skill, which replaces the governing partial differential equations of fluid flow with numbers and then these numbers in space and/or time is used to get the whole flow field of the analysis. The final result of CFD is just a combination of numbers[23]*"*

This part of the chapter presents the governing equations with numerical approximation according to the current research. The fluid motion can be completely described by the partial differential equations for the conservation of mass, energy, and momentum in fluid flows. These equations are combinedly referred to as Navier-Stokes equations. These equations describe continuum fluid flow, which is explained by the classic work of Schlichting [24]. Considered Continuum, meaning that flow quantities such as pressure and temperature are approximately uniform within fluid elements [25]. The set of equations is known as the compressible Navier Stokes equations:

Continuity equation [26]:

$$\frac{\partial \boldsymbol{U}}{\partial \boldsymbol{x}} + \frac{\partial \boldsymbol{V}}{\partial \boldsymbol{y}} + \frac{\partial \boldsymbol{W}}{\partial \boldsymbol{z}} = \boldsymbol{0} \quad \textbf{(20)}$$

x- Momentum [26]:

$$\frac{\partial \boldsymbol{U}}{\partial \boldsymbol{t}} + \boldsymbol{U}\frac{\partial \boldsymbol{U}}{\partial \boldsymbol{x}} + \boldsymbol{V}\frac{\partial \boldsymbol{U}}{\partial \boldsymbol{y}} + \boldsymbol{W}\frac{\partial \boldsymbol{U}}{\partial \boldsymbol{z}} = \boldsymbol{\nu}\left(\frac{\partial^2 \boldsymbol{U}}{\partial \boldsymbol{x}^2} + \frac{\partial^2 \boldsymbol{U}}{\partial \boldsymbol{y}^2} + \frac{\partial^2 \boldsymbol{U}}{\partial \boldsymbol{z}^2}\right) - \frac{\partial \boldsymbol{P}}{\partial \boldsymbol{x}}\frac{\boldsymbol{1}}{\boldsymbol{\rho}} \quad \textbf{(21)}$$

y- Momentum:

$$\frac{\partial \boldsymbol{V}}{\partial \boldsymbol{t}} + \boldsymbol{U}\frac{\partial \boldsymbol{V}}{\partial \boldsymbol{x}} + \boldsymbol{V}\frac{\partial \boldsymbol{V}}{\partial \boldsymbol{y}} + \boldsymbol{W}\frac{\partial \boldsymbol{V}}{\partial \boldsymbol{z}} = \boldsymbol{\beta g(T - T_o)} + \boldsymbol{\nu}\left(\frac{\partial^2 \boldsymbol{V}}{\partial \boldsymbol{x}^2} + \frac{\partial^2 \boldsymbol{V}}{\partial \boldsymbol{y}^2} + \frac{\partial^2 \boldsymbol{V}}{\partial \boldsymbol{z}^2}\right) - \frac{\partial \boldsymbol{P}}{\partial \boldsymbol{y}}\frac{\boldsymbol{1}}{\boldsymbol{\rho}} \quad \textbf{(22)}$$

z- Momentum:

$$\frac{\partial W}{\partial t} + U\frac{\partial W}{\partial x} + V\frac{\partial W}{\partial y} + W\frac{\partial W}{\partial z} = \nu\left(\frac{\partial^2 W}{\partial x^2} + \frac{\partial^2 W}{\partial y^2} + \frac{\partial^2 W}{\partial z^2}\right) - \frac{\partial P}{\partial z}\frac{1}{\rho} \quad (23)$$

Energy Equation [26]:

$$\frac{\partial T}{\partial t} + U\frac{\partial T}{\partial x} + V\frac{\partial T}{\partial y} + W\frac{\partial T}{\partial z} = \alpha\left(\frac{\partial^2 T}{\partial x^2} + \frac{\partial^2 T}{\partial y^2} + \frac{\partial^2 T}{\partial z^2}\right) \quad (24)$$

Equation (20) presents the conservation of mass, while the equation (21-24) represents the momentum conservation of the fluid volume.

2.5 Boussinesq Model

The Boussinesq approximation is used in the field of fluid dynamics. This method is normally used for free convection where buoyancy effects come into play. It ignores any change in the density, besides where it comes in multiples of g [27]. It caters to the change in density just in the buoyancy term of the momentum equation. The purpose of using this model is that it leads to quick convergence as compared to simulations in which fluid density is used as a function of temperature.

$$(\rho - \rho_0)g \approx -\rho_0\beta(T - T_0)g \quad (25)$$

β is a thermal expansion coefficient. Boussinesq approximation holds true when changes in density are small. It is valid when $\beta(T-T_0) << 1$.

In this research work a CFD based analysis is carried out to validate a downsized model with the experimental data. Furthermore, new models are to be created by varying their geometric parameters, and simulated further on different boundary conditions. Later, mathematical corelations for inner and outer Nusselt numbers are to be deduced and further validated with the past studies to determine its authenticity. Lastly, the relationship between different geometric parameters and heat transfer coefficient of the helical coil is to be established.

Summary

The chapter 2 includes the details of literature review related to the past research done on helical coil-based heat exchangers. Studies done on heat exchangers of different configurations and orientation are discussed in this chapter. Furthermore, this chapter includes the details of mathematical correlations derived in past for inner and outer Nusselt numbers. This chapter also elaborates the unique characteristic of helical coil and its effects on the flowing fluid. Moreover, details of unique dimensionless number used for the helical coils are also discussed. Lastly, use of Boussinesq equation model for determining the effects of free convection is explored in this chapter.

References

[1] S.R. Shakeel, J. Takala, W. Shakeel, Renewable energy sources in power generation in Pakistan, Renew. Sustain. Energy Rev. 64 (2016) 421–434. https://doi.org/10.1016/j.rser.2016.06.016.

[2] N.D. Shirgire, Review on Comparative Study between Helical Coil and Straight Tube Heat Exchanger, IOSR J. Mech. Civ. Eng. 8 (2013) 55–59. https://doi.org/10.9790/1684-0825559.

[3] J. Fernández-Seara, F.J. Uhía, J. Sieres, Experimental analysis of a domestic electric hot water storage tank. Part II: dynamic mode of operation, Appl. Therm. Eng. 27 (2007) 137–144. https://doi.org/10.1016/j.applthermaleng.2006.05.004.

[4] R.C. Xin, M.A. Ebadian, Natural convection heat transfer from helicoidal pipes, J. Thermophys. Heat Transf. 10 (1996) 297–302. https://doi.org/10.2514/3.787.

[5] M.A. Abdalla, A four-region, moving-boundary model of a once-through, helical-coil steam generator, Ann. Nucl. Energy. 21 (1994) 541–562. https://doi.org/10.1016/0306-4549(94)90078-7.

[6] D.G. Prabhanjan, T.J. Rennie, G.S.V. Raghavan, Natural convection heat transfer from helical coiled tubes, Int. J. Therm. Sci. 43 (2004) 359–365. https://doi.org/10.1016/j.ijthermalsci.2003.08.005.

[7] Handbook of single-phase convective heat transfer|INIS, (1987). https://inis.iaea.org/Search/search.aspx?orig_q=RN:18090434.

[8] J.H. Masliyah, Bifurcation in steady laminar flow through curved tubes, J. Fluid Mech. 119 (1982) 475–490.

[9] R. Maradona, S. Rajkumar, CFD Analysis of Heat Transfer Characteristics of Helical Coil Heat Exchangers, Appl. Mech. Mater. 787 (2015) 172–176. https://doi.org/10.4028/www.scientific.net/amm.787.172.

[10] E.F. Schmidt, Wärmeübergang und Druckverlust in Rohrschlangen, Chemie Ing.

Tech. 39 (1967) 781–789. https://doi.org/10.1002/cite.330391302.

[11] R.C. Xin, M.A. Ebadian, The effects of Prandtl numbers on local and average convective heat transfer characteristics in helical pipes, J. Heat Transfer. 119 (1997) 467–473. https://doi.org/10.1115/1.2824120.

[12] J.S. Jayakumar, S.M. Mahajani, J.C. Mandal, P.K. Vijayan, R. Bhoi, Experimental and CFD estimation of heat transfer in helically coiled heat exchangers, Chem. Eng. Res. Des. 86 (2008) 221–232. https://doi.org/10.1016/j.cherd.2007.10.021.

[13] J.S. Jayakumar, S.M. Mahajani, J.C. Mandal, K.N. Iyer, P.K. Vijayan, CFD analysis of single-phase flows inside helically coiled tubes, Comput. Chem. Eng. 34 (2010) 430–446. https://doi.org/10.1016/j.compchemeng.2009.11.008.

[14] M. Mahmoudi, M.R. Tavakoli, M.A. Mirsoleimani, A. Gholami, M.R. Salimpour, Étude expérimentale et numérique du transfert de chaleur par convection forcée et de la chute de pression dans des canalisations enroulées en hélice utilisant le nanofluide TiO2/eau, Int. J. Refrig. 74 (2017) 625–641. https://doi.org/10.1016/j.ijrefrig.2016.11.014.

[15] X. Xu, Y. Zhang, C. Liu, S. Zhang, C. Dang, Experimental investigation of heat transfer of supercritical CO2 cooled in helically coiled tubes based on exergy analysis, Int. J. Refrig. 89 (2018) 177–185. https://doi.org/10.1016/j.ijrefrig.2018.03.011.

[16] M.E. Ali, Experimental investigation of natural convection from vertical helical coiled tubes, Int. J. Heat Mass Transf. 37 (1994) 665–671. https://doi.org/10.1016/0017-9310(94)90138-4.

[17] M.E. Ali, Natural convection heat transfer from vertical helical coils in oil, Heat Transf. Eng. 27 (2006) 79–85. https://doi.org/10.1080/01457630500458617.

[18] Z. Lavan, J. Thompson, Experimental study of thermally stratified hot water storage tanks, Sol. Energy. 19 (1976).

[19] Y.P. Chandra, T. Matuska, Stratification analysis of domestic hot water storage tanks: A comprehensive review, Energy Build. 187 (2019) 110–131. https://doi.org/10.1016/J.ENBUILD.2019.01.052.

[20] A. Karim, A. Burnett, S. Fawzia, Investigation of Stratified Thermal Storage Tank Performance for Heating and Cooling Applications, Energies 2018, Vol. 11, Page 1049. 11 (2018) 1049. https://doi.org/10.3390/EN11051049.

[21] B.A. Mujawar, M. Raja Rao, Flow of Non-Newtonian Fluids through Helical Coils, Ind. Eng. Chem. Process Des. Dev. 17 (1978) 22. https://pubs.acs.org/sharingguidelines.

[22] J.M. Richardson, J.F. Coulson, Chemical Engineering Vol. 1 - Fluid Flow, Heat and Mass Transfer (1999).pdf, 1999.

[23] A. Stein, S. Niazi, L.N. Sankar, Computational Analysis of Stall and Separation Control in Centrifugal Compressors, Https://Doi.Org/10.2514/2.5532. 16 (2012) 65–71. https://doi.org/10.2514/2.5532.

[24] H.W. Coleman, B.K. Hodge, R.P. Taylor, A Re-Evaluation of Schlichting's Surface Roughness Experiment, J. Fluids Eng. 106 (1984) 60–65. https://doi.org/10.1115/1.3242406.

[25] E. Sundstrom, Flow instabilities in centrifugal compressors at low mass flow rate, Department of Mechanics, Royal Institute of Technology, SE-100 44 Stockholm, Sweden, 2017.

[26] M.M.U. Rehman, T.A. Cheema, F. Ahmad, M. Khan, A. Abbas, Thermodynamic assessment of microchannel heat sinks with novel sidewall ribs, J. Thermophys. Heat Transf. 34 (2020) 243–254. https://doi.org/10.2514/1.T5770.

[27] D.J. Tritton, Physical fluid dynamics, Clarendon Press, 1988.

Chapter 3: Methodology & Experimental Setup

3.1 Research methodology

This chapter will mainly cover the step-by-step research methodology followed during the research. As shown in Figure 3-1, first a comprehensive literature review was conducted.

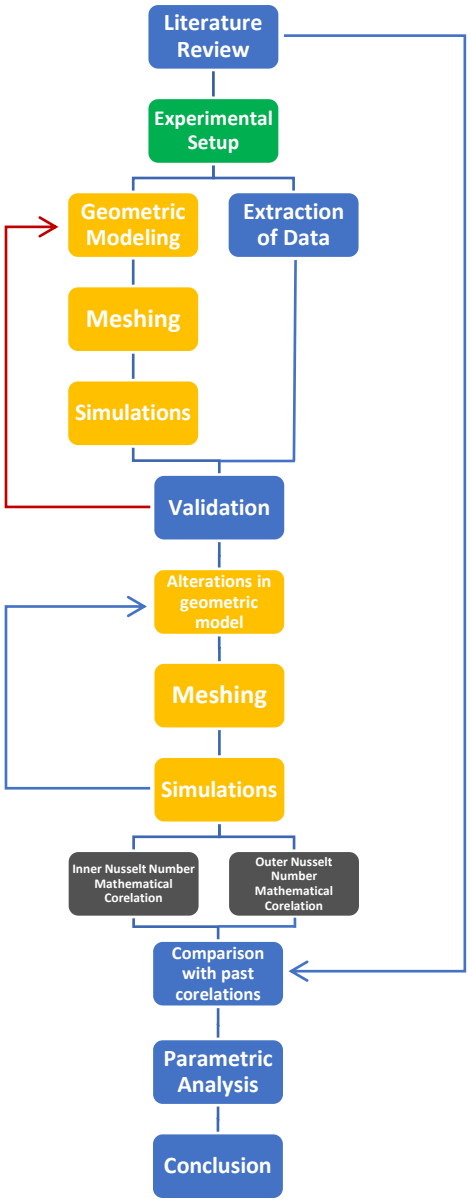

Figure 3-1 Flow sheet diagram of research methodology

In the next section, the experimental setup and procedure of experimentation are illustrated. Afterward, the system under consideration was modelled and its CFD-based analysis is carried out followed by the comparison of simulated data with experimental results. Subsequently, after validation of the CFD model, geometric alternations were performed on the model and the new model was further passed through a grid independence test. Later, more simulations were executed and co-relations for internal and external heat transfer coefficients were devised from the extracted data. Lastly, these co-relations were compared with relations present in past papers, and their percentage errors were also calculated. No considerable work was done in the past that shows transient state CFD-based simulations were carried on the tank, where 50% water-glycol solution in the coil is dynamic and water inside the tank is in static flow condition, while the only changes inside the tank are due to natural convection. Lastly, thermal stratification analysis of the tank was studied and observed results were registered.

3.2 Experimental setup & procedure

3.2.1 Experimental setup

The whole setup investigated in this study consist of a evacuated flat plate solar collector coupled with a thermal energy storage tank, both were connected through PVC pipes. The whole system is set up on the rooftop of the United States Pakistan Centre of Advanced Study in Energy, NUST Islamabad, Pakistan. Experimentations were carried out at the end of January and the start of February. The schematic and the physical experimental setup can be seen in Figures 3-2 & 3-3.

Two TS-400 type evacuated flat plate solar collectors are used in this experimental setup, both collectors are connected in series. Specifications of the solar collector are in Table 3-1. A 100 Ltr water tank with an aspect ratio of 3 is used as a thermal energy storage medium. 50/50% water-glycol solution is used as a working fluid that absorbs solar radiation in the solar collector and then passes the thermal energy to the water inside the tank, copper-based helical coil heat exchanger is used for this purpose which is enclosed inside the tank

Table 3-1 Specifications of TS-400

TS-400 Specifications	
Cover glass	4mm safety solar ESG white glass
Absorber Tube	Cu 10 x 0.5 mm
Casing	Non-corrosive AL Mg sheet
Thermal Insulation	0.8 bar
Liquid Capacity	1.6 Ltrs
Heat Transfer Fluid	Water - Glycol
Mix ratio	50 / 50 %
Flow rate	120 - 180 Lh^{-1}
Gross area	2.031 m^2
Absorber area	1.7 m^2
Tilt angle	30°
Surface azimuth angle	0°
Longitude and latitude	33.64215° N, 72.98441° E

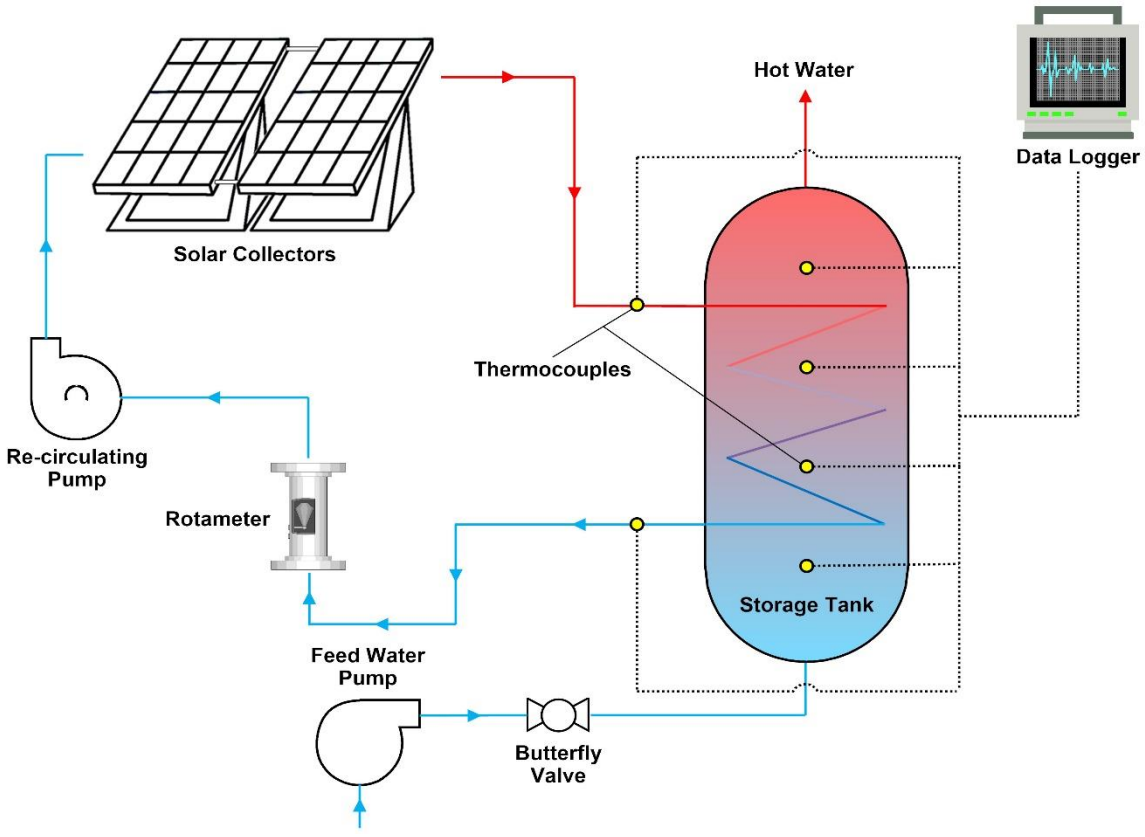

Figure 3-2 Schematic of experimental setup

Table 3-2 Specifications of coil

Coil Specifications	
Inner Diameter (d_i) (mm)	17.65
Outer Diameter (d_o) (mm)	19.05
Thickness (mm)	0.7
Coil Diameter (D) (mm)	260
Curvature Ratio (δ) (mm)	0.0679
Internal Surface Area (m^2)	0.6317
External Surface Area (m^2)	0.6568
Length of Coil (m)	11.4

Figure 3-3 Experimental setup

Six PT-1000 type thermocouples were integrated into the whole experimental setup. One thermocouple at the inlet and exit of the storage tank. Whereas, the remaining four were placed at regular intervals from the bottom of the storage tank, to investigate the thermal stratification inside the tank. All of the thermocouples were integrated with a data logger that stores data at a regular 1-second interval. The storage tank mentioned is made up of galvanized steel and is further padded with a 50 mm thick sheet of glass wool to prevent heat losses. Figure 3-4 illustrates the whole configuration of the storage tank. While

detailed drawing of the parts and assembly of the storage tank was created on Solidworks® 2018, and is available in Appendix 1,2,3.

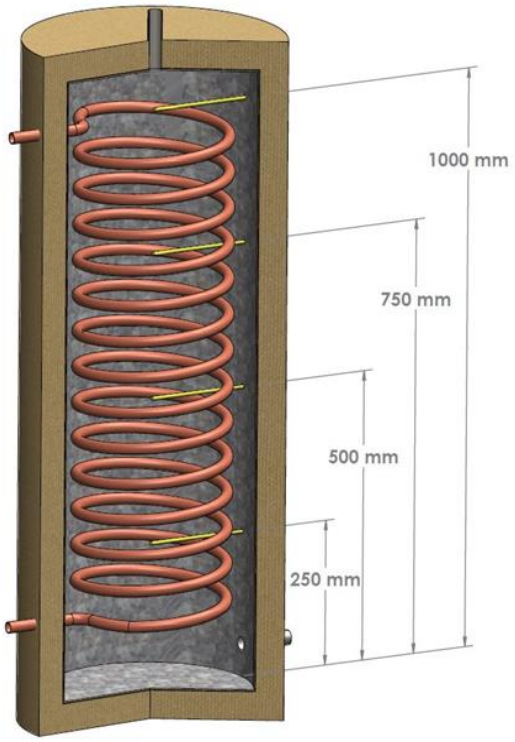

Figure 3-4 Model of storage tank

3.2.2 Experimental procedure

Initially, freshwater was added inside the tank, and it was ensured that the whole tank is at a uniform temperature. Later on, experimentation was carried out with two volume flow rates; 2 LPM and 3 LPM. Measurements with 2 LPM were carried on 27th January, while with 3 LPM were carried on 28th January. During each experiment, the flow rate of glycol solution remains constant and water remains at static flow condition. Both of the experiments were carried out for 65 minutes and the temperature inside the tank was measured at the end. Hot glycol solution was flown through the storage tank for 60 minutes and then stopped for 5 minutes so that water maintains a stable thermal stratification inside the tank, therefore the final reading of the tank was taken at the end of 65 minutes. During the whole experimentation, the tank's external surface temperature was measured at regular intervals so that the mean surface temperature could be determined.

Additional experimentation was also carried on 9th February with a flow rate of 2 LPM for 25 minutes. Results of this experiment were used as a source for determining the grid dependency of the CFD model.

Summary

This chapter includes the details and flow chart of the whole research methodology, and the strategy adopted to perform this study. Furthermore, the specification of the whole experimental setup is elaborated. Dimensions of the coil and storage tank with flow rates are also detailed in this chapter. Later on, experimental procedure acquired to extract the data is also discussed.

Chapter 4: CFD Modelling & Simulation

All the simulations were executed on the commercial version of FLUENT® 19.1. Numerous case scenarios for various Reynolds numbers in the laminar flow regime were simulated. Additionally, governing equations of mass, momentum, and energy, were simulated in double-precision, and 3D version methods using parallel processing.

4.1 CFD modelling & simulation

Two basic models were created to validate it with the experimental results. Both models were created in ANSYS® 19.1 Design modeler. Model-II is the duplicate of the storage tank as seen in the experimental setup Figure 3-3, while model-I is the symmetrical downsized version of the original tank. Model-I tank volume is half the size of the original tank (50 Ltr), and the length of the coil is also reduced to half.

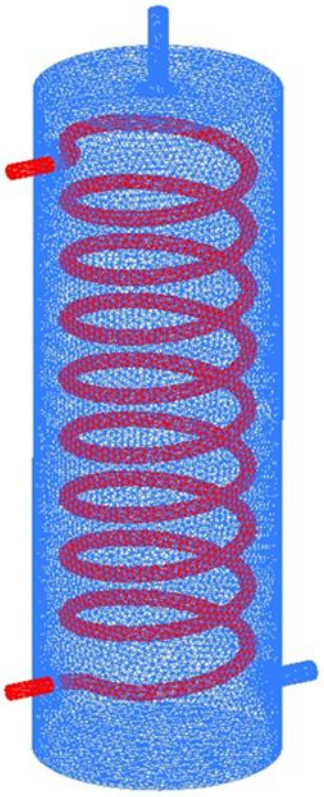

Figure 4-1 Computational domain

However, the aspect ratio of both tank and coil is kept constant, even though, the internal diameter and thickness of the pipe in both cases are similar. Moreover, the distance between the top of the coil at the inlet, and the upper boundary of the tank is reduced in

symmetry with the original dimension of the tank. Likewise, the gap between the bottom of the coil at the outlet and the lower boundary of the tank was also adjusted. Figure 4-1 illustrates the coiled pipe, storage tank, and the complete computational domain for the case study.

4.1.1 Boundary conditions

Coiled pipe having a thickness of 0.7 mm was not modelled in the design modeler, but its effects are catered in the examination by using the shell conduction model of Fluent. This results in the reduction of mesh elements and computation time. The interface between the hot fluid and water is thermally coupled considering a conjugate heat transfer. Forced convection between the fluid and the pipe, conductive heat transfer within the pipe, and natural convection between the pipe and water in the tank. A no-slip condition is applied for the flowing fluid.

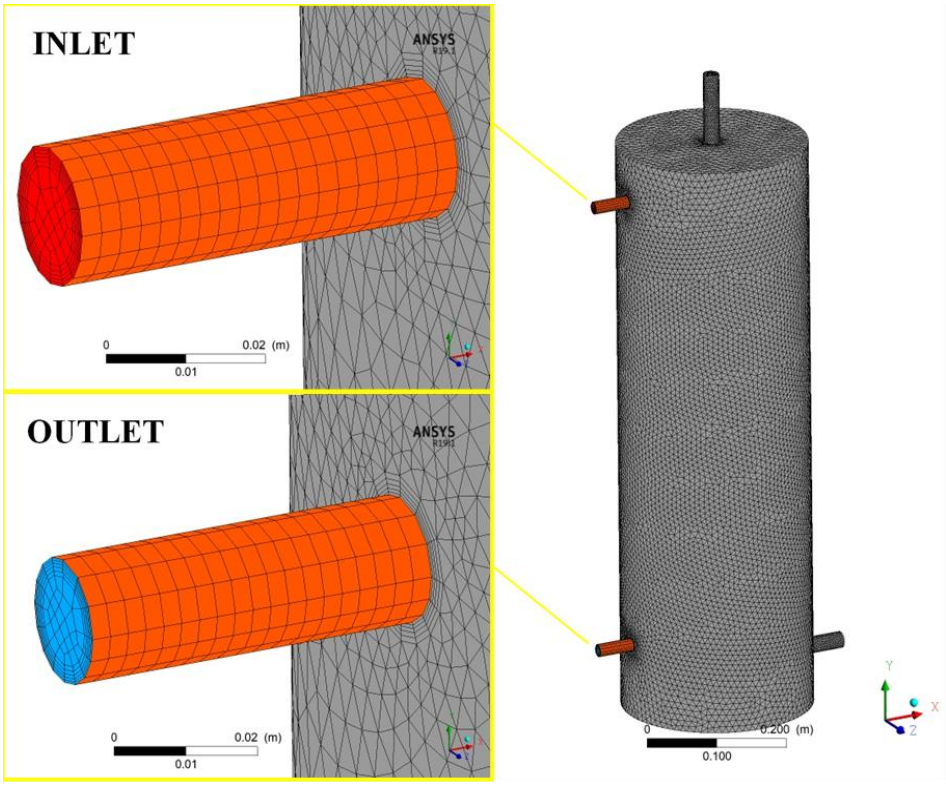

Figure 4-2 Inlet & outlet of coil, and grid of the storage tank used for analysis

The material of the coil is copper having properties; thermal conductivity = 387.6 W/m.K, density = 8978 kg/m^3, and specific heat = 381 J/kg.K. The wall of the tank is steel with

properties; thermal conductivity = 502.48 W/m.K, density = 8030 kg/m^3, and specific heat = 16.27 J/kg.K. Furthermore, 50 mm glass wool padding on the tank wall having thermal conductivity 0.0315 W/m.K, density = 50 kg/m^3, and specific heat = 840 J/kg.K. Both steel wall and glass wool thickness were specified through the shell conduction model. Additionally, a constant mean temperature was applied at the outer surface of the glass wool, measured during the experimentation. Hot fluid enters from the top of the coil taken as mass flow inlet boundary condition and cold fluid leaves from the bottom of the coil specified as an outflow boundary condition. See Figure 4-2. As the hot fluid flowing through the storage tank comes from the solar collector, the temperature at the inlet of the tank is not constant. The temperature of hot glycol solution changes with the amount of solar radiation captured by the solar collector.

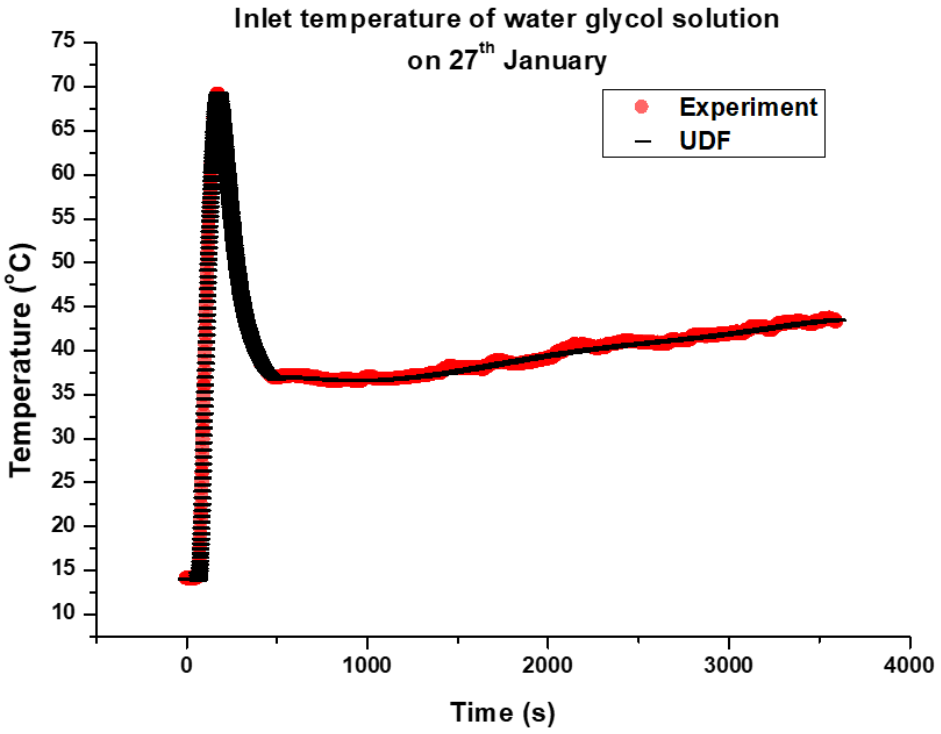

Figure 4-3 Comparison between experimental values and UDF generated values

To simulate a similar boundary condition, UDF was coded in C language for each case scenario that determines the temperature of water-glycol at the inlet of the storage tank. See appendix 4,5 & 6. The comparison between the experimental values of temperature and UDF generated temperature values, of the inlet glycol, on different dates are shown in Figure 4-3,4-4 & 4-5.

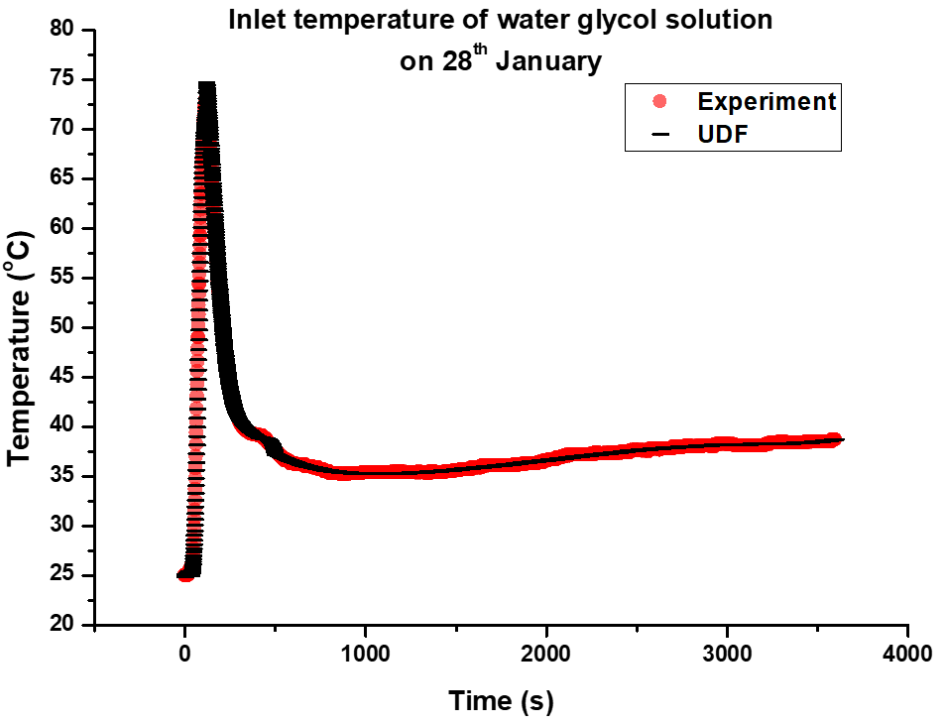

Figure 4-4 Comparison between experimental values and UDF generated values

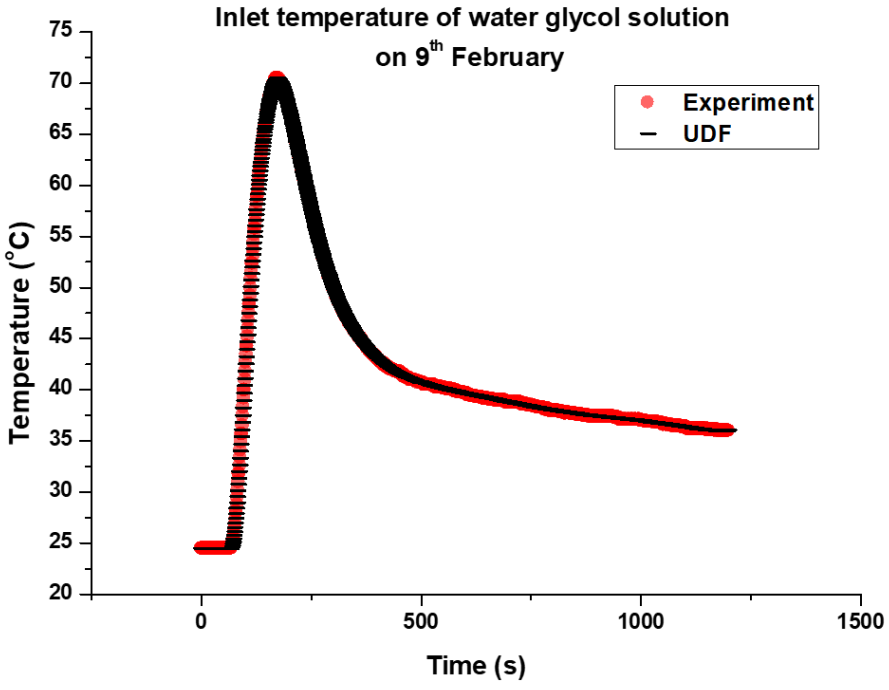

Figure 4-5 Comparison between experimental values and UDF generated values

4.1.2 Determination of density & β of water

For simulating the case scenarios, a water-glycol solution was specified with constant properties. It was deduced by J.S Jayakumar & et al [1], at low Dean number, a hot fluid with similar boundary conditions having constant or temperature-dependent thermal properties results in a similar inner Nusselt number. Properties of water-glycol solution were decided by calculating its mean temperature from the received experimental data. The same methodology was also adopted for deciding the properties of water. However, water inside the tank is in static flow condition, consequently, a phenomenon of natural convection would eventuate due to the rise in temperature of the water with time. To ensure the effects of buoyancy within the tank, Boussinesq approximations are selected for simulating the effects of buoyancy on water inside the tank. So, a numeric value of density and thermal expansion coefficient for water needs to be decided, because both properties changes with temperature.

There are four scenarios with which these values can be determined. The first scenario is initial density/initial thermal expansion coefficient. The value of density and thermal expansion coefficient will be taken at the temperature at which the simulation was initialized. The second scenario, initial density/average thermal expansion coefficient. The value of density will be taken at the temperature at which the simulation was initialized, while the value of the thermal expansion coefficient will be taken at the mean. The third scenario, average density/initial thermal expansion coefficient. A value of density will be taken at a mean temperature. While value thermal expansion coefficient would be taken at the temperature on which the simulation was initialized. The fourth scenario, average density/average thermal expansion coefficient, both the values of density and thermal expansion coefficient will be taken at an average temperature. All of these scenarios, in which the density of water is calculated through the Boussinesq model, are compared with the original values of density of water at different temperatures. As shown in Figure 4-6.

From the below Figure, it can be deduced that case scenario 2 (initial density/average thermal expansion coefficient) is most close to the original values of density. Furthermore, to solve coupling equations for determining pressure and velocity distributions, a SIMPLE

algorithm was used. Second-order upwind was used as a solution method for energy and momentum, while body force weighted was used for pressure [2]. Lastly, an absolute convergence criterion of 10^{-3} is used for continuity and velocities at the x,y, and z-axis, and 10^{-6} for the energy equation.

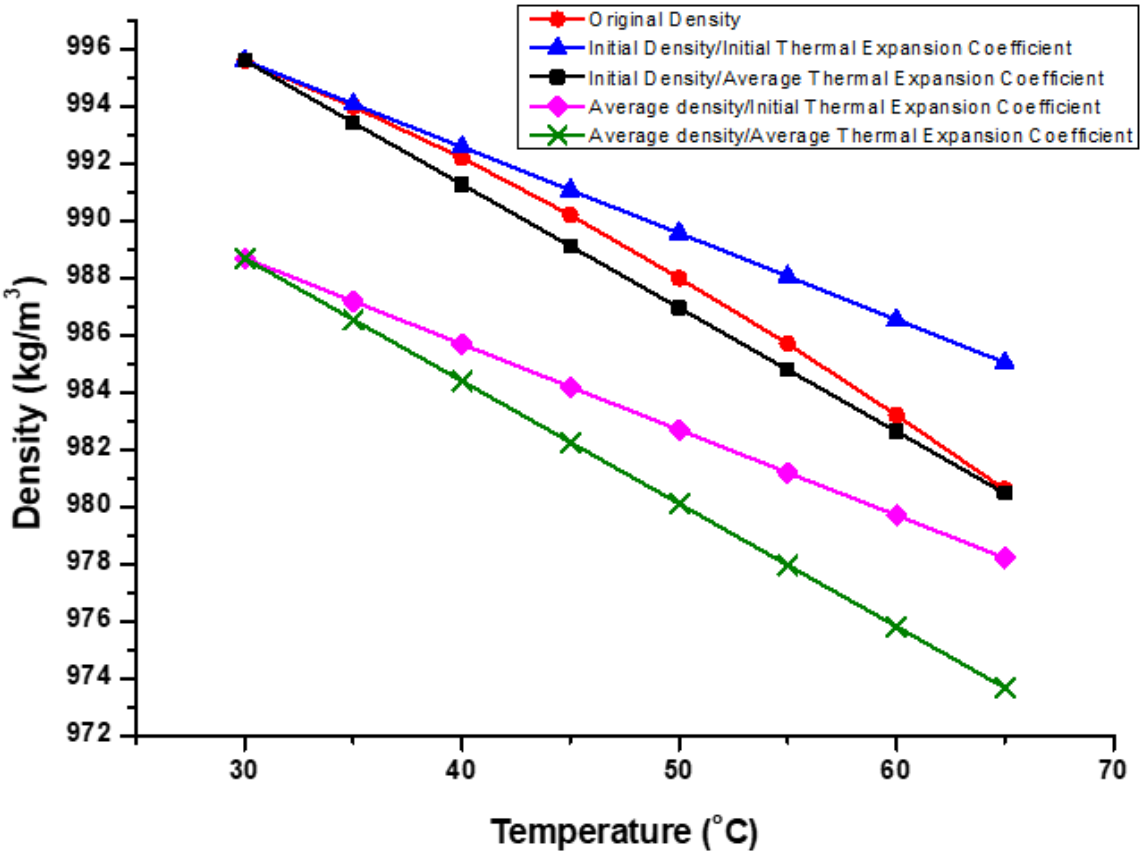

Figure 4-6 Density of water determined through Boussinesq model

4.2 Grid generation

The mesh was generated in the ANSYS® meshing tool. In the model, the structured mesh was generated for the volume of hot fluid, by combining edge sizing techniques with multi-zone methods. For the water domain, the patch conforming method is used. Moreover, inflation is applied on both sides of the interface. As the mesh generated in the tank is dependent on the mesh size of the coil passing through the whole tank, so as the mesh sizing of the coil is changed it affects the number of elements of the tank.

Table 4-1 Models with number of nodes & elements

Model #	Coil		Tank		Total		Flow Time (minutes)	Real Time (hrs)
	Nodes	Elements	Nodes	Elements	Nodes	Elements		
Model-I	258280	239394	534622	2167284	758252	2406678	65	456
Model-II	72993	57868	589168	2605275	632173	2663143	65	456
Model-III	821730	767380	1379171	5222921	2097792	5990301	25	384

Specifications of the meshed model are listed in Table 4-1. Mesh in model-II is coarser, thus, there is no great difference between the number of mesh elements in model-I and model-II as the volume of the tank, and length of the coil in model-II is double. However, model-III is a model with original dimensions and fine mesh. See Figure 4-7.

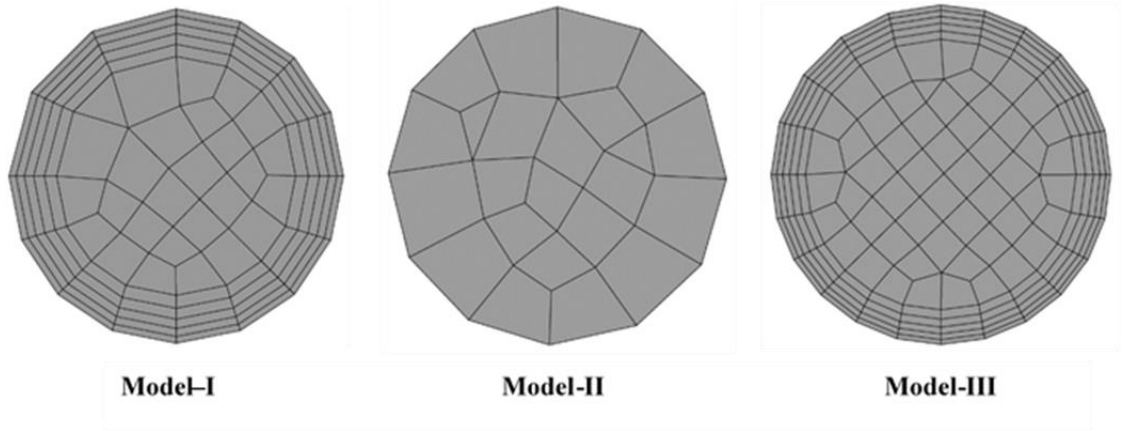

Figure 4-7 Grid of the helical pipe at a cross section

65 minutes of flow time simulation took around 456 hours to complete, for each model-I and model-II. While 25 minutes of simulation on model-III took around 384 hours to complete. Simulations were run on a workstation having specifications of intel, Xenon Gold 2.3 GHz (2 processors) with 32 GB RAM.

Summary

In this chapter the computational domain of the system is discussed in detail. Furthermore, the boundary conditions used for running the simulation are also explained, moreover the variation in the inlet temperature of the glycol from the experimentation is catered by developing a UDF. The comparison between the UDF and experimental data is elaborated in this chapter. Furthermore, use of Boussinesq approximation for determining the buoyancy effects induced in the water, and constant properties of water selected through a certain methodology that shows closest value to the original value of the water is also explained in this chapter. Lastly, the technique adopted for grid generation and comparison of the number of elements and nodes of different models are also discussed.

References

[1] J.S. Jayakumar, S.M. Mahajani, J.C. Mandal, P.K. Vijayan, R. Bhoi, Experimental and CFD estimation of heat transfer in helically coiled heat exchangers, Chem. Eng. Res. Des. 86 (2008) 221–232. https://doi.org/10.1016/j.cherd.2007.10.021.

[2] C. Hochenauer, J. Wurm, Numerical Investigation of Heat Transfer with Thermal Radiation in an Enclosure in Case of Buoyancy Driven Flow, Smart Sci. 2 (2016) 116–125. https://doi.org/10.1080/23080477.2014.11665614.

Chapter 5: Results & Discussions

5.1 Validation of the numerical results with experiment

A numerical model was designed in accordance with the experimental setup to validate its accuracy. All the geometric parameters and boundary conditions were kept similar to the setup, and the initial model simulated was based on 27th January conditions. At 10:50, hot fluid was flown at 2 LPM for 60 minutes and then stopped for 5 minutes so that the tank maintains a stable thermocline. Then, a comparison was drawn between simulated and experimental tank temperature data, as shown in Figure 5-1.

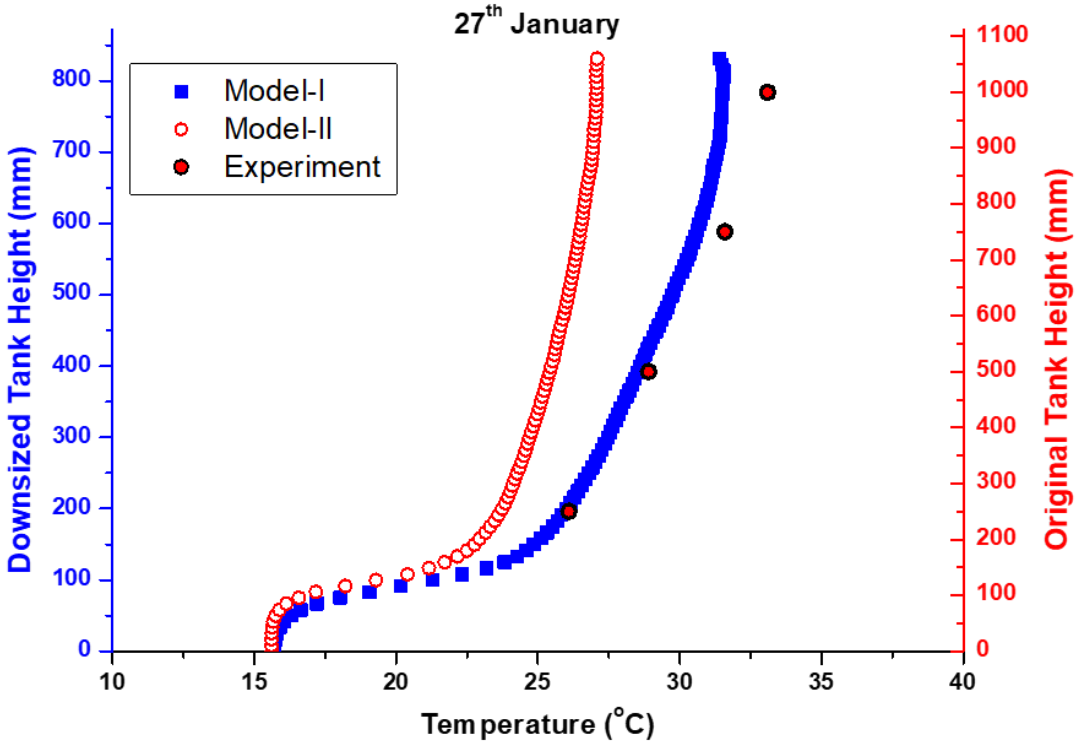

Figure 5-1 Tank temperature profile after 65 minutes on 27th January

A similar geometrical model was simulated for 28th January boundary conditions having a hot fluid volume flow rate of 3 LPM. The experiment started at 14:10 and the results are shown in Figure 5-2. For 27th January conditions, Model-I showed an average percentage error of 2.5%, however, the average percentage error for model-II is 13.93%. For 28th January conditions, Model-I showed an average percentage error of 4.85%, however, the average percentage error for model-II is 17.43%.

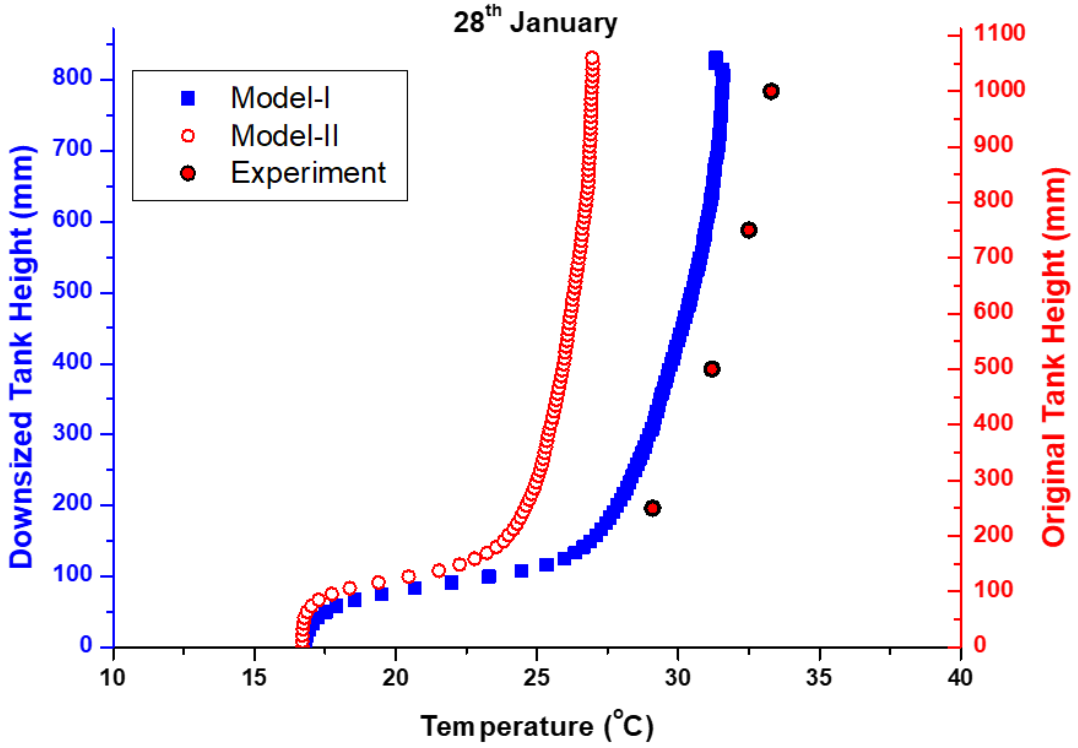

Figure 5-2 Tank temperature profile after 65 minutes on 28th January

Model-II geometric parameters are the replica of the physical tank but its simulation is showing a greater percentage of error as compared to model-I, which is a downsized model with half the volume flow rate. So further simulations were run on model-III, which has the exact geometrical parameters as of model-I but with finer mesh. So, another experiment was conducted on 9th February at 15:14, and results were extracted from the setup. The water-glycol solution was flown at 2 LPM for 20 minutes and then the whole tank was kept static for 5 minutes. Furthermore, simulation was also carried for 25 minutes of flow time. In contrast with the past cases, lesser flow time for this case was due to large computational demand, due to finer mesh. Model-I and Model-II are also simulated on the 9th February boundary condition so a better comparison could be laid out, as shown in Figure 5-3. The average percentage error for model-I is 2.41%, while the average percentage error for model-II is 6.35%. However, the error for model-III is 1.85%, which is the lowest among all other models. Moreover, outlet HTF temperature comparison was drawn between the CFD-based models and experimental data. In the 27th January case, the average percentage error for model-I is 4.93%, while the average percentage error for model-II is 16.65%. The comparison can be observed in Figure 5-4.

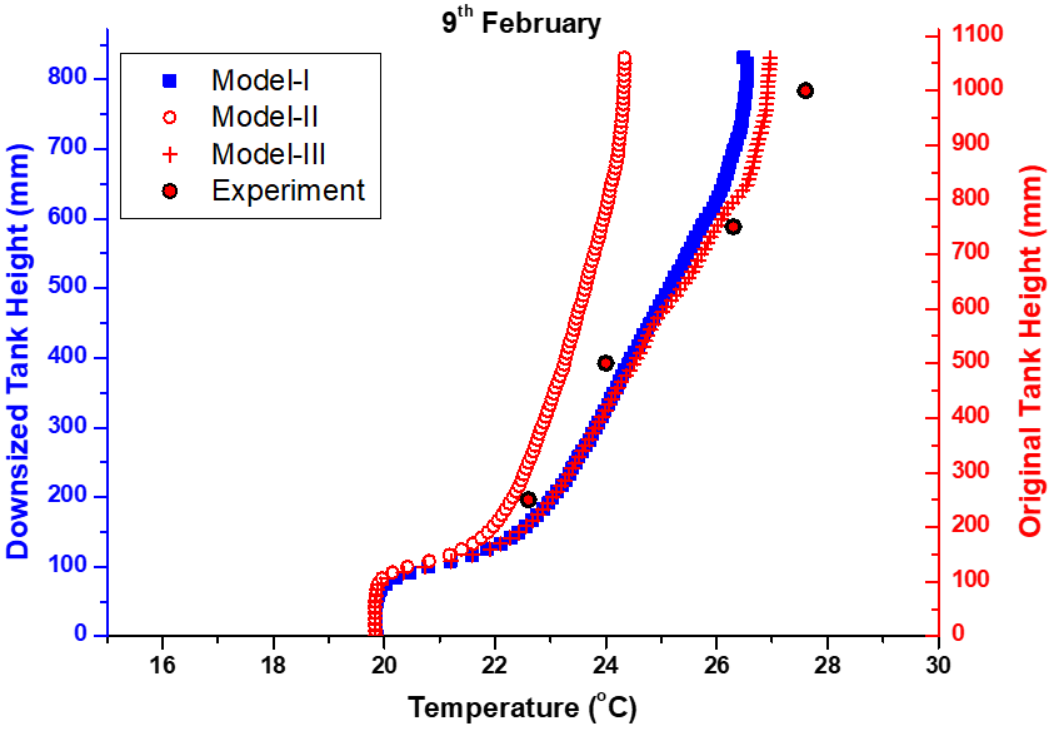

Figure 5-3 Tank temperature profile after 25 minutes on 9th February

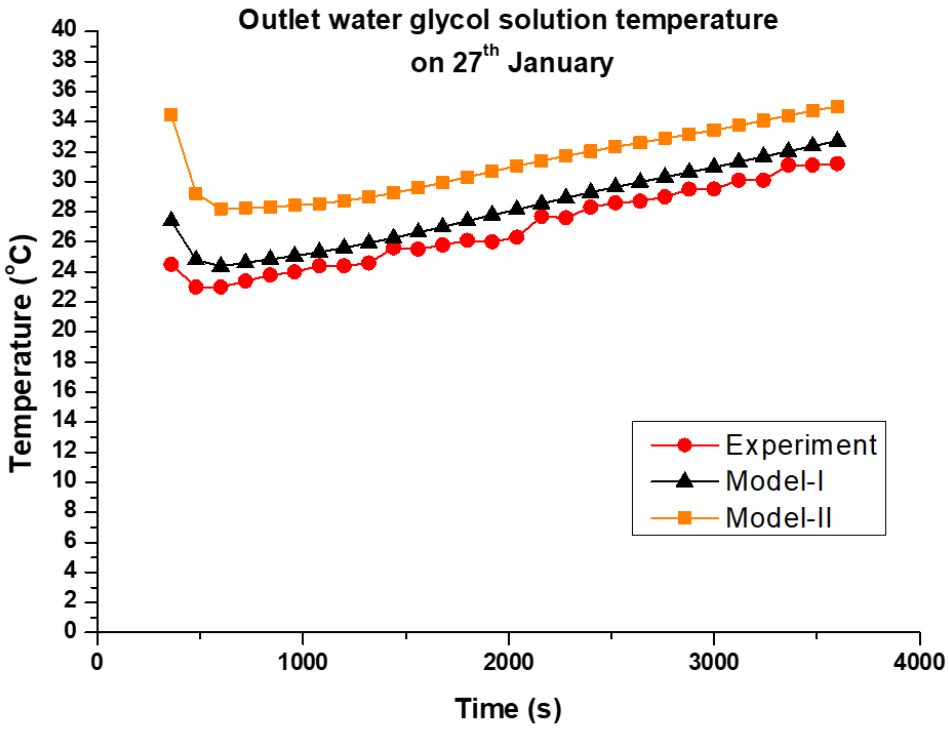

Figure 5-4 Comparison of outlet water glycol solution temperature on 27th January

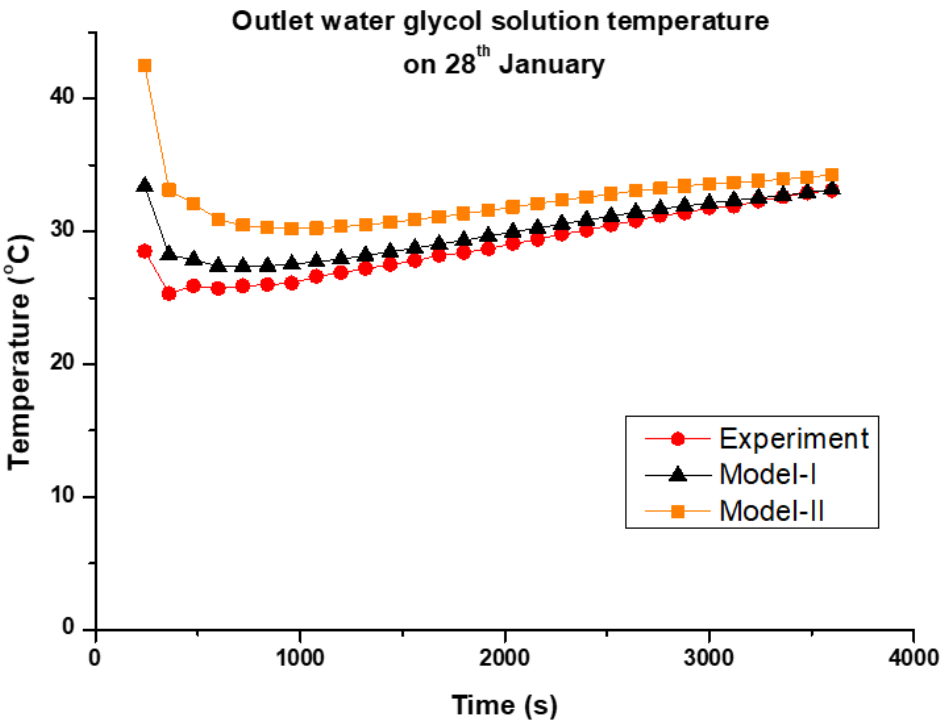

Figure 5-5 Comparison of outlet water glycol solution temperature on 28th January

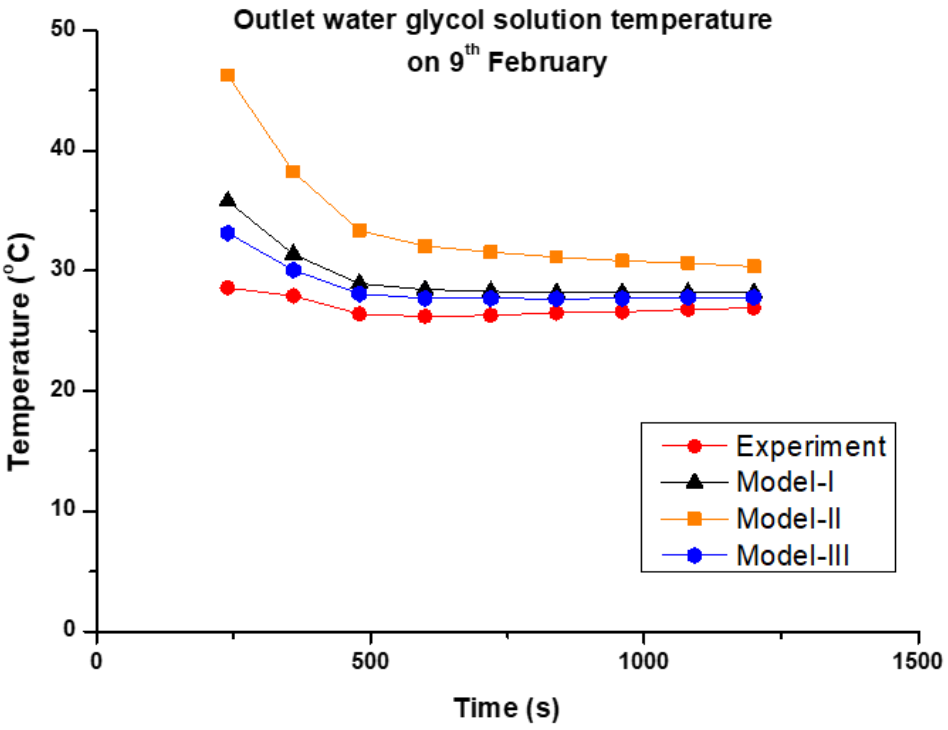

Figure 5-6 Comparison of outlet water glycol solution temperature on 9th February

In the 28th January case, the average percentage error for model-I is 3.78%, while the average percentage error for model-II is 12.29%. Lastly, for 9th February, the average percentage error for model-I is 9.54%, and the average percentage error for model-II is 25.32%, while for model-III the average percentage error is 6.31%. Greater percentage error for model-I, in this case, is due to a lesser number of data points. Since, the simulation was of 20 minutes of flow time, during which the heat transfer was taking place. It can also be observed from the above comparisons that as time proceeds the percentage error between the experimental data and simulated data decreases. Both comparisons can be seen in Figure 5-5 & 5-6.

So, from the above results, it can be deduced that the above model used has quite promising accuracy to the experimented data. The increase in percentage error for model-II is due to the lesser mesh elements, as compared to its volume. Lastly, it can also be deduced that symmetric downsizing of the tank shows results with greater accuracy as compared to maintaining the same geometric parameters and increasing the mesh size.

5.2 Mathematical model

To determine the heat transfer from the hot fluid to the storage tank, the following equation is used:

$$\boldsymbol{Q = \dot{m} C_p (T_{in} - T_{out})} \quad \textbf{(26)}$$

Internal heat transfer coefficient h_i, shell side heat transfer coefficient h_o, and overall heat transfer coefficient UA are the basic parameters that define the overall heat transfer from the hot fluid to the water inside the tank. So, it is preferable to determine which parameter affects the process in what manner.

$$\boldsymbol{Q = UA\Delta T} \quad \textbf{(27)}$$

For calculating the overall heat transfer coefficient following relation was used:

$$\boldsymbol{\frac{1}{UA} = \frac{1}{h_i A_i} + \frac{\ln(\frac{r_o}{r_i})}{2\pi kL} + \frac{1}{h_o A_o}} \quad \textbf{(28)}$$

ΔT is the mean temperature difference between the average bulk temperature of the hot fluid inside the coil and the water inside the tank. The internal heat transfer coefficient is determined through the following relation:

$$\boldsymbol{h_i = \frac{Q}{A_i \Delta T_i}} \quad \textbf{(29)}$$

A_i is the internal surface area of the coiled pipe. While ΔT_i is the mean temperature difference between the average bulk temperature of the hot fluid in the pipe and the inner wall of the coiled pipe. Furthermore, the external heat transfer coefficient is determined through the following relation:

$$\boldsymbol{h_o = \frac{Q}{A_o \Delta T_o}} \quad \textbf{(30)}$$

A_o is the external surface area of the coiled pipe. While ΔT_o is the mean temperature difference between the average temperature of the external surface of the coil and the average bulk temperature of the water. Furthermore, the Nusselt numbers are calculated through the following relation:

$$\boldsymbol{Nu = \frac{hL_c}{k}} \quad \textbf{(31)}$$

5.3 Modelling & simulation of new models

New geometries were modelled, details are mentioned in Table 5-1 and can be seen in Figure 5-7, 5-8 & 5-9. All of the cases were simulated by using the same hot working fluid, water-glycol mixture. The water inside the tank is taken at 30ºC and water-glycol at 65ºC. Initially, all the above cases were simulated by using a flow rate of 40 LPH at 65 ºC with coil external surface area of 0.35 m^2. Material properties of the hot fluid are taken at the average temperature of the hot fluid inlet and water inside the tank. Since, insignificant changes in inner Nusselt number are observed on simulating helical coil model either with constant material properties or temperature-dependent properties, especially at lower Dean number [1].

Hence, cases A1 to A8 had approximately the same inner heat transfer coefficient. Cases A1 to A3 show that the aspect ratio of the Nusselt number does not have any significant

effect on the inner heat transfer coefficient. While from cases A3 and A4 it can be deduced that the position of the coil inside the tank also does not have any significant effect. From cases A5, A6, and A8 it is observed that increasing the pitch of the coil did not have any significant effect on the inner heat transfer coefficient, but for cases B1, B2, and B3, with lesser curvature ratios, an increase in inner heat transfer coefficient is observed. Thus, for further numerical simulations only cases A6, A7 and B3 are considered.

Furthermore, additional simulations are carried out on flow rates 30, 40, 50, 60, 80, and 100 LPH with hot fluid inlet temperatures of 50ºC, 65ºC, and 80ºC. As the heat transfer area and the critical Reynolds number remained constant for all the simulated scenarios, however, Reynolds number, M number, heat transfer coefficient, Dean number, and Nu number were calculated separately for each scenario.

Table 5-1 Specifications of new models

Case #	Inner Diameter (d_i) (mm)	Coil Diameter (D) (mm)	Length of Coil (m)	Height of the coil (mm)	Pitch (mm)	Distance from top of tank (mm)	Distance from bottom of tank (mm)	Diameter of tank (mm)	Height of tank (mm)
Case A1	23	200	4.5	434	60	21.5	68.5	349	524
Case A2	23	200	4.5	434	60	111.5	88.5	317	634
Case A3	23	200	4.5	434	60	308.5	88.5	277	831
Case A4	23	200	4.5	434	60	21.5	375.5	277	831
Case A5	23	200	4.5	633	90	109.5	88.5	277	831
Case A6	23	200	4.5	696	99	46.5	88.5	277	831
Case A7	23	125	4.5	667	60	75.5	88.5	277	831
Case A8	23	200	4.5	228	30	513.5	88.5	277	831
Case B1	18	200	5.7	281	30	459	91	277	831
Case B2	18	200	5.7	543	60	197	91	277	831
Case B3	18	200	5.7	630	70	110	91	277	831

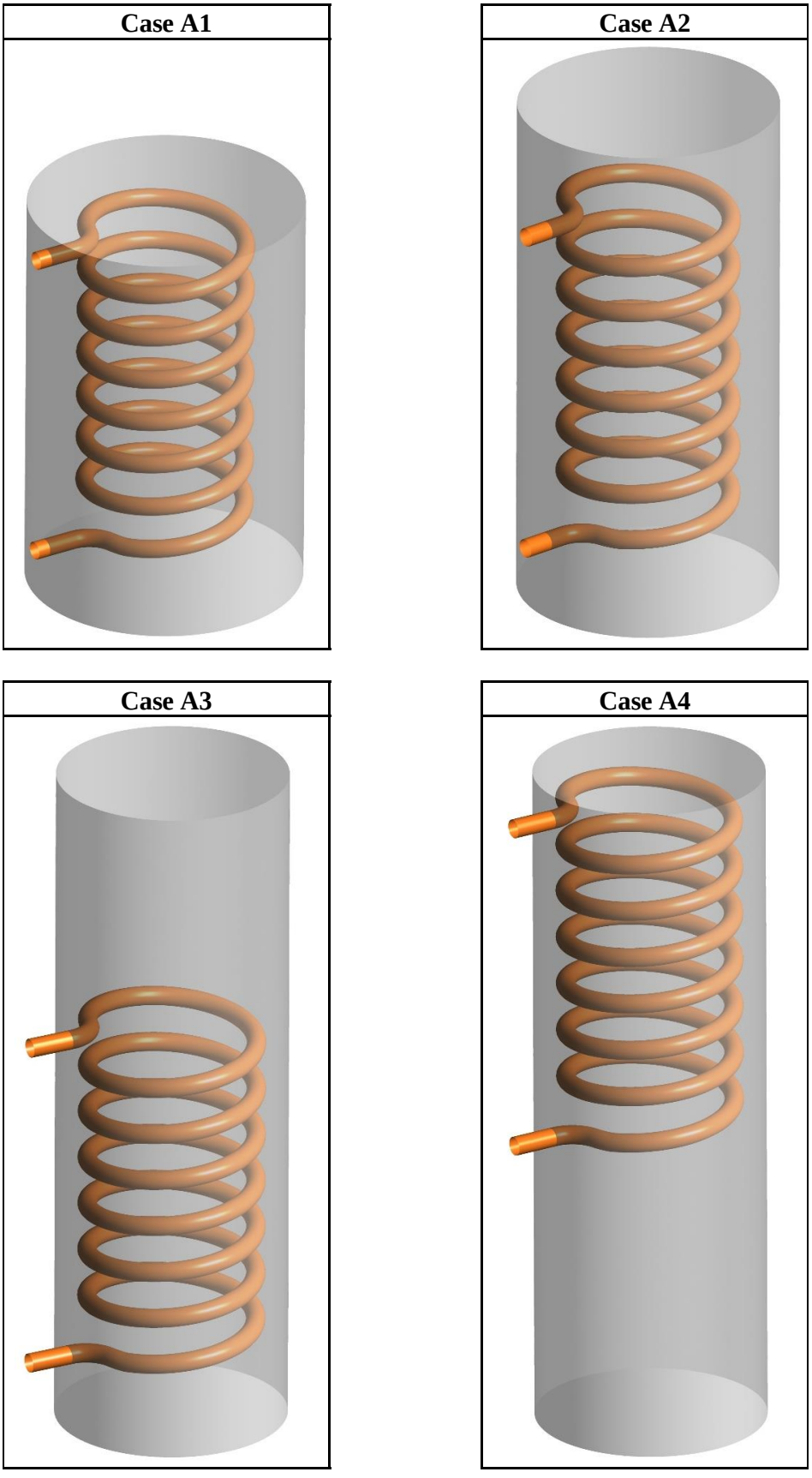

Figure 5-7 Case A1, Case A2, Case A3 & Case A4

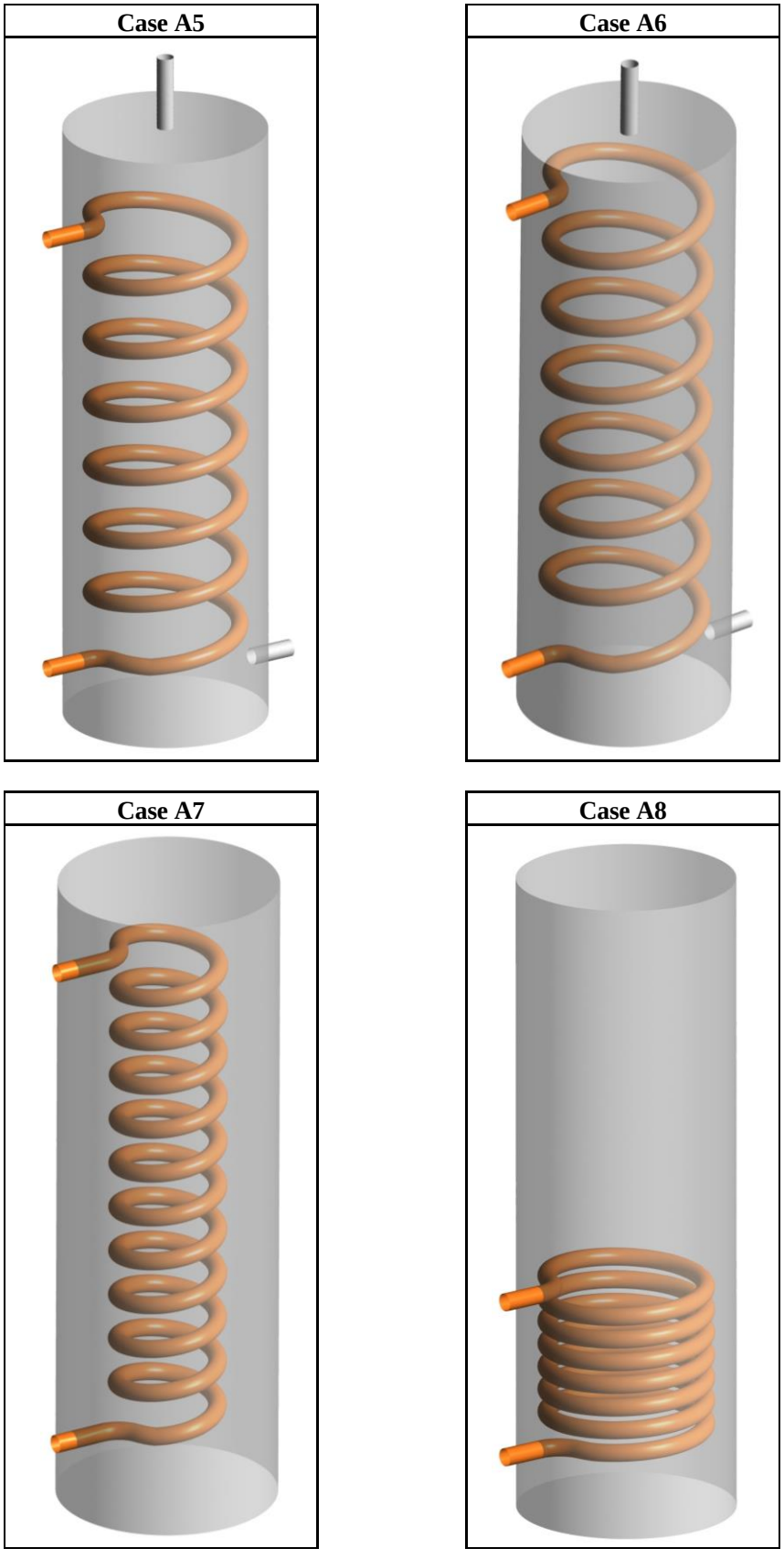

Figure 5-8 Case A5, Case A6, Case A7 & Case A8

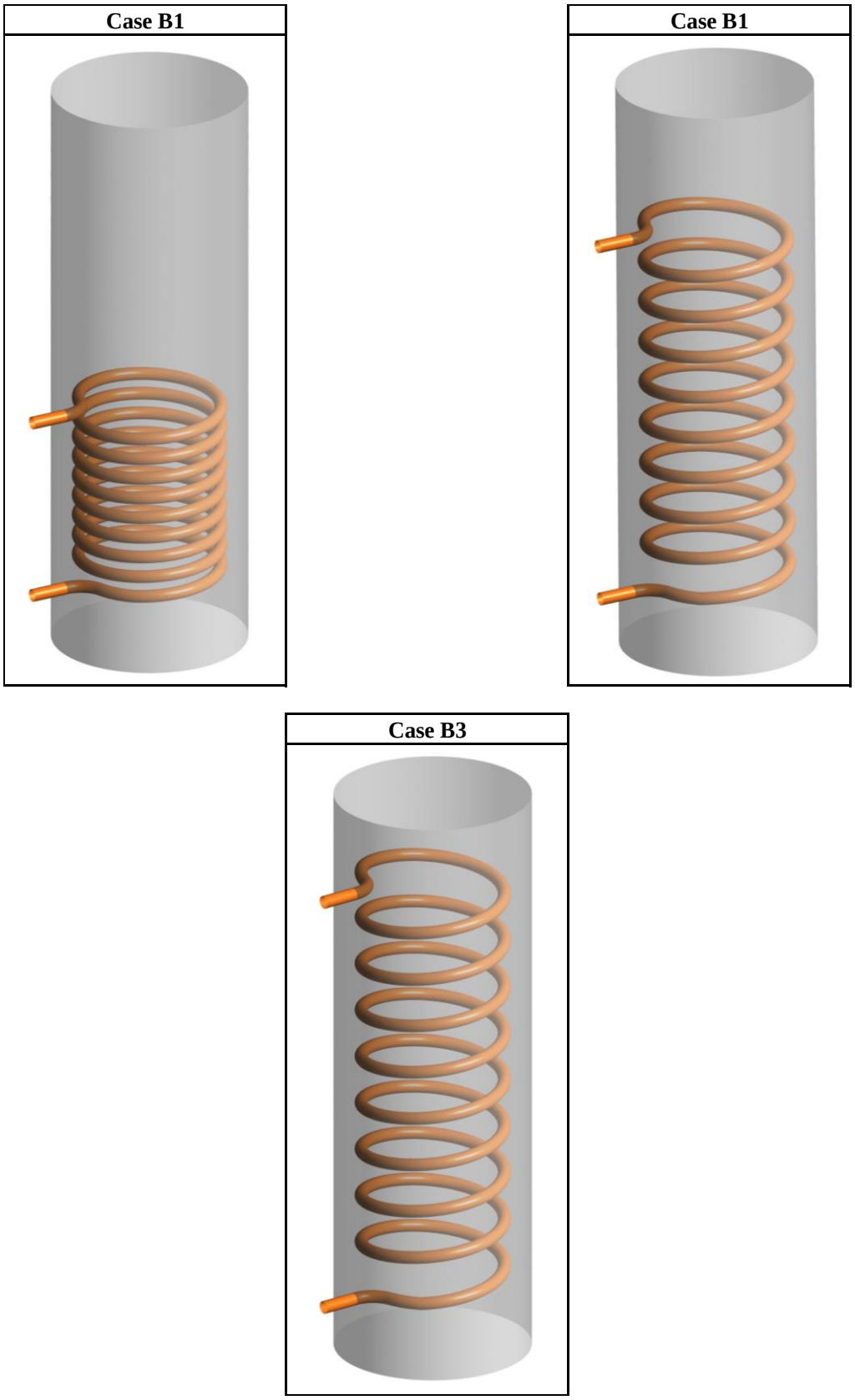

Figure 5-9 Case B1, Case B2 & Case B3

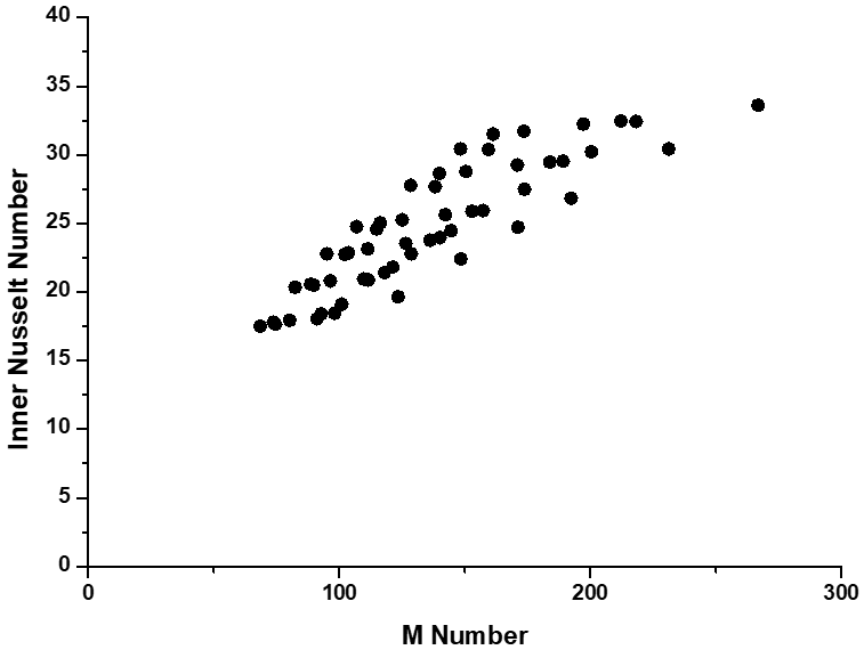

Figure 5-10 Comparison between M number and Inner Nusselt number

A general trend of increased inner Nusselt number with the increase of M number is observed in Figure 5-10. The same trend is not observed with the Reynolds number, because curvature ratio plays a vital role in determining the hydrodynamic nature of the fluid and the inner Nusselt number of the coil.

5.4 Flow dynamics and heat transfer in helical coil

In helical coils, the curvature of the pipe induces centrifugal forces that affect the fluid flowing inside the coil. The magnitude of the centrifugal force depends upon the curvature ratio [2] and the axial velocity of the flowing fluid. In the case of straight pipe, a general pattern is observed, the velocity of the fluid at the core of the pipe is highest compared to the fluid particles closer to the wall of the pipe. In helically coiled pipes, due to the variation in the velocity of flowing fluid, particles closer to the wall experiences lesser centrifugal force as compared to the particles at the core of the helical pipe. Therefore, particles of the fluid at the core get pushed toward the outer bend of the coil. It can be studied in Figure 5-11 that fluid particles with the highest velocity are at an offset from the centre of the pipe.

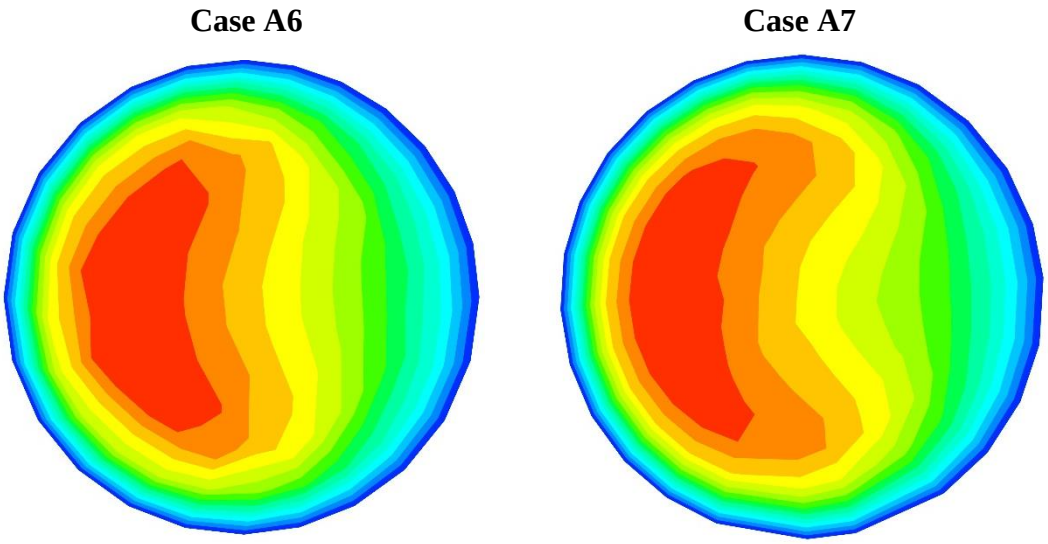

Figure 5-11 Velocity contour of helical pipe cross-section

In Case A7 high-velocity contour is closer to the outer bend due to greater centrifugal force. Moreover, this effect of centrifugal force causes the bifurcation of the stream at the outer wall of the pipe. After the bifurcation, fluid flows over the periphery of the pipe and returns to the inner bend. This causes the generation of counter-rotating vortices also known as secondary flows in the helical pipe.

Thus, secondary flows lead to a greater heat transfer coefficient in helical pipes as compared to a straight pipe. Due to the additional transport of fluid, greater heat transfer takes place. However, from past investigations, it is also observed that curvature of the coil restricts the emergence of turbulence in the flowing fluid and the effect of suppression increase with an increase in curvature ratio [2]. Due to suppression of turbulent fluctuations, flow is more stable and requires a higher Reynolds number for the hydrodynamic nature of the fluid to become turbulent.

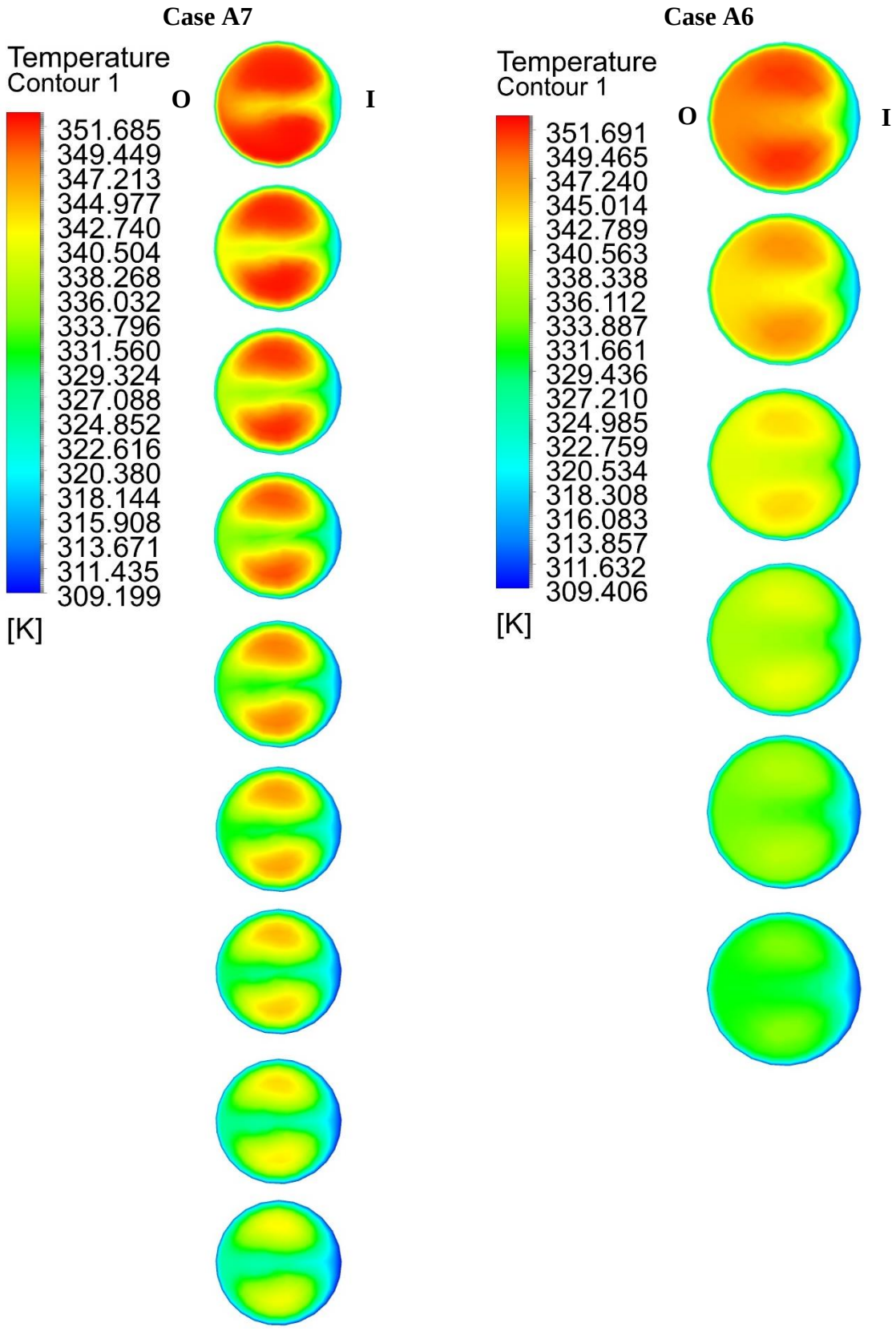

Figure 5-12 Temperature contour of helical pipe cross-section

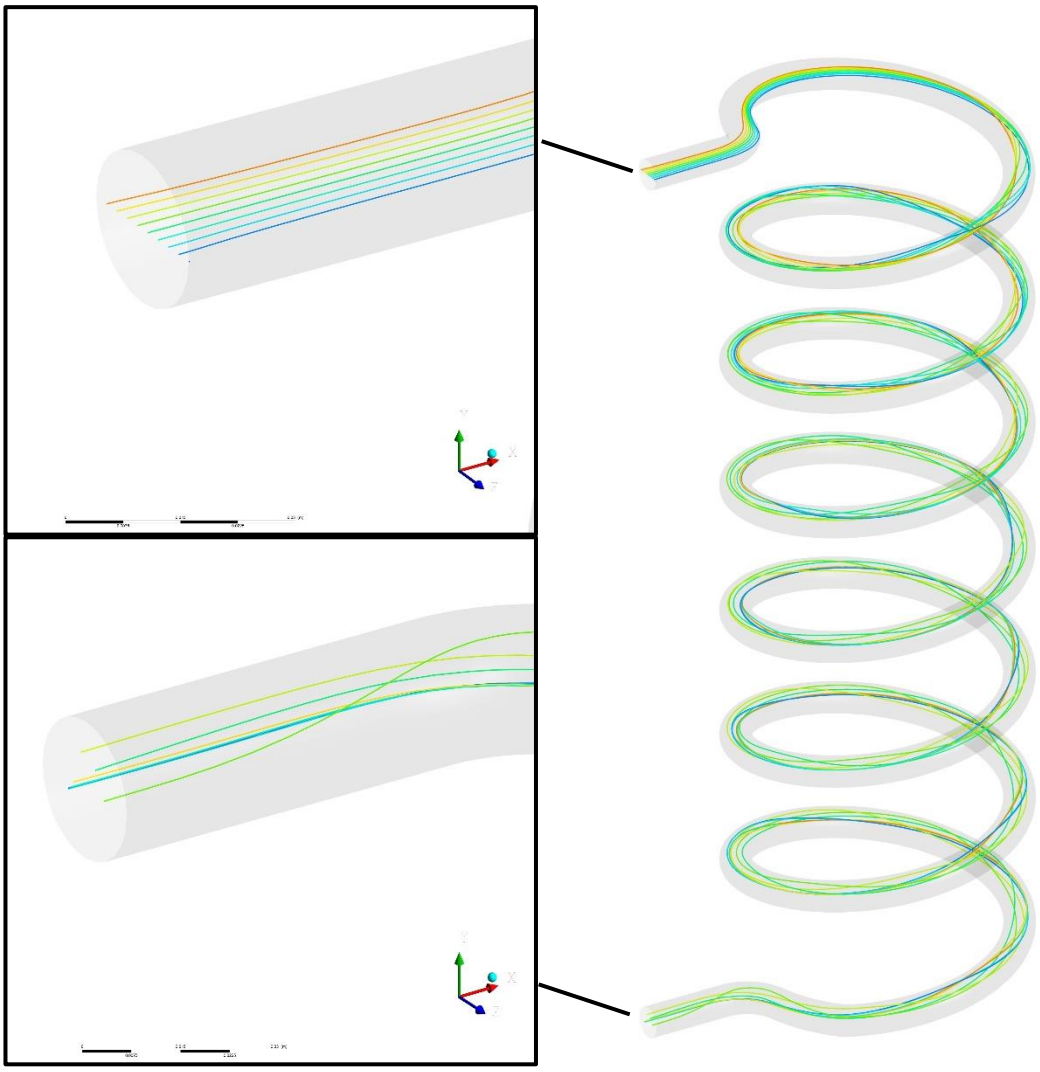

Figure 5-13 Trace of fluid particles parallel to Z-axis at the inlet

From Figure 5-13 it can be noted that the inlet fluid particles are along a line parallel to the Z-axis. While in Figure 5-14 fluid particles are along the line parallel to the Y-axis. In both scenarios at the outlet of the pipe fluid particles are scattered and during flow fluid particles are adopting different trajectories due to the secondary flow induced in the helical pipes. All the particles undergo a movement displaced from the inner side of the coil towards the outer bend. This rotational movement leads to a change in the local Nusselt number.

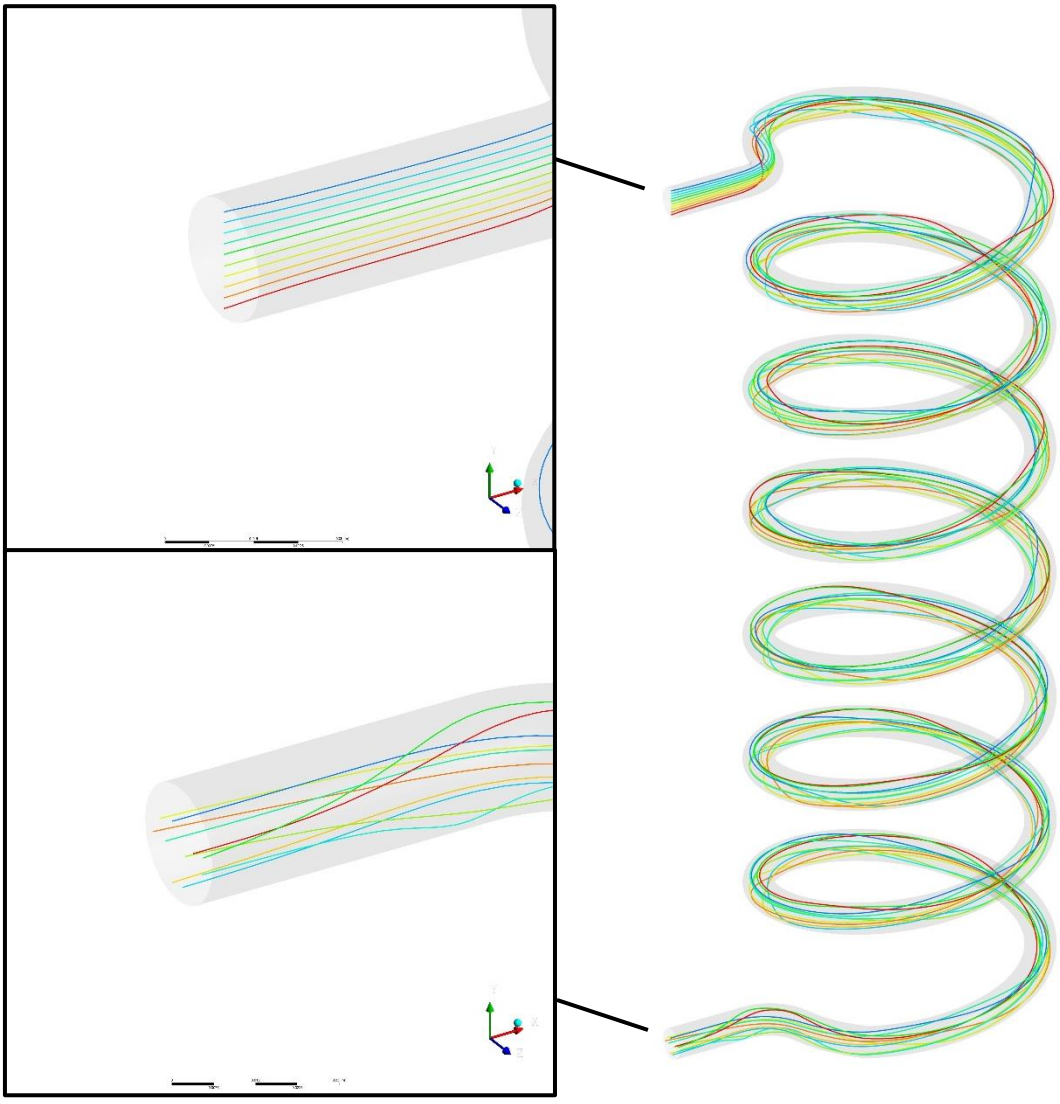

Figure 5-14 Trace of fluid particles parallel to Z-axis at the inlet

The temperature contours plot also shows that the low temperature of water/glycol solution appears near the inner side and the high temperature of water/glycol solution is at the outer side. This result shows that the heat transfer on the outer side is superior to that on the inner side due to higher velocity occurred on the outer side of the coiled tube. Moreover, it is found that the local Nusselt number on the outer side of the coil is higher than those at any other location at that cross-section. The rotational movement or the secondary flow in the coiled tube influences the heat transfer at the wall of the pipe.

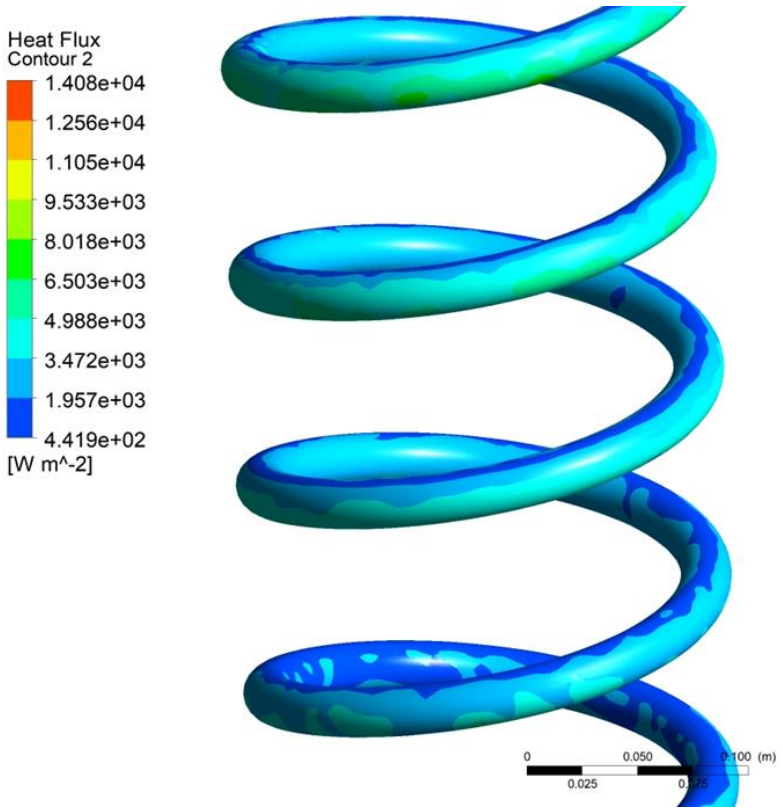

Figure 5-15 Heat flux contour of helical pipe

From the above Figure 5-15, it can be observed that heat flux at the outer periphery of the coil is greater than the inner periphery due to the difference in local Nusselt number.

5.5 Development and validation of inner Nusselt number relations

A correlation was developed in form of $Nu = a(Re^{b})(Pr^{0.4})$, and a and b were the constants to be determined. The heat transfer data acquired from 54 simulations, conducted for 50/50% water/glycol mixture, were used for generating the required mathematical correlation. The equation is constructed by using MATLAB® 2018 curve fitting tool, that induced the following correlation:

$$\boldsymbol{Nu = 0.43296(Re^{0.44564})Pr^{0.4}} \quad \textbf{(32)}$$

Valid for Reynolds number $56.045 \leq Re \leq 382.63$, $74.135 \leq Pr \leq 122.09$ and $0.09 \leq \delta \leq 0.184$.

Dean number is another dimensionless number used to understand the fluid flow in the helical-based coil. In this case, an equation is developed by plotting $Nu/Pr^{0.4}$ on the y-axis and De number on the x-axis on a linear scale for 54 simulated data Figure 5-16. The following co-relation is developed using the least-squares fitting-power law.

$$\boldsymbol{Nu = 0.7396(De^{0.4282})Pr^{0.4}} \quad \textbf{(33)}$$

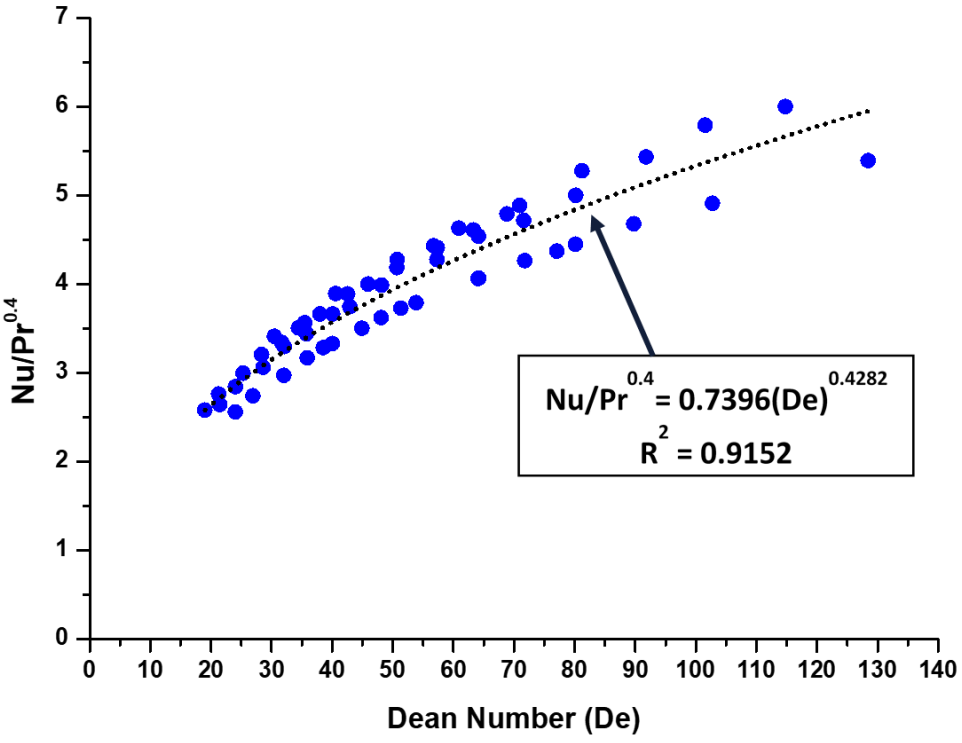

Figure 5-16 Development of correlation (33) with Nu as function of De & Pr

Heat transfer data generated from 54 simulated data under is plotted on a linear scale as $Nu/Pr^{0.4}$ vs. M to get a unique correlation without δ. The least squares-power law fitting curve through the data points shown by the dark line in Figure 5-17 resulted in the following correlation.

$$\boldsymbol{Nu = 0.175(M^{0.6364})Pr^{0.4}} \quad \textbf{(34)}$$

Applicable for range $68.615 \leq M \leq 266.834$, $74.135 \leq Pr \leq 122.09$.

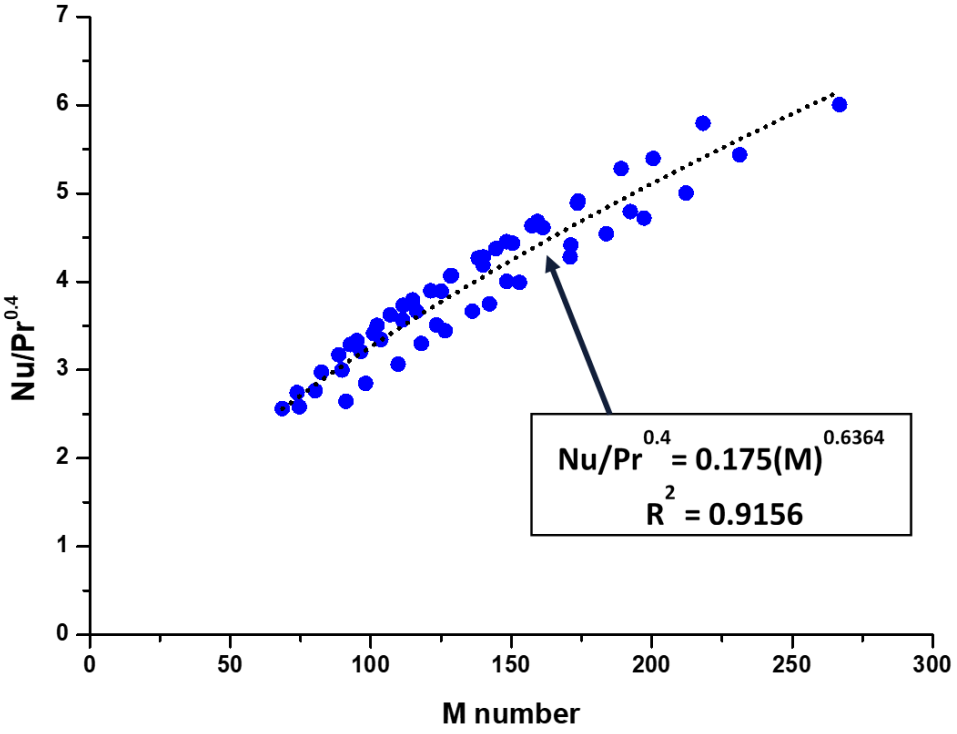

Figure 5-17 Development of correlation (34) with Nu as function of M and Pr

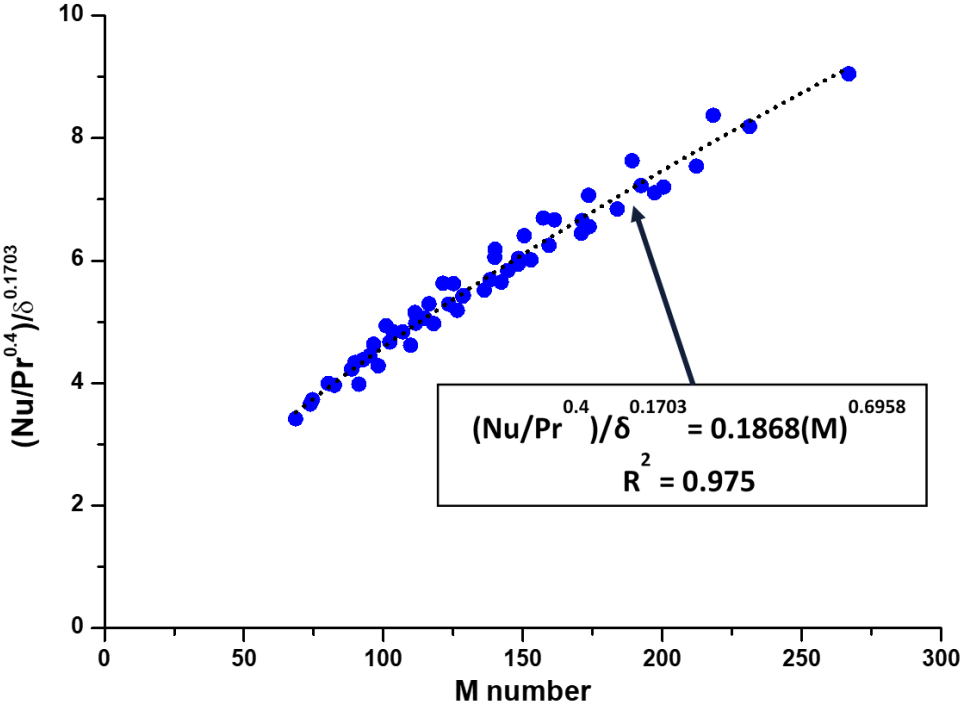

Figure 5-18 Development of correlation (35) with Nu as function of M,δ & Pr

However, these correlations give the best results when the flow rate is variable for a constant value of δ. Therefore, to modify the existing equation to make it applicable for constant or variable values of flow rates and also for constant/variable value of coil curvature, coil curvature ratio, δ needs to be introduced. A final correlation was developed by using MATLAB. All 54 simulated data points were used to develop a comprehensive correlation Figure 5-18. Which is as follows:

$$\boldsymbol{Nu = 0.1868\left(M^{0.6958}\right)\delta^{0.1703}Pr^{0.4}} \qquad \textbf{(35)}$$

Applicable for range 68.615 ≤ M ≤ 266.834, 74.135 ≤ Pr ≤ 122.09 and 0.09 ≤ δ ≤ 0.184.

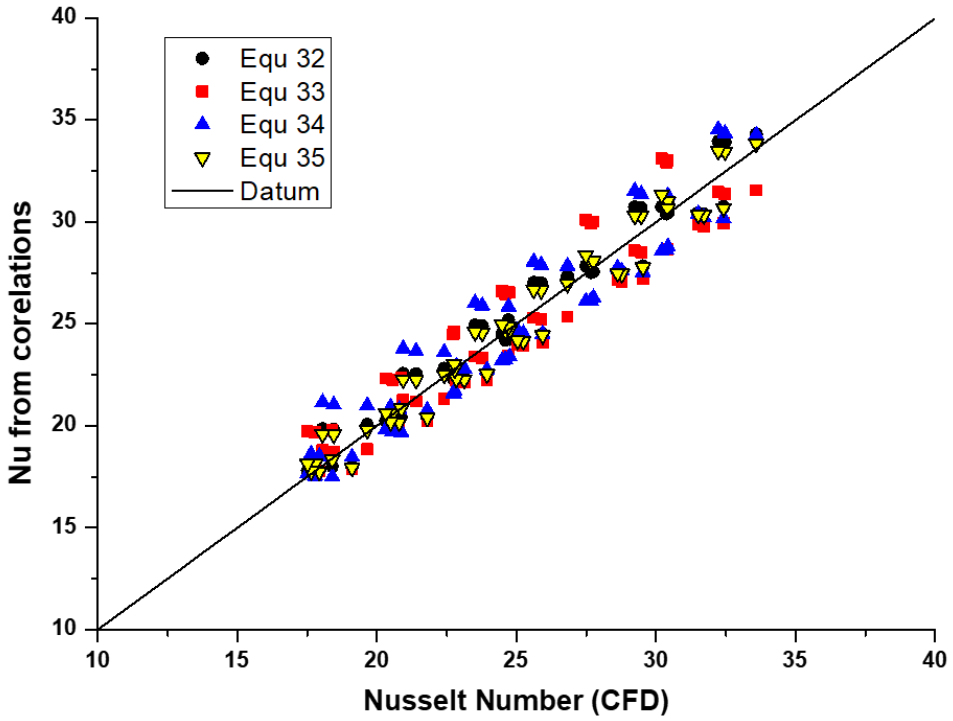

Figure 5-19 Comparison of all the developed correlations

From the above Figure 5-19, it is quite visible that the correlation which caters to the curvature ratio is most close to inner Nusselt numbers generated through simulations. Comparison of mathematical correlations (33)-(35), and the simulated data with the work done by previous investigators are presented in Figure 5-20.

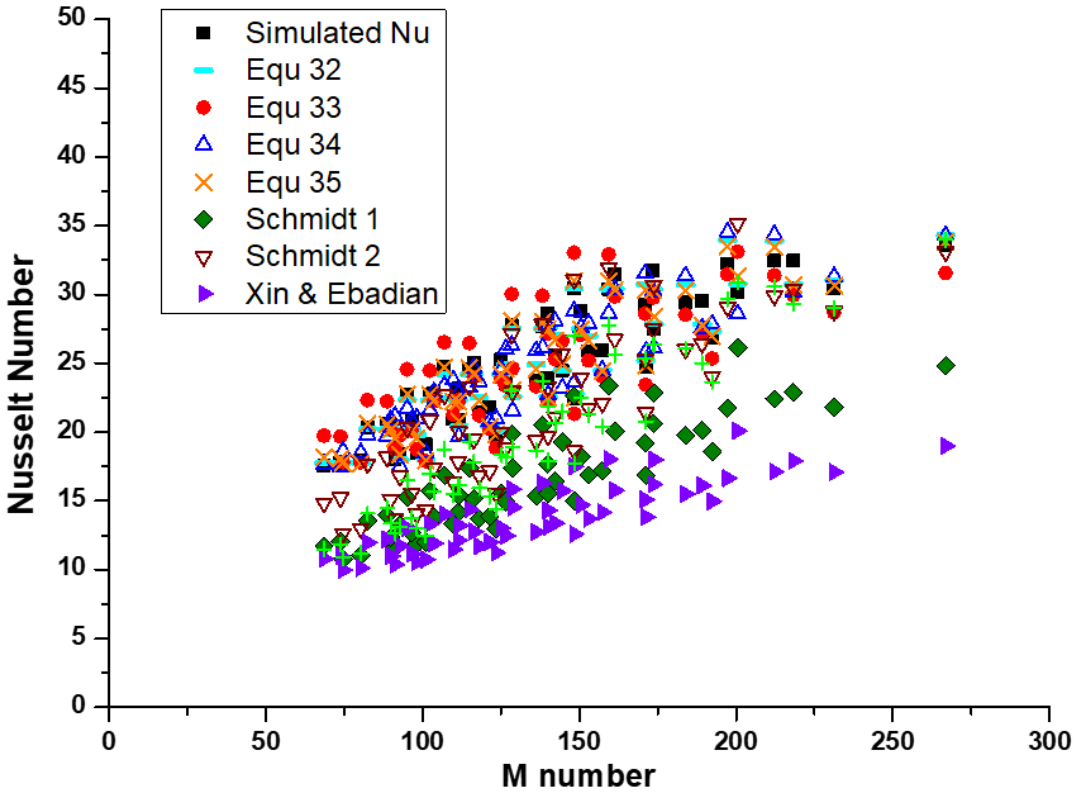

Figure 5-20 Comparison of simulated data, developed correlations & past relations

Numerically generated Nusselt number and mathematical correlations (33)-(35) predicted values of inner Nusselt number with mean percentage error of 32.4%, 32.6%, 32.3% and 32.4%, along with mean percentage error of 12.7%, 13.15%, 12.4%, and 12.8% to those predicted by Schmidt [3](1&2). Moreover, with average percentage error of 43.7%, 44%, 43.7% and 43.8%, and 21.2%, 21.3%, 21.2% and 21.4% with those predicted in researches [4] and [5], respectively.

5.6 Development and validation of external Nusselt number relations

The heat transfer process begins with cold water inside the tank at a constant temperature of 30ºC. Simulations were carried out by having the same 50% water-glycol mixture at the inlet with a volume flow rate of 40 LPH, and a temperature of 65ºC. Simulations were carried out for all the cases mentioned in Table 5-1. All the cases were simulated for a flow time of 30 minutes, and the time took to complete the simulation of each case was around 216 hours. Inside the tank heat transfer takes place due to free convection. Equ

(30) is used for calculating the external heat transfer coefficient, and then equ (31) is used for calculating the external Nusselt number. Conventionally, in cases of natural convection, Nusselt numbers are mathematically correlated as the power law of the Rayleigh number. These forms of numerical correlations are desirable for solving engineering problems.

$$\boldsymbol{Nu_o = a(Ra)^b} \tag{36}$$

As the heat transfer process takes place, the average temperature of the external surface of the coil, and the bulk temperature of the water inside the tank change with time. So, measurements of the simulations were recorded at the regular interval of 120s to study the phenomenon of natural convection, Boussinesq approximations (Equ 25) were used to determine the effects of buoyancy during the CFD based simulations. Both, the external Nusselt number and Rayleigh number were calculated by taking the length of the coil (L), diameter of the tube (d_o), and height of the coil (H) as the characteristic length L_c.

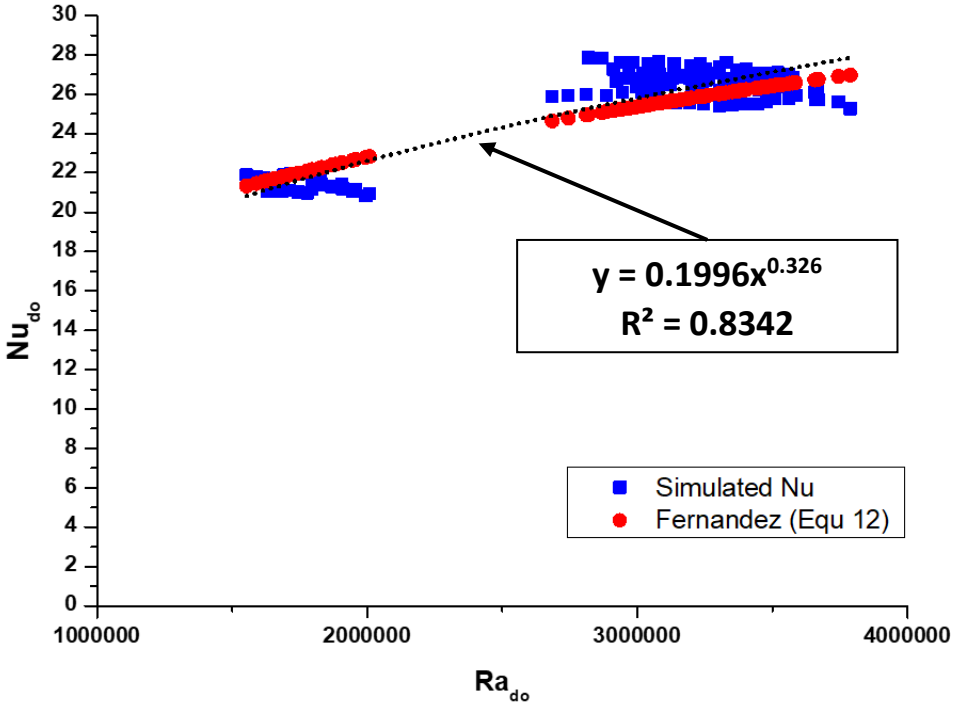

Figure 5-21 Average Nu in comparison with Ra, taking d_0 as L_c

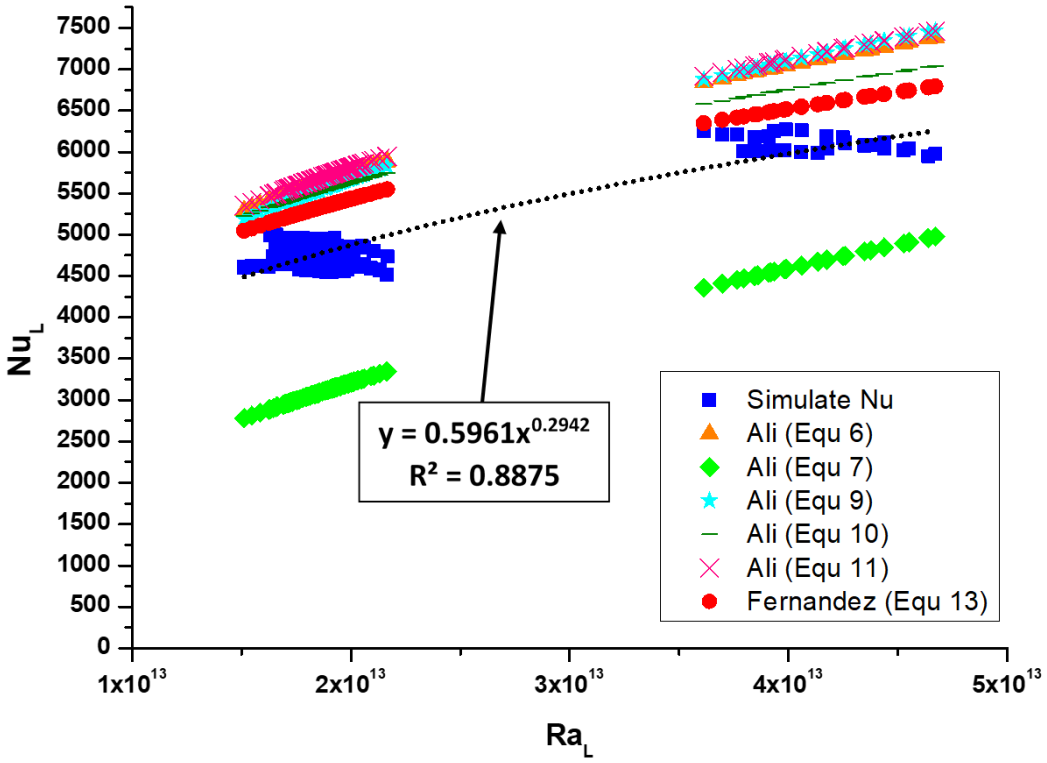

Figure 5-22 Average Nu in comparison with Ra, taking L as L_c

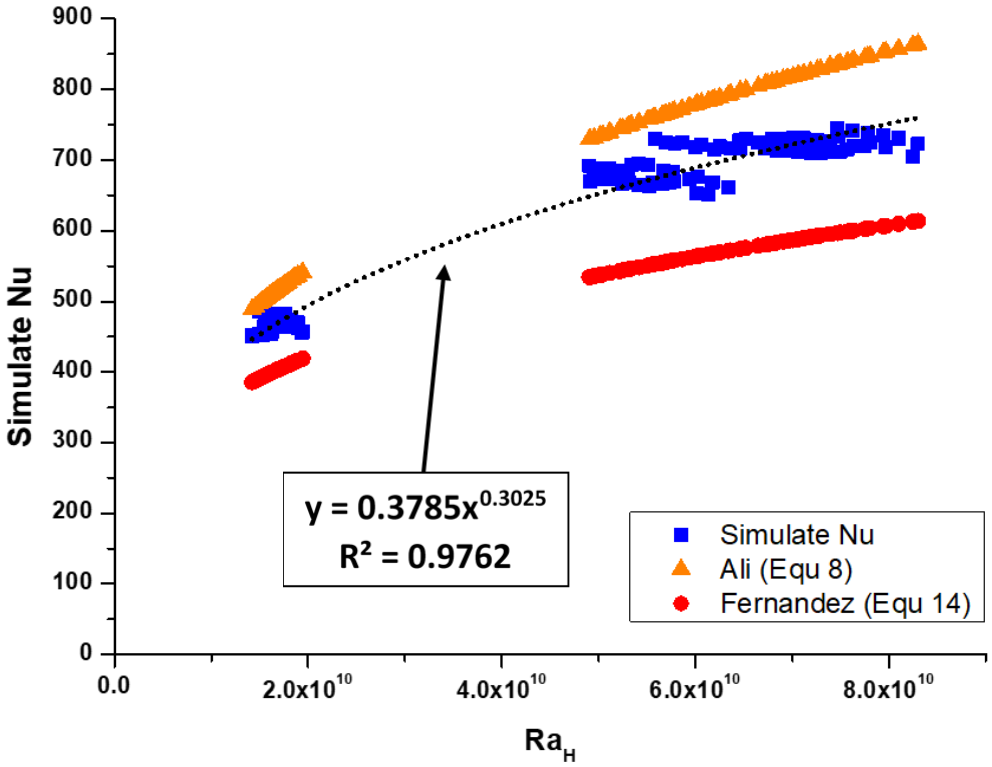

Figure 5-23 Average Nu in comparison with Ra, taking H as L_c

Table 5-2 Coefficient a & b of relation $Nu_o = aRa^b$, Ra range, and correlation coefficient

Characteristic length	a	b	Rayleigh range	Correlation coefficient	Figure number
Diameter of tube	0.1996	0.326	$1.55x10^6$ - $3.78x10^6$	0.9133	5.15
length of tube	0.5961	0.2942	$1.51x10^{13}$ - $4.67x10^{13}$	0.9421	5.16
Height of coil	0.3785	0.3025	$1.42x10^{10}$ - $8.3x10^{10}$	0.988	5.17

In Figure 5-21, numerically generated external Nusselt number and correlation derived using the diameter of the tube as its characteristic length has to mean percentage error of 1.29% and 1.37% with the correlation derived in past study [6]. In Figure 5-22, the numerically generated Nusselt number and the correlation derived by using the length of the tube as its characteristic length are compared with mathematical correlations produced in the past by using an experimental setup. Simulated Nusselt number have mean percentage error of 17.4%, 32.45% with past relation [7] (equ 6,7), average percentage error of 16.8%, 15.12% and 19.22% with past co-relation [8] (equ 9,10,11), and 11.11% with derived relation [6] (equ 13). Similarly, mathematical correlation has error of 17.7%, 32.5%, 16.65%, 14.95%, 19.04% and 10.95%, respectively. Furthermore, Figure 5-23 using the height of the coil as the characteristic length, simulated Nusselt number have percentage mean error of 11.79% and 16.47% with [7] (equ 8) and [6] (equ 14). Similarly, an arithmetic correlation has an average error of 11.7% and 16.54%, respectively.

5.7 Parametric analysis

Following are the parametric analysis performed in this study

5.7.1 Thermal stratification analysis

As 3d models of different configurations were used for the numerical simulations, different thermal stratification was observed inside the water tank. It turns out that the position of the coil, the inlet, and the outlet position of the hot fluid also plays a vital role in determining the thermocline inside the storage tank. In all the cases mentioned in Figure 5-24, the surface area of the pipe, the diameter of the pipe, length of the pipe, and diameter of the coil are similar. Even for case A3 and case A4 pitch of the coil is also equal. From the above Figure 5-24, it can be observed that coils with similar configurations have different effects on the storage tank due to their positioning.

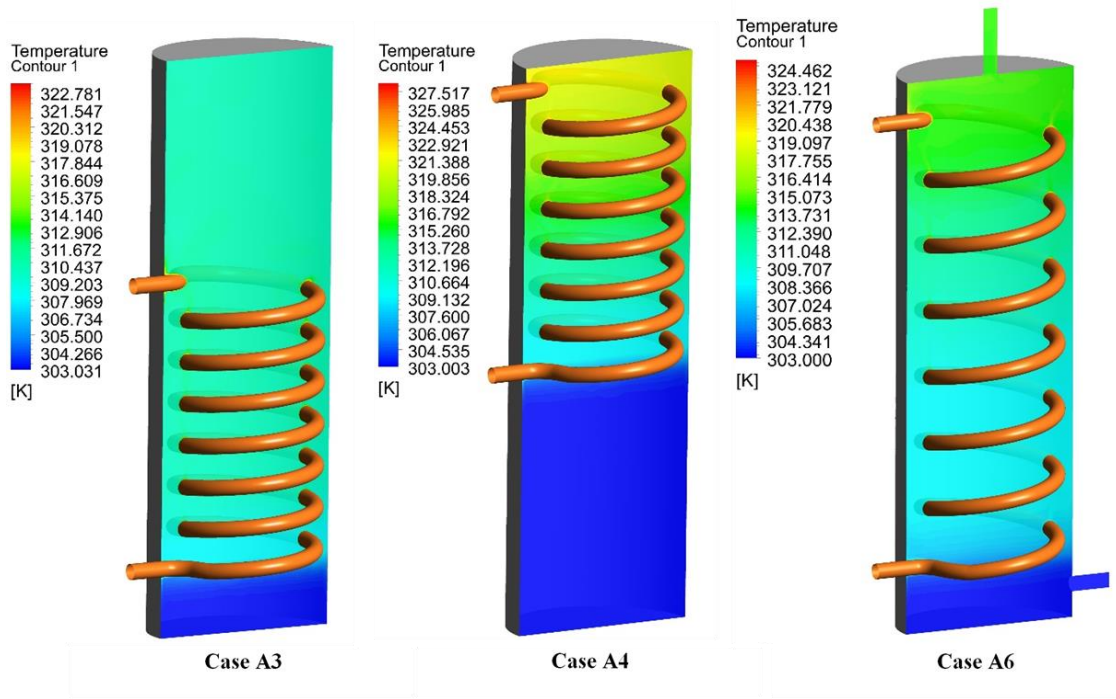

Figure 5-24 Temperature contours of A3, A4 and A6 after 30 minutes of flow time

As for case A3, when the coil is placed at the bottom of the tank highest heat transfer takes place. As the thermal energy is transferred from the coil to water, water in contact with the coil shows upward movement due to the buoyancy effect. During its upward movement, it starts mixing with the water at a lower temperature, as a result, all the water above the coil has a uniform temperature. In the case of A4 when the coil is placed at the top of the tank, the highest temperature of the water is observed at the top of the tank, but the amount of heat transfer decreases with time significantly. The reason for the decrease in heat transfer is due to the water beneath the coil, which does not play a significant role in storing energy. While in Case A6 the pitch of the coil is increased so that the coil could be extended throughout the whole tank. The approximately same amount of heat transfer is observed as that of case A3, discussed before. But in this case, the stratification is distributed throughout the whole water tank, and water with a greater temperature range is available inside the tank. Although, a longer simulation is required, in the future, to observe the extent of the decline in heat transfer in both Case A3 and A6 with longer flow time.

Table 5-1 contains configurations of water storage tanks with different aspect ratios. A comparison between case A1 and case A6 is studied further. In both cases, the water

storage tank is of 50 ltr volume but with different aspect ratios. As in case A1 with a lower aspect ratio, the height of the coil is small but it is still spread along with the height of the tank. Correspondingly, in case A6 pitch of the coil is increased so that it could also be distributed along with the height of the coil. However, other parameters of the coil in both cases are identical. After 30 minutes of flow time simulation, the temperature of the water at the uppermost part of the tank in case A1 is observed to be higher than in case A6. This is due to the lesser distance between the upper wall of the tank and the inlet of the hot fluid. Afterward, the inlet flow of the hot fluid is stopped and the whole model was kept at a static position for the next 330 minutes of flow time. During this simulation, boundary conditions of the outer wall of the tank are kept equal to the average of data received through the experimental process. A comparison of both models can be seen in Figure 5-25.

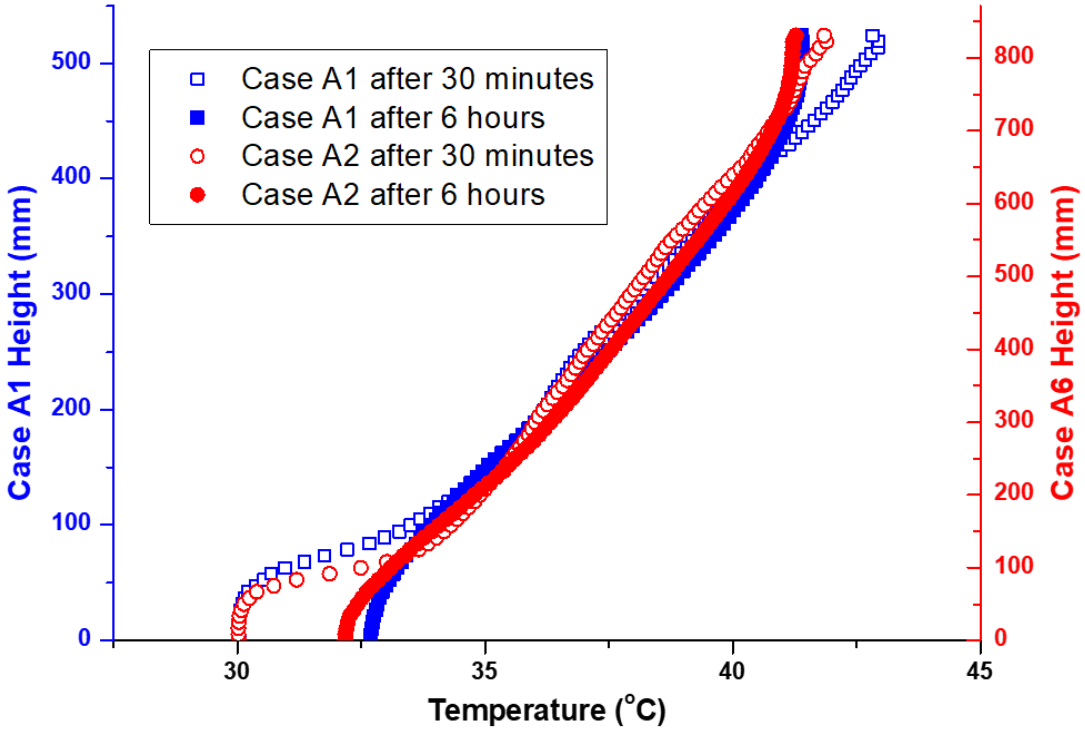

Figure 5-25 Temperature profile of tank after 30 minutes and 6 hours of flow time

From Figure 5-25 it can be studied that the greater degree of temperature increase is seen for case A1 from the bottom of the tank. Likewise, a greater amount of temperature decrease is observed at the top of the tank, for case A1. So, it can be deduced, in a small aspect ratio, a greater amount of thermal energy gets distributed along with the height of

the tank, with time, as compared to a tank with a high aspect ratio. Tanks with a small aspect ratio have a greater cross-section which leads to a greater surface area for different layers of water that helps in faster heat transfer, and overall thermal equilibrium inside the tank.

5.7.2 Inner Heat Transfer Coefficient

Coils with different configurations have varying set of parameters, those parameters are altered to study their effects on the inner heat transfer coefficient of the coil. A comparison is drawn between the heat transfer coefficient, M number, and Reynolds number in Figure 5-26 & 5-27. In all of the following comparisons values of HTC are in SI units.

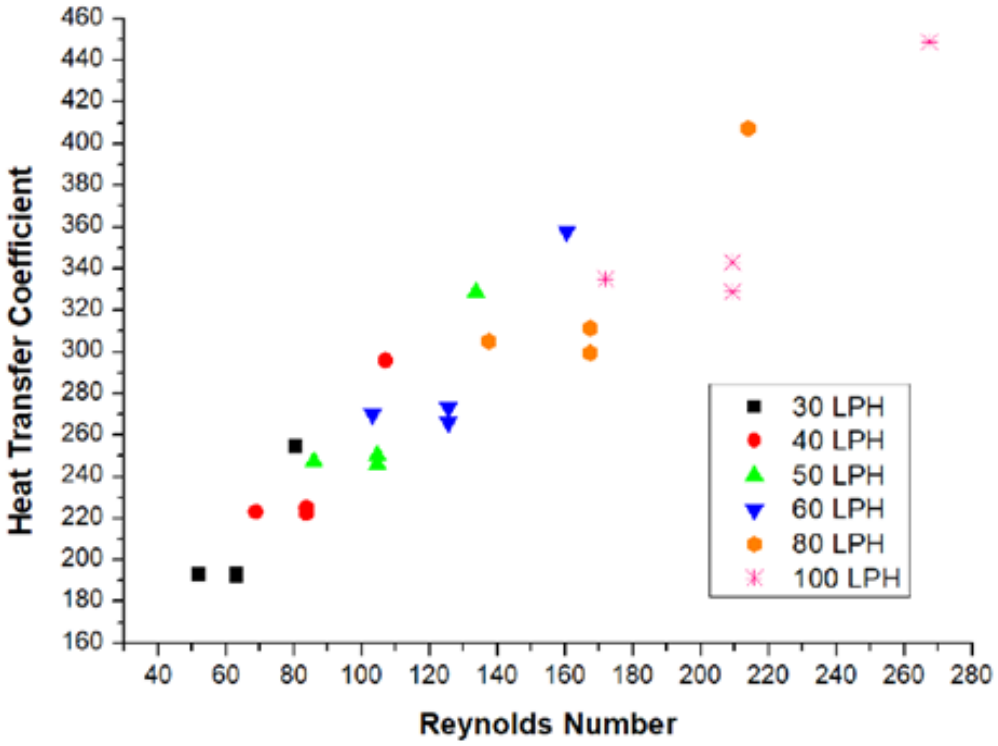

Figure 5-26 Comparison between Reynolds Number and HTC

From the Figure, a trend of increase in heat transfer coefficient with M number can be observed but the same cannot be said about the Reynolds number. In Figure 5-26 it can be observed that some cases have the same Reynolds number but different heat transfer coefficients but the same is not observed for M number. Reynold's number does not cater

to the effects of curvature. Therefore, the M number is a better dimensionless number for predicting the heat transfer coefficient for coiled heat exchangers, as seen in Figure 5-27.

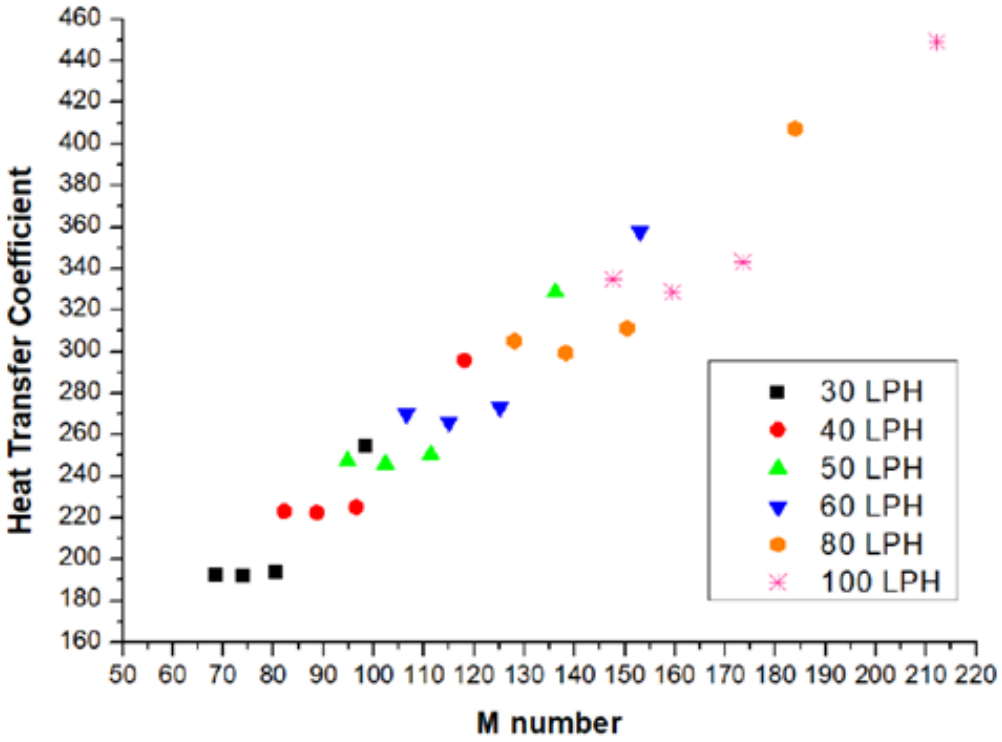

Figure 5-27 Comparison between M number and HTC

A variation in the M number by varying the geometric parameters of the coil is observed, while same cannot be deduced for the Reynolds number. Due to complex flow patterns in the coil different dimensionless number are used to understand the mechanics of the flow inside the coil.

Later on, a comparison of heat transfer coefficients is drawn with the diameter and length of the pipe. In both comparisons, simulations are performed with different mass flow rates by keeping surface area and coil diameter constant. The results of the comparison can be seen in Figure 5-28 & 5-29.

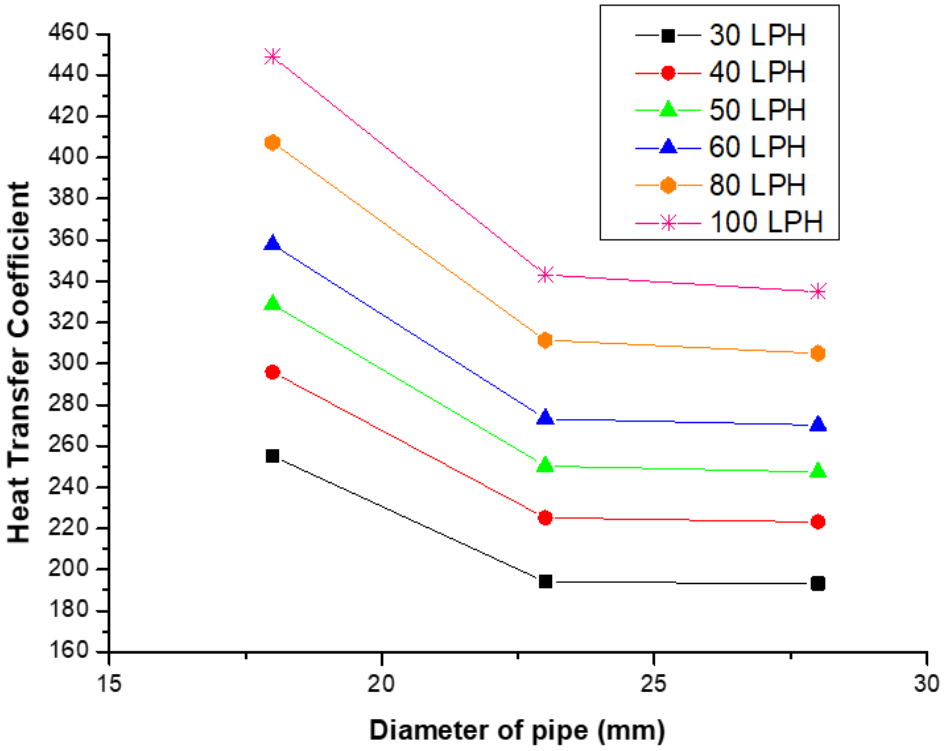

Figure 5-28 Variation in HTC with diameter of the pipe

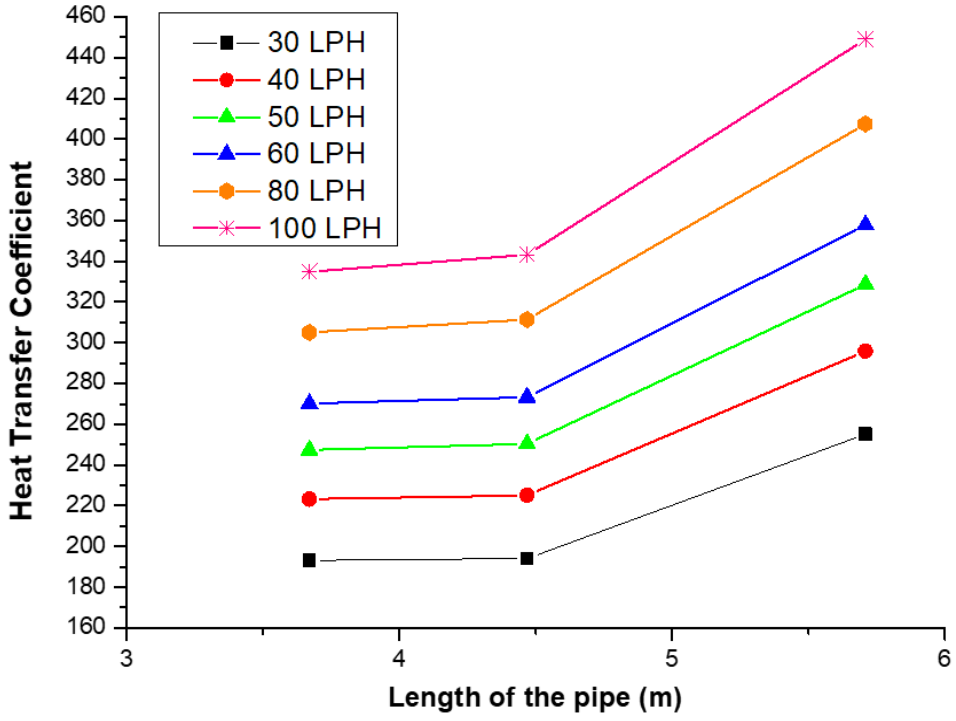

Figure 5-29 Variation in HTC with the length of the pipe

An increase in the diameter of the pipe leads to a trend of decrease in the heat transfer coefficient. But on the contrary, increasing the length of the pipe leads to an increase in the heat transfer coefficient.

Moreover, in both comparisons increase in flow rates causes a considerable increase in heat transfer coefficient. Lastly, comparisons are drawn by varying the Pitch and curvature ratio (δ = diameter of the coil/ diameter of the pipe) of the coil. All the comparisons were carried out for volume flow rates varying from 30-100 LPH. In all of the scenarios surface area of the coil was kept constant. Both comparisons with pitch and curvature ratio are demonstrated in Figure 5-30 & 5-31.

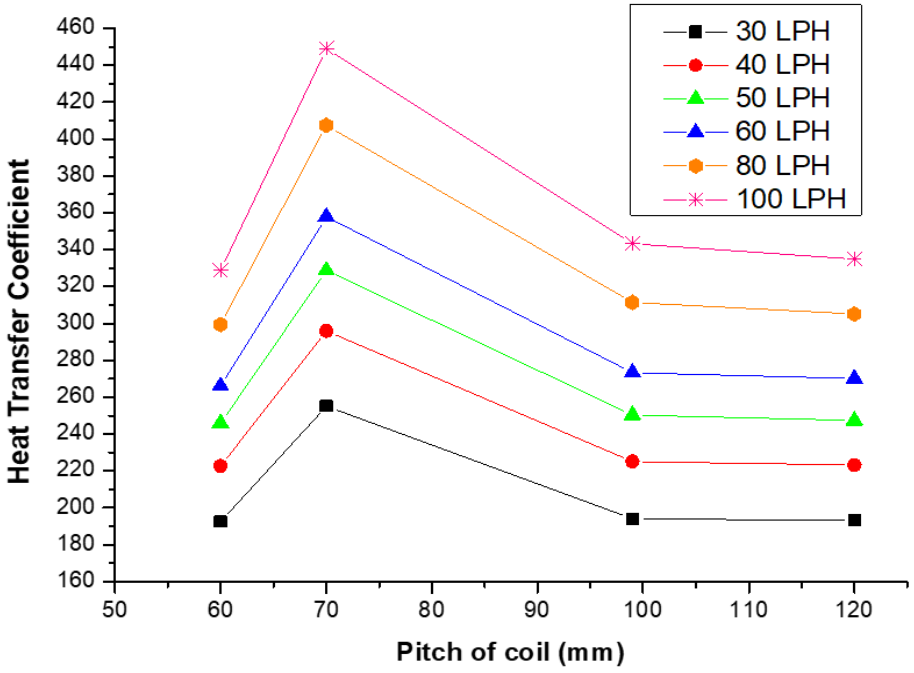

Figure 5-30 Variation in HTC with pitch of the coil

A trend of increase in the heat transfer coefficient with curvature ratio can be studied in Figure 5-31. For the laminar flow regime in coils, an increase in curvature ratio leads to a decrease in the centrifugal effects. Centrifugal effects cause a delay in the critical Reynolds number that eventually leads to a lesser heat transfer coefficient. The centrifugal effects also lead to the increase in the heat transfer coefficient as compared to straight pipes, due to its secondary flows, but it also keeps the hydrodynamic nature of the flow laminar for higher flow rates. Moreover, it was observed that coils having a pipe with

equal diameter have different HTC due to changes in there in coil diameter. Hence, the curvature ratio of the coil plays an essential role in determining the inner HTC of the coil.

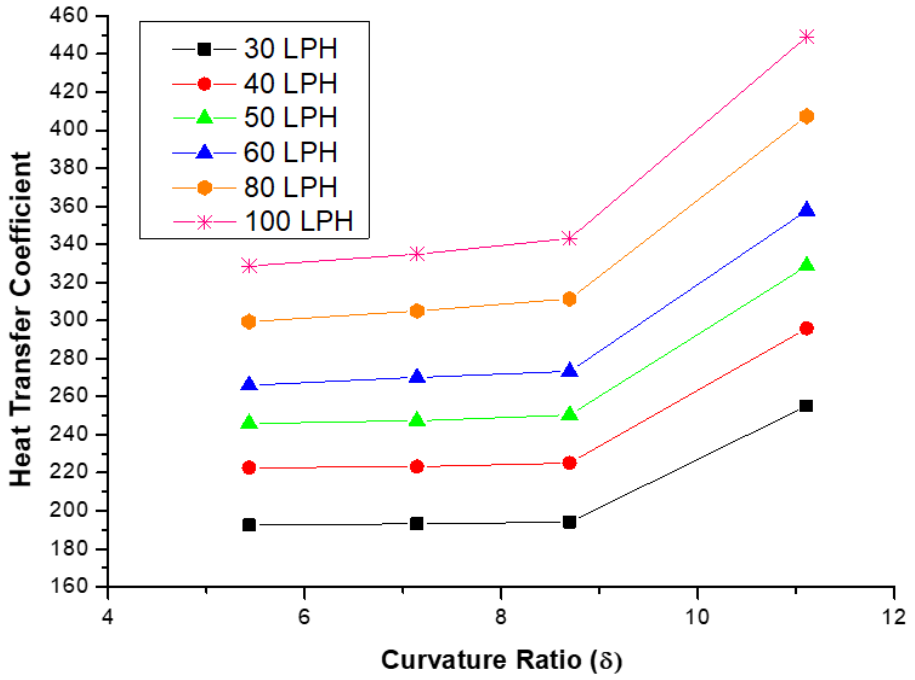

Figure 5-31 Variation in HTC with curvature ratio

From Figure 5-30 it can be observed that there is no clear trend for heat transfer coefficient with the variation in pitch. And the spike in the heat transfer coefficient in Figure 5-30 is because that model had the greatest curvature ratio, but lesser pitch as compared to the following models. It shows that pitch variation does not have a significant effect on inner Nusselt number and torsion effects are quite insignificant for coil-based heat exchangers.

Furthermore, a trend of increase in heat transfer coefficients with the rise in flow rates is quite evident.

5.7.3 Outer Heat Transfer Coefficient

As the heat transfer takes place between coil and water, the average temperature and thermal profile of the tank changes with time. This change leads to variation of external HTC of coil. So, for each model more than one plots of HTC can be seen. Each model is simulated for real time of 30 minutes.

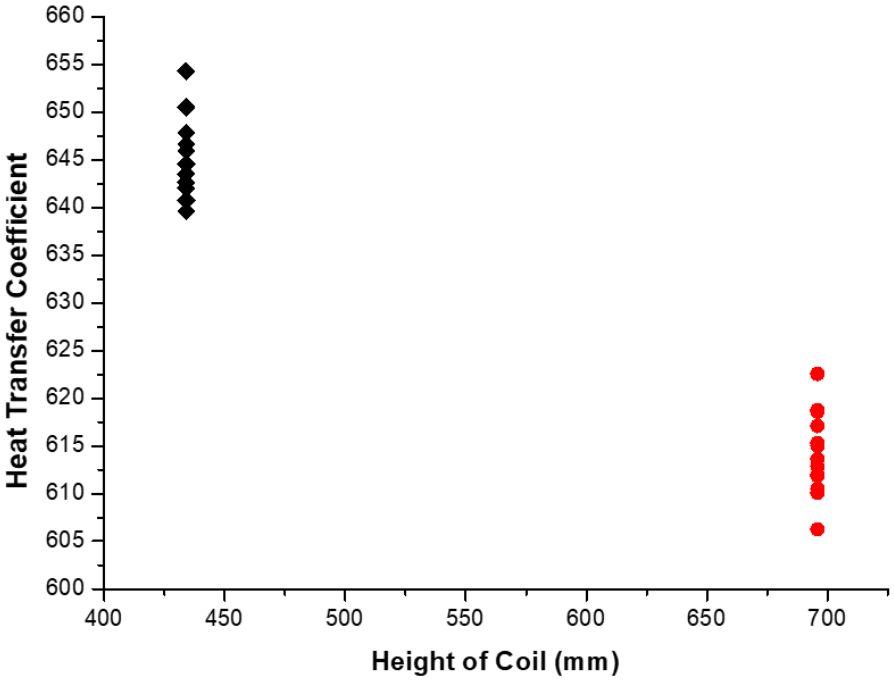

Figure 5-32 Variation in HTC with coil height

From the above Figure 5-32 a general trend of decrease in HTC with the height of the coil is noted. Because as the height of the coil is increased greater it is extended throughout the whole tank which leads to lesser upward movement of water from the upper part of the coil, after heat transfer, which eventually results in lesser outer HTC.

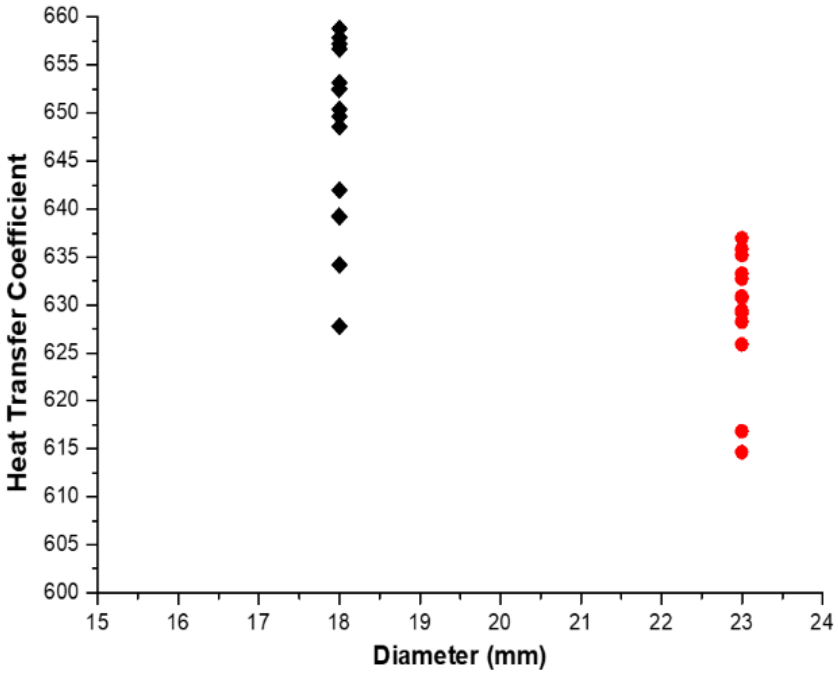

Figure 5-33 Variation in HTC with coil diameter

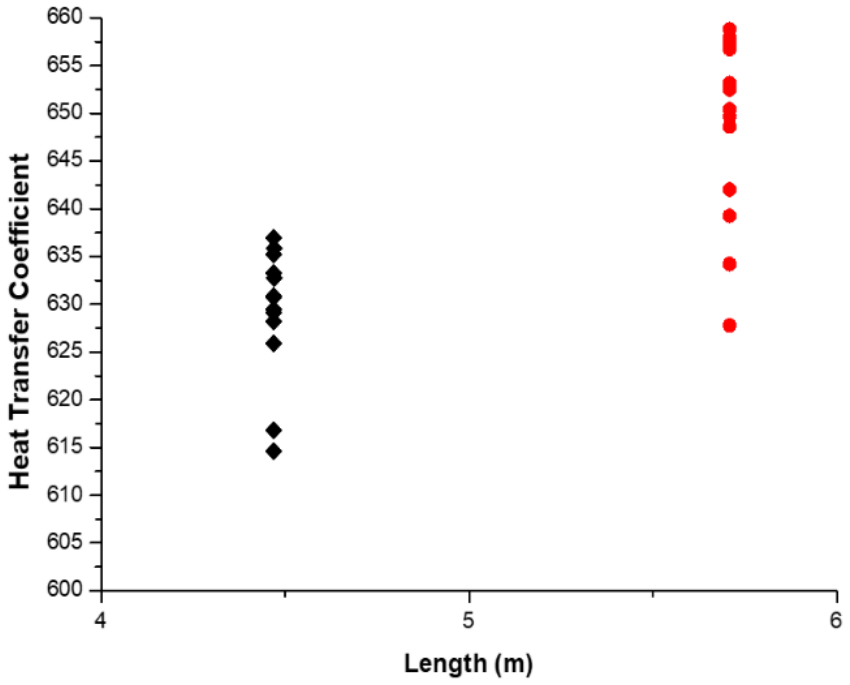

Figure 5-34 Variation in HTC with length

In Figure 5-33 & 5-34 coils with equal surface area, height and coil diameter are taken into consideration. A comparison showed a trend of decrease in HTC with increase in diameter of the coil, while a trend of increase in HTC with increase in length of the tube is observed.

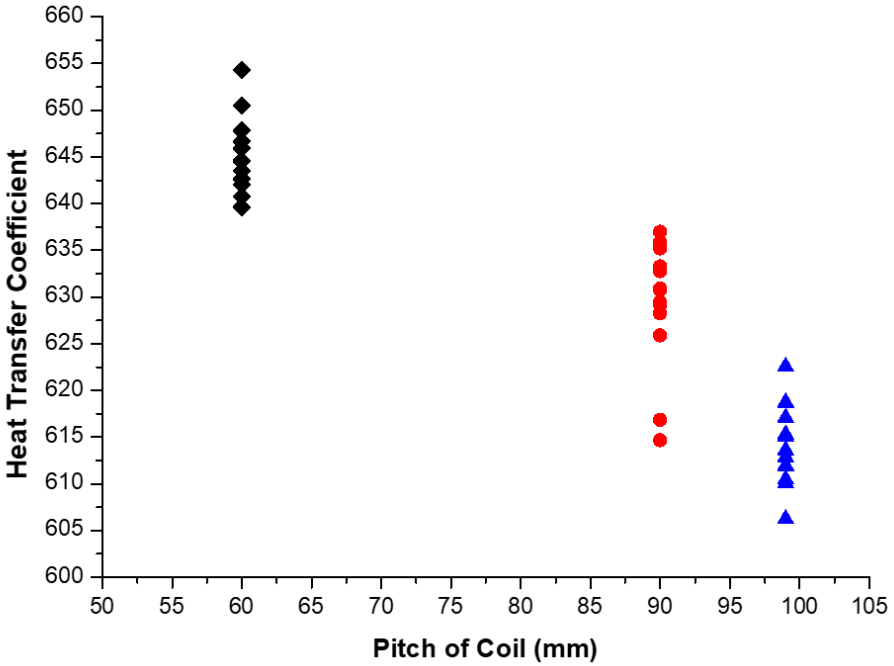

Figure 5-35 Variation in HTC with pitch of coil

In Figure 5-35 a comparison between the pitch of the coil and HTC is drawn. In all of the above three cases diameter of the pipe, diameter of the coil, surface area of the coil, length of the pipe and curvature ratios are kept equal. Study demonstrated a trend of decrease in HTC with increase in the pitch of the coil. As greater pitch leads to increase in height of the coil so same trend was observed in this comparison.

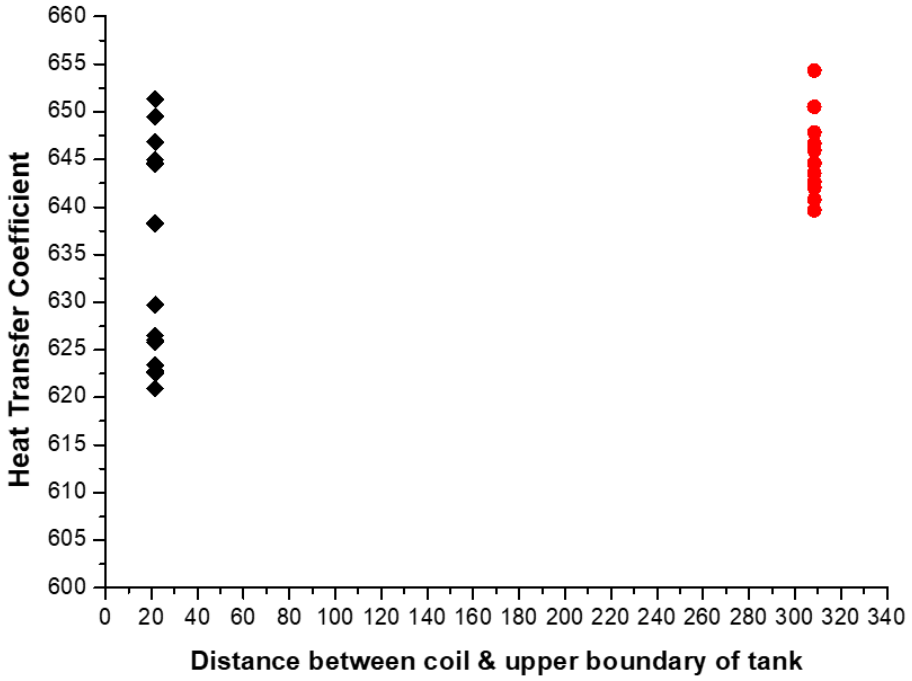

Figure 5-36 Variation in HTC with longitudinal gap

In Figure 5-36 a comparison between the HTC and longitudinal gap between the coil and upper boundary of the tank is drawn. Larger spectrum of HTC values can be noticed for the case with less gap. Because, as the heat transfer starts from helical coil to the water inside the tank, temperature of the water rises which leads to upward movement of water due to decrease in its density. This phenomenon is more prominent in case with larger gap. In the case with smaller gap there is low space for the upward movement of water in result high temperature water accumulates at the top of the tank and thermocline starts developing in the water tank which leads to decrease in natural convection with time. While, in case of larger gap high temperature water mixes with the water above the coil and forms a uniform temperature which leads to greater temperature difference between the water and upper part of the coil for longer periods. In comparison of pitches with HTC,

low pitch coil showing greater HTC is also because of the greater distance longitudinal between the coil and upper boundary of the tank.

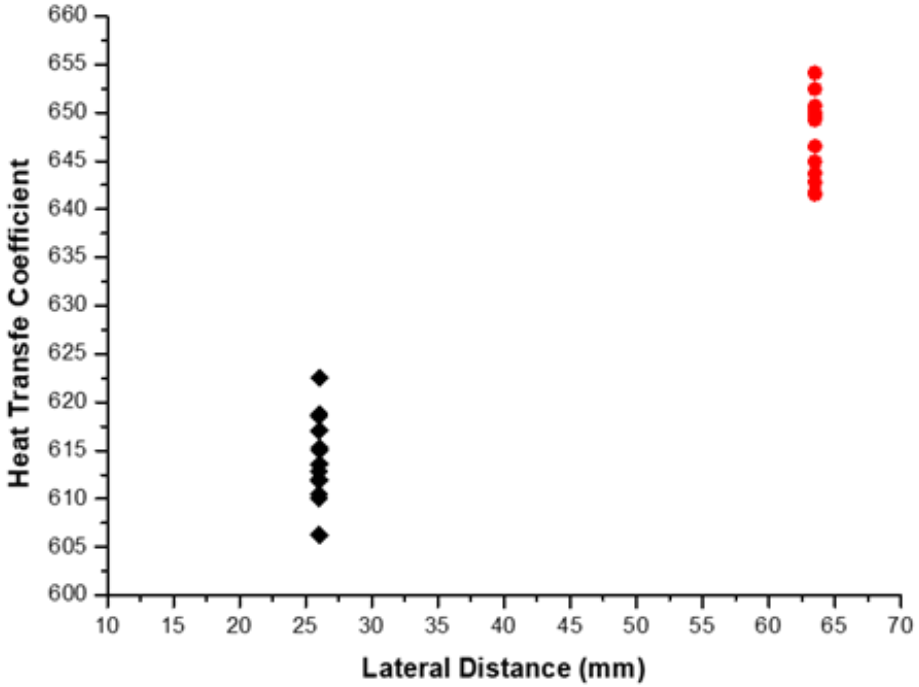

Figure 5-37 Variation in HTC with lateral gap

Above Figure 5-37 is the comparison between the lateral distance of the coil and side boundary of the tank. In both cases, length of the coil, diameter of the pipe and surface area of the coil is kept constant. The variation in the lateral gap was established by fluctuating the coil diameter of the coil. A rise in HTC was noticed with increase in the lateral gap.

In the second Figure 5-38 the lateral gap was changed by varying the aspect ratio of the tank while keeping the volume of water constant. In this comparison, coil diameter, pipe diameter, pitch of the coil, height of the coil and surface are of the pipe were kept constant. Same trend of increase in HTC with increase in lateral gap is observed.

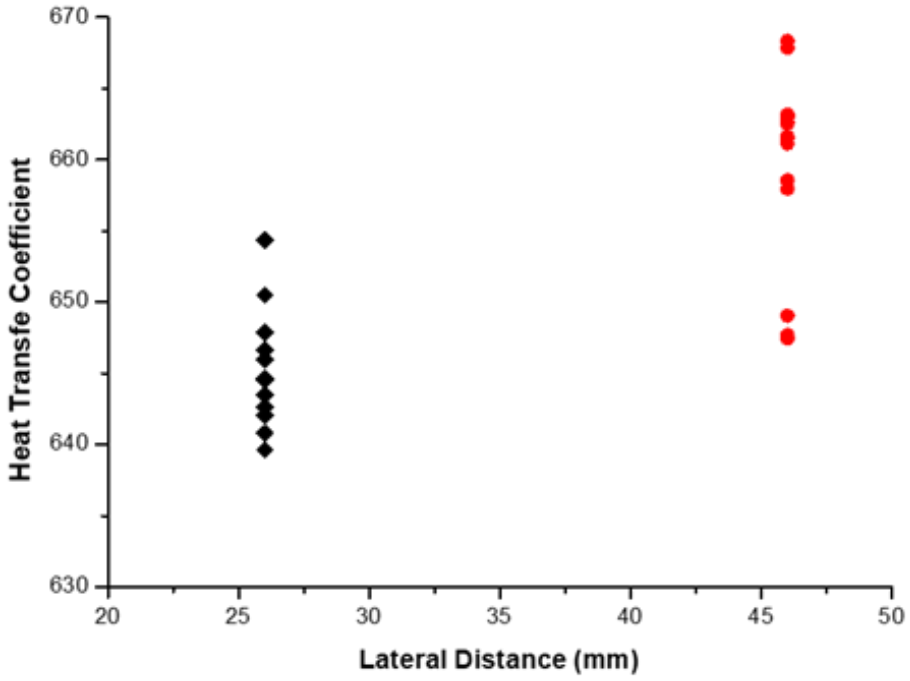

Figure 5-38 Variation in HTC with lateral gap

In Figure 5-39, curvature ratio is compared with external HTC of the coil. No specific trend for change in HTC with curvature ratio is discovered.

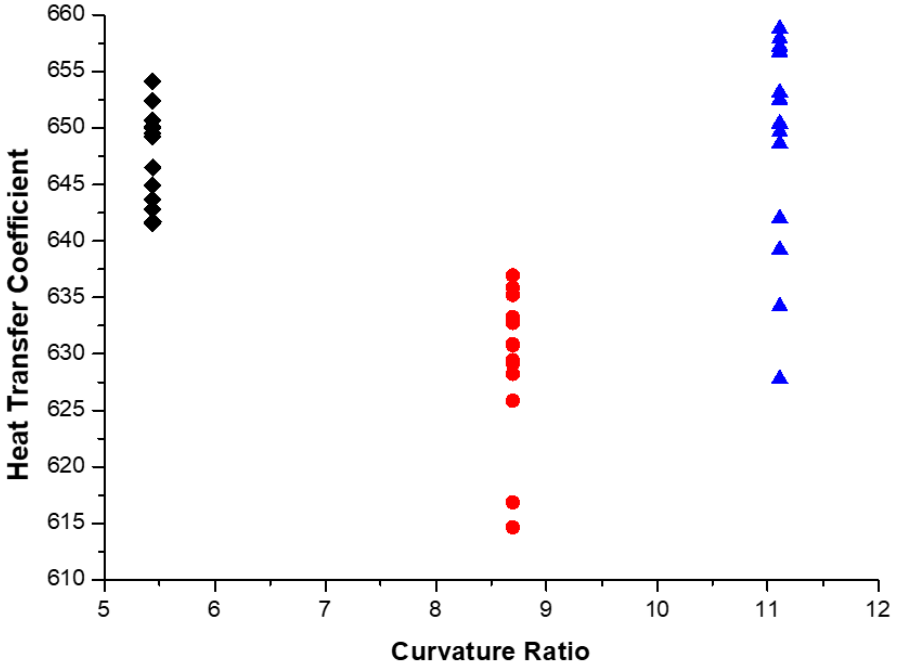

Figure 5-39 Variation in HTC with curvature ratio

However, in last 2 cases diameter of the coil is same which means the lateral distance between the coil and side boundary of the tank is also equal. In case of equal lateral distance, increase in curvature ratio leads to increase in HTC. While, in first 2 cases diameter of the pipe is same, but the first case had lesser coil diameter as compared to second case which means greater lateral distance. That eventually lead to greater HTC even with lesser curvature ratio. So lateral distance is a better geometric factor for predicting the outer HTC as compared to curvature ratio of the coil.

Summary

This chapter includes the details of obtained results which are further analysed for making certain deductions. First, the CFD-based model is validated with the experimental data, then, new models were generated and simulated for extraction of relations and parametric analysis. Moreover, the flow dynamics of the HTF fluid in the coiled pipe is also studied in this chapter. Later on, inner Nusselt number and outer Nusselt number correlations were derived on the basis of the data extracted from the simulated models. These relations are further validated with the past correlations. Lastly, parametric analysis of the thermal stratification inside the tank, and sensitive analysis of inner and outer heat transfer coefficients of the coil are also discussed.

References

[1] J.S. Jayakumar, S.M. Mahajani, J.C. Mandal, P.K. Vijayan, R. Bhoi, Experimental and CFD estimation of heat transfer in helically coiled heat exchangers, Chem. Eng. Res. Des. 86 (2008) 221–232. https://doi.org/10.1016/j.cherd.2007.10.021.

[2] J. Mitrovic, Heat Exchangers - Basics Design Applications, Heat Exch. - Basics Des. Appl. (2012). https://doi.org/10.5772/1997.

[3] E.F. Schmidt, Wärmeübergang und Druckverlust in Rohrschlangen, Chemie Ing. Tech. 39 (1967) 781–789. https://doi.org/10.1002/cite.330391302.

[4] R.C. Xin, M.A. Ebadian, Natural convection heat transfer from helicoidal pipes, J. Thermophys. Heat Transf. 10 (1996) 297–302. https://doi.org/10.2514/3.787.

[5] J.S. Jayakumar, S.M. Mahajani, J.C. Mandal, K.N. Iyer, P.K. Vijayan, CFD analysis of single-phase flows inside helically coiled tubes, Comput. Chem. Eng. 34 (2010) 430–446. https://doi.org/10.1016/j.compchemeng.2009.11.008.

[6] J. Fernández-Seara, F.J. Uhía, J. Sieres, Experimental analysis of a domestic electric hot water storage tank. Part II: dynamic mode of operation, Appl. Therm. Eng. 27 (2007) 137–144. https://doi.org/10.1016/j.applthermaleng.2006.05.004.

[7] M.E. Ali, Experimental investigation of natural convection from vertical helical coiled tubes, Int. J. Heat Mass Transf. 37 (1994) 665–671. https://doi.org/10.1016/0017-9310(94)90138-4.

[8] M.E. Ali, Natural convection heat transfer from vertical helical coils in oil, Heat Transf. Eng. 27 (2006) 79–85. https://doi.org/10.1080/01457630500458617.

Chapter 6: Conclusions & Recommendations

6.1 Conclusions

A fluid-fluid conjugate heat transfer CFD model for a helical coil-based storage tank is simulated, which considers both the effects of forced and natural convection. The CFD model was validated by comparing the simulated results with the experimental data. Additionally, a symmetrical downsized version of the storage tank was modelled, which helped in simulating transient conditions of the storage tank with MAPE of 3.25% and consuming 55% lesser time.

This developed model can be used for simulating future models and predicting the inner state of the storage tank. Secondly, an inner Nusselt number correlation is formed by comparing it with M number, Prandtl number, and curvature ratio. $Nu_i = 0.1868\ M^{0.6958}\ \delta^{0.1703}\ Pr^{0.4}$ showed good agreement with the correlations derived by past investigators through experimental studies. Additionally, outer Nusselt numbers were correlated with Rayleigh's number and the mathematical correlation derived showed good agreement with work done by the past investigators. $Nu_{do} = 0.1996\ (Ra_{do})^{0.326}$ showed least MAPE of 2.06%. Hence, the simulation based on the Boussinesq approximation holds very true and could be further used for studying heat transfer effects on water in the case of natural convection.

Thirdly, it is better to extend the coil through the whole tank to increase its storage capacity and increase the degree of utilization of water inside the tank. Lastly, a tank with aspect ratio 3 led to lesser diffusion of the thermal energy with time, in result increasing the usability of stored energy inside the tank for a longer period.

Furthermore, a general trend of decrease in inner heat transfer coefficient with the increase of diameter and inverse relation for the increase in the length of pipe is observed. The Pitch of the coil did not show any trend and do not have any significant effect on heat transfer. Finally, curvature ratio turned out to be the most salient geometric parameter to determine the heat transfer coefficient of the helical coil heat exchanger, and as the flow

rate increases, a greater degree of increase in HTC with change in curvature ratio is observed.

Lastly, it was deduced from the study that the external HTC of the helical coil increases with the increase in length of the pipe and decreases with an increase in diameter of the pipe, and also pitch and height of the coil. Secondly, it was also observed that the vertical gap between the coil and upper boundary of the tank, and lateral distance between the coil and side boundary of the tank plays an important role in determining the HTC. While curvature ratio of the coil did not demonstrate a specific pattern in comparison with the external HTC.

6.2 Recommendations & future work

As the above research showed reasonable agreement with the past investigations, but more work could be done to drive more comprehensive mathematical correlations.

- All the above simulations need to be repeated by using the thermal properties of the 50% water-glycol solution as a function of its temperature. Then a comparison is needed to be drawn to study the difference with the present simulated results as well as the experimental data.
- Different working fluids need to be used in the laminar flow regime to get more data points for deducing a better general correlation.
- 50% water-glycol solution should be experimented and simulated for turbulent flow regime to study the concordance of the symmetrical downsized model for the turbulent flow regime.
- Mathematical correlation for the inner and outer Nusselt numbers are to be derived for the turbulent flow regime of 50% water-glycol solution.
- More simulations with a different working fluid, with turbulent flow, could lead us to more comprehensive relations.
- All the data points for the laminar as well as turbulent flow could be combined to derive a universal arithmetic relation.
- For external HTC, more variations in the coil configuration and use of different working fluid at different temperatures could lead us to better general corelations.

Appendix I - Coil

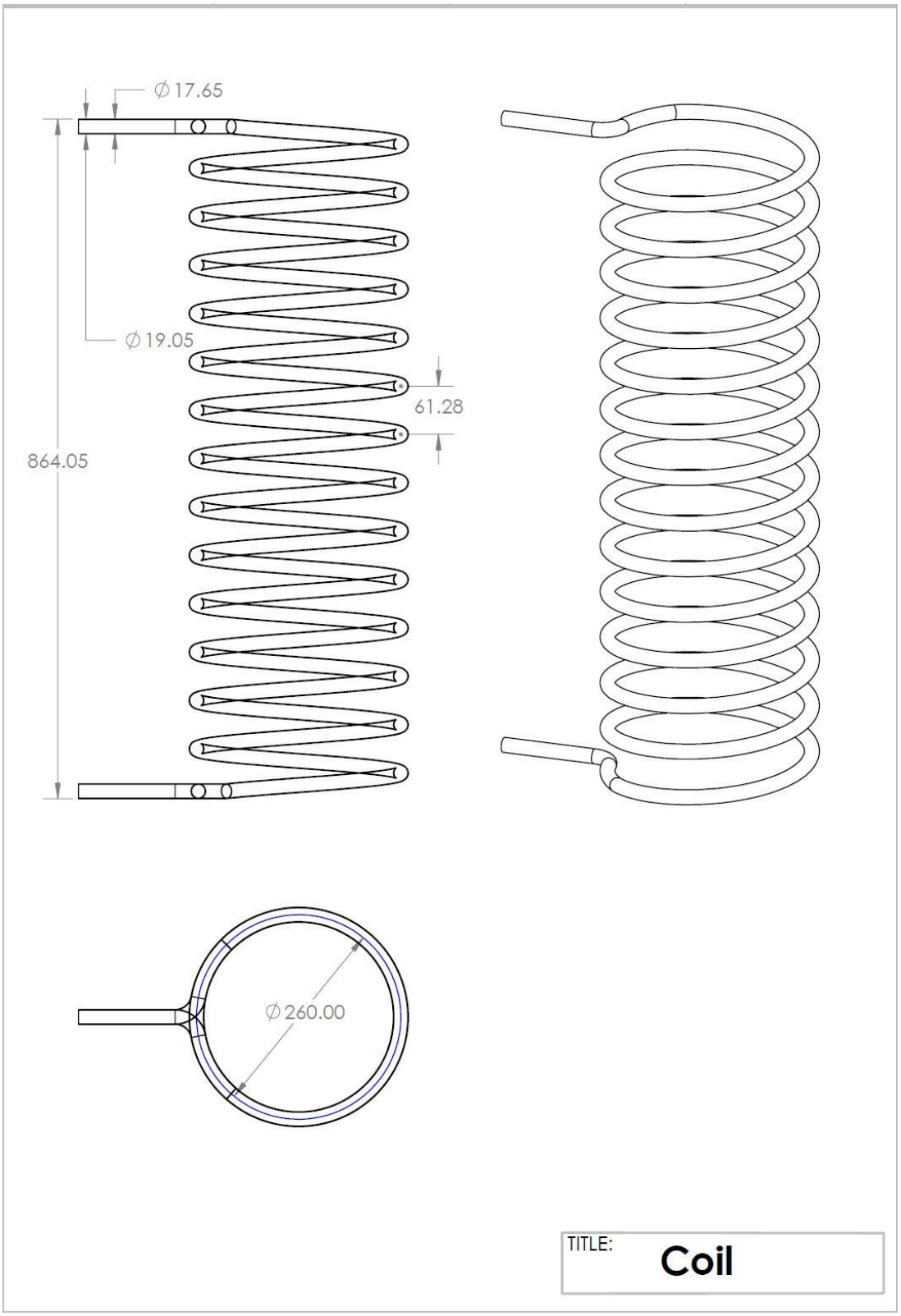

Appendix II - Tank

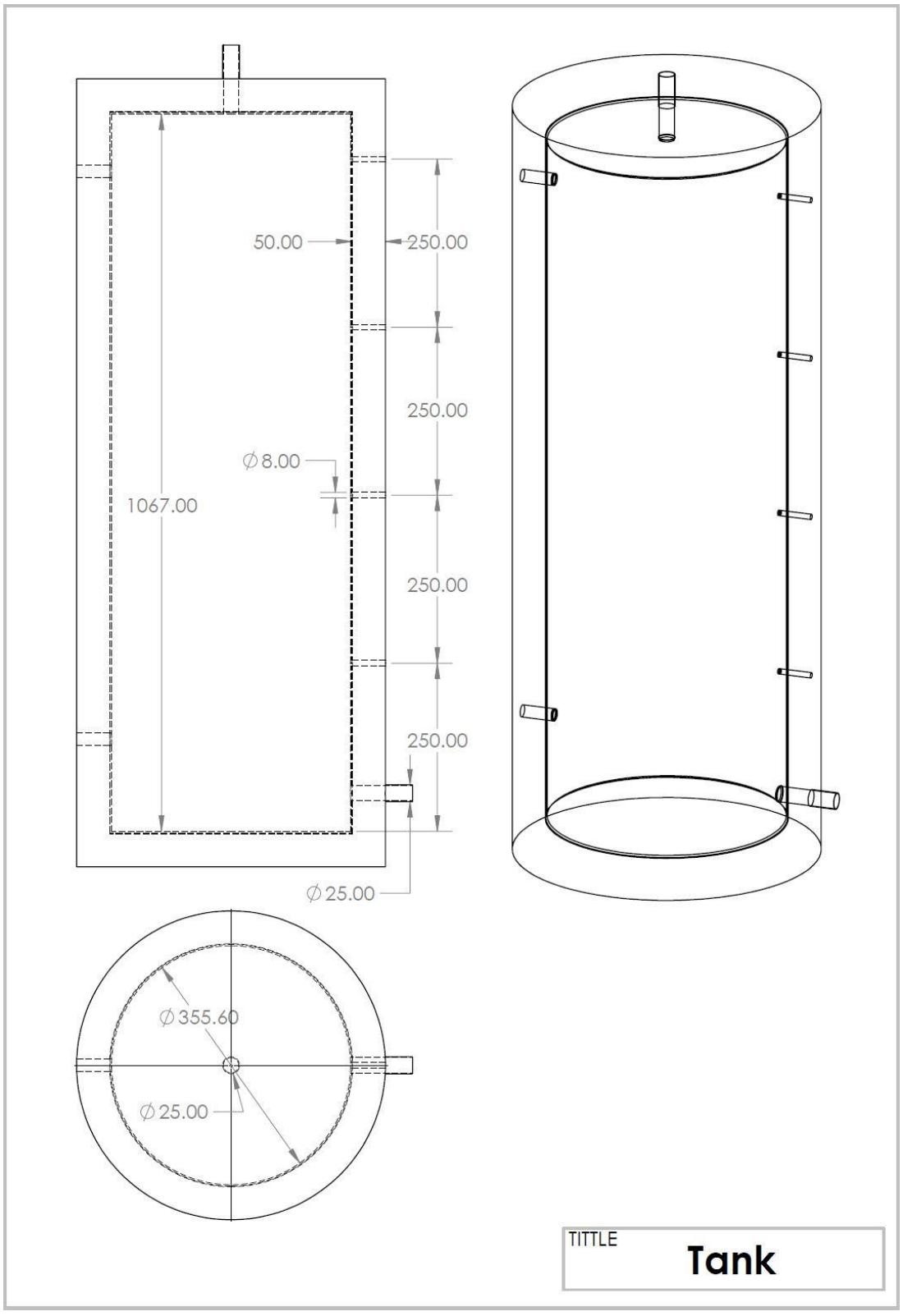

Appendix III - Assembly

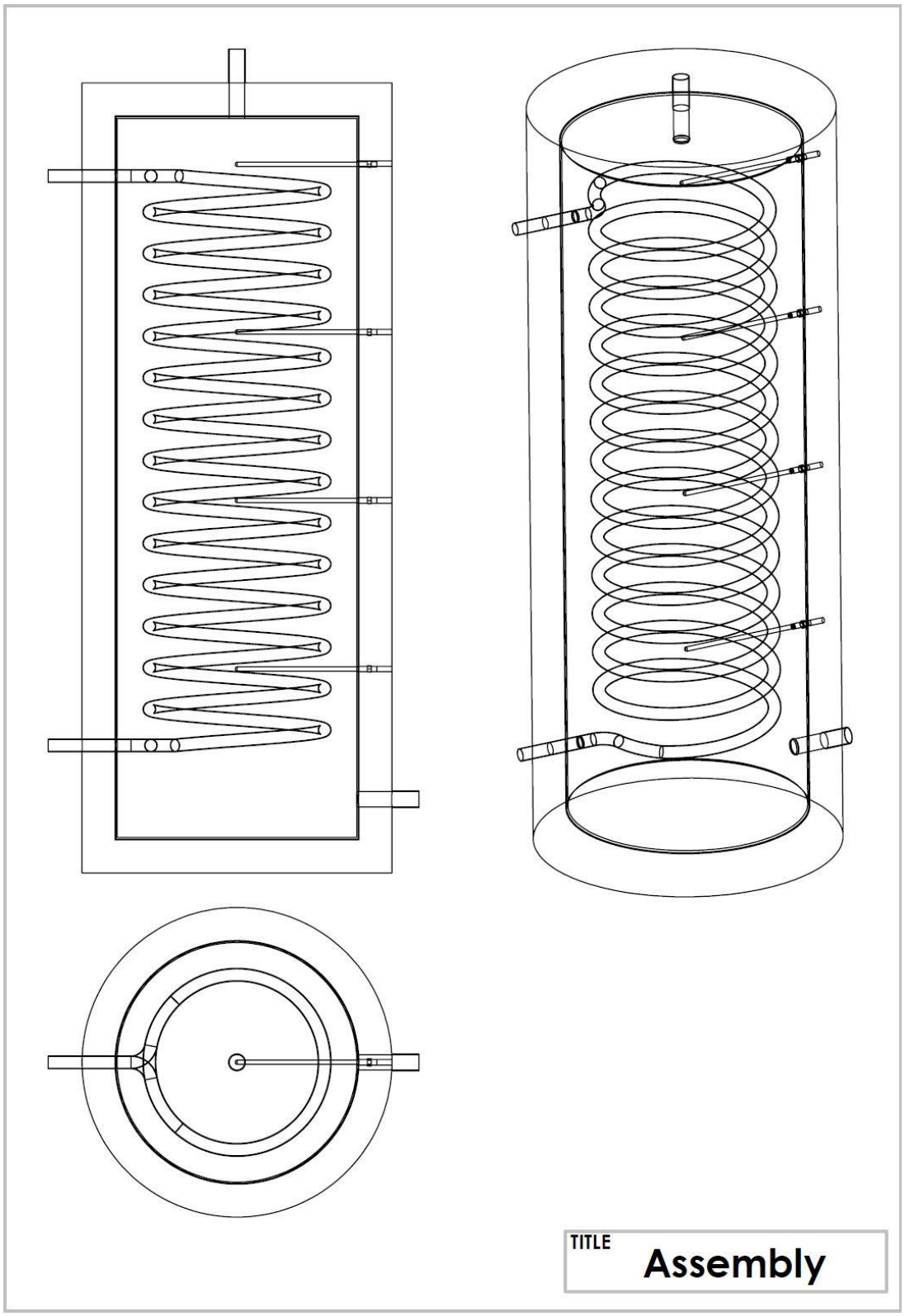

Appendix IV

Inlet glycol temperature UDF for 27th January

```
#include "udf.h"
DEFINE_PROFILE(temperature_profile, thread, i)
{
        face_t f;
        real t = CURRENT_TIME;

        begin_f_loop(f,thread)
           {
              if ( t <= 59.0)
                 {
                    F_PROFILE(f,thread,i) = 287;
                 }
              else if ( 59.0 < t && t <= 180.0)
                 {
                    F_PROFILE(f,thread,i) = -1.00200287947254*pow(10,-10)*pow(t,6)
                                            + 6.24985836462119*pow(10,-8)*pow(t,5)
                                            - 0.00001441188665544O8*pow(t,4) +
                                            0.0013527024232768 2*pow(t,3) -
                                            0.016040078488962 2*pow(t,2) -
                                            4.13409215804316*t + 171.175106591746
                                            + 273;
                 }
              else if ( 180.0 < t && t <= 500.0)
                 {
                    F_PROFILE(f,thread,i) = -3.49474743671764*pow(10,-13)*pow(t,6)
                                            + 7.7782256639084*pow(10,-10)*pow(t,5)
                                            - 7.08023036812959*pow(10,-7)*pow(t,4)
                                            + 0.000335756674295324*pow(t,3) -
                                            0.0866271677163242*pow(t,2) +
```

```
                                        11.2586051598903*t - 500.351981938507
                                        + 273;
            }
        else
            {
                F_PROFILE(f,thread,i) = -2.77345396607473*pow(10,-
                                        19)*pow(t,6) +
                                        3.4329995870785*pow(10,-15)*pow(t,5) -
                                        1.63943936083565*pow(10,-11)*pow(t,4)
                                        + 3.74395528525629*pow(10,-
                                        8)*pow(t,3) -
                                        0.00004042599095197 01*pow(t,2) +
                                        0.0189538119908156*t +
                                        33.9019882953471 + 273;
            }
    }
end_f_loop(f,thread)
}
```

Appendix V

Inlet glycol temperature UDF for 28th January

```
#include "udf.h"

DEFINE_PROFILE(temperature_profile, thread, i)

{

        face_t f;

        real t = CURRENT_TIME;


        begin_f_loop(f,thread)

            {

                if (t <= 120.0)

                    {

                        F_PROFILE(f,thread,i) = 7.40540472612137*pow(10,-10)*pow(t,6) -
                                                2.47756714005787*pow(10,-7)*pow(t,5) +
                                                0.0000287171981894208*pow(t,4) -
                                                0.0013260150823l289*pow(t,3) +
                                                0.024782570075331*pow(t,2) -
                                                0.144212479084672*t +
                                                25.0811604709888 + 273;

                    }

                else if ( 120.0 < t && t <= 500.0)

                    {

                        F_PROFILE(f,thread,i) = -3.08761426082361*pow(10,-13)*pow(t,6)
                                                + 6.04553591516324*pow(10,-
                                                10)*pow(t,5) -
                                                4.75987851744901*pow(10,-7)*pow(t,4) +
                                                0.000190088472159797*pow(t,3) -
                                                0.0394023022379041*pow(t,2) +
                                                3.70949601285095*t - 46.7115431212819
                                                + 273;
```

```
            }

        else

            {

                F_PROFILE(f,thread,i) = 1.69651048446063*pow(10,-19)*pow(t,6) -
                                        2.1281181194726*pow(10,-15)*pow(t,5) +
                                        1.0917877165945*pow(10,-11)*pow(t,4) -
                                        2.98970435012836*pow(10,-8)*pow(t,3) +
                                        0.0000469988812779033*pow(t,2) -
                                        0.038854233457603*t +
                                        48.0507346035389 + 273;

            }

    }

end_f_loop(f,thread)

}
```

Appendix VI

Inlet glycol temperature UDF for 9th February

```
#include "udf.h"
DEFINE_PROFILE(temperature_profile, thread, i)
{
        face_t f;
        real t = CURRENT_TIME;

        begin_f_loop(f,thread)
           {
              if ( t <= 69.0)
                 {
                    F_PROFILE(f,thread,i) = 297.5;
                 }
              else if ( 69.0 < t && t <= 181.0)
                 {
                    F_PROFILE(f,thread,i) = -1.06381172445321*pow(10,-8)*pow(t,5) +
                                            7.37136102242674*pow(10,-6)*pow(t,4) -
                                            0.00202742863550365*pow(t,3) +
                                            0.271582377783658*pow(t,2) -
                                            16.9388773936251*(t) +
                                            415.859463553446 + 273;
                 }
              else if ( 181.0 < t && t <= 500.0)
                 {
                    F_PROFILE(f,thread,i) = -2.77311395237524*pow(10,-13)*pow(t,6)
                                            + 6.19789026546321*pow(10,-
                                            10)*pow(t,5) -
                                            5.67821496876113*pow(10,-7)*pow(t,4) +
                                            0.000271574591118843*pow(t,3) -
                                            0.0707705580117591*pow(t,2) +
```

```
                                        9.28755695158169*t - 403.866866096332
                                        + 273;
                }
            else
                {
                  F_PROFILE(f,thread,i) =  9.12353055894359*pow(10,-16)*pow(t,6) -
                                        4.56925420831289*pow(10,-12)*pow(t,5)
                                        + 9.37007953253601*pow(10,-9)*pow(t,4)
                                        - 0.0000100700798028302*pow(t,3) +
                                        0.00598833738929065*pow(t,2) -
                                        1.87962587834124*t + 285.174980542304
                                        + 273;
                }
        }
end_f_loop(f,thread)
}
```

Appendix VII - Publication

Development and Validation of Nusselt number correlations for a Helical Coil Based Energy Storage Integrated with Solar Water Heating System

Saqib Ayuob[1], Mariam Mahmood[1*], Naveed Ahmad[1], Adeel Waqas[1], Hamza Saeed[1], Muhammad Bilal Sajid[1], Majid Ali[1], Nadia Shahzad[1]

[1]US-Pakistan Centre for Advanced Studies in Energy, National University of Sciences and Technology, Islamabad, Pakistan.

Abstract

Storage tanks based on helical coil heat exchangers are an integral part of solar water heating (SWH) systems and require optimal design configuration to achieve maximum heat transfer and a longer storage period. This study is focused on thermal analysis of a vertical helical coil-based water storage tank and derivation of inner and outer Nusselt number correlations by considering the storage tank as well as helical coil and catering to both forced and natural convection effects. A fluid-fluid conjugate heat transfer transient state model is validated with experiments performed with 50/50% water-glycol mixture as HTF at flow rates of 2 and 3 L/minute in a solar water heating system, while water remains at static flow condition inside the tank. To reduce the computational cost, a symmetrical downsized model is also designed and validated, which showed a mean absolute percentage error of 3.25%. In order to derive the mathematical correlations, alterations were made to the validated model by using coils with curvature ratios ranging from 0.09-0.184 with HTF flow rates in laminar flow regimes, ranging from 30 to 100 liters per hour at temperatures from 40^{o}C to 80^{o}C. Furthermore, Nu_i mathematical correlations based on M number, curvature ratio, and Prandtl number showed good agreement with correlations derived by past investigators. Similarly, the outer Nusselt number of the coil was related to Rayleigh's number and the derived relations showed good agreement with the past studies, while $Nu_o = 0.1996 (Ra_{do}^{0.326})$ showed the least error of 2.06%. Finally, thermal stratification analysis helped to understand that coil position and aspect ratio determine the thermocline developed inside the storage tank and hot water storage for longer periods.

Keywords: Thermal Energy Storage (TES), Nusselt Number, Helical Coil, Computational Fluid Dynamics (CFD), Thermal Stratification

EST-D-22-00865- Journal of Energy Storage (Under review)